



M Ű E G Y E T E M 1 7 8 2

Budapest University of Technology and Economics
Faculty of Electrical Engineering and Informatics
Department of Networked Systems and Services

Analysis of some Cooperative Methods for Wireless Communications

Ph.D. Dissertation

by

Arwa Mahmoud Yousef Jwaifel

Supervisor

Prof. Tien Van Do

Budapest University of Technology and Economics

Budapest, Hungary

September, 2025

Declaration

I, the undersigned *Arwa Mahmoud Yousef Jwaifel*, hereby declare, that this PhD. dissertation was made by myself, and I only used the sources given at the end. Every part that was quoted word-for-word, or was taken over with the same content, I noted explicitly by giving the reference of the source.

The reviews of the dissertation and the report of the thesis discussion are available at the Deans Office of the Faculty of Electrical Engineering and Informatics of the Budapest University of Technology and Economics.

Budapest, Sunday 7th September, 2025

Arwa Mahmoud Yousef Jwaifel

Abstract

Unmanned Aerial Vehicles (UAVs) have gained significant attention in recent years due to their potential for carrying out a wide range of tasks, including carrying gNB to provide mobile services in various applications such as disaster management, surveillance, and extended coverage. First, I investigated the joint optimization of resource allocation and trajectory planning for UAV-enabled communication systems, focusing on integrating Deep Reinforcement Learning (DRL) algorithms. The primary goal of this research is to develop an innovative approach that leverages the capabilities of UAVs to optimize the trajectory while utilizing gNB radio resources for wireless communication.

The proposed framework integrates DRL algorithms to enable the gNB, which is carried by UAV, to dynamically allocate radio resources based on changing environmental conditions and task requirements. By using DRL, the UAVs, and the carried gNB can learn and adapt their trajectory and radio resource allocation over time to maximize the efficiency of radio resource utilization. The research methodology involves the development of a simulation environment to model the joint optimization problem and evaluate the performance of the proposed approach. The simulation results demonstrate the effectiveness of the integrated DRL and gNB-based resource allocation and trajectory optimization strategy carried out by UAVs, showcasing improvements in network throughput, user satisfaction, and overall system efficiency.

In our second study, I investigated the impact of co-channel interference on the performance of cooperative UAV-enabled ad-hoc networks operating over α - μ fading channels. UAV-enabled ad-hoc networks have emerged as a promising communication paradigm for applications requiring flexible and dynamic connectivity. The primary objective is to analyze and quantify the effects of co-channel interference on the reliability and throughput of cooperative communication in challenging fading environments, specifically in the context of UAV deployments.

The research methodology involves the development of a comprehensive analytical framework to model cooperative UAV-enabled ad-hoc networks under the influence of co-channel interference and α - μ fading channels. The framework considers various performance metrics, including outage probability and bit error rate, to assess the impact of interference on the network's communication reliability and efficiency.

The derived results provide insights into the trade-offs between cooperative diversity, interference mitigation, and network performance in the presence of α - μ fading and co-channel interference in UAV-enabled ad-hoc networks. The findings highlight the challenges and opportunities associated with cooperative communication in adverse fading environments, shedding light on potential strategies to improve the reliability and throughput of UAV-enabled ad-hoc networks under co-channel interference.

Then, I extended the research in the third study to investigate the impact of co-channel interference on the performance of cooperative diversity networks. Integrating cooperative diversity and dual-hop communication mechanisms plays a crucial role in mitigating the impact of co-channel interference and enhancing the overall network performance. Cooperative diversity leverages the spatial diversity offered by multiple cooperative nodes to combat fading and improve the reliability of communication links. Meanwhile, dual-hop communication involves data transmission over two consecutive hops, providing an additional layer of diversity and enabling more effective interference management.

Utilizing cooperative diversity within dual-hop communication scenarios in UAV-enabled ad-hoc networks over α - μ fading channels presents a compelling approach to address the challenges posed by co-channel interference. By leveraging the cooperative transmission and reception capabilities of UAVs and ground nodes, the network can exploit the benefits of spatial diversity and cooperative beamforming to combat fading effects and mitigate interference. The dual-hop nature of the communication further enhances the diversity gain by allowing the network to leverage multiple transmission paths, thereby reducing the impact of fading and interference on the overall communication reliability.

Integrating cooperative diversity and dual-hop communication in the context of UAV-enabled ad-hoc networks over α - μ fading channels offers a synergistic approach to improving the network's robustness and performance in challenging communication environments. By jointly leveraging the benefits of cooperative diversity and dual-hop communication, the network can effectively manage co-channel interference, combat fading effects, and enhance communication links' overall reliability and throughput. This integrated approach enables the network to adapt to dynamic fading conditions and mitigate the adverse impact of interference, thereby improving the quality of service and enhancing the network's resilience in challenging communication scenarios.

Acknowledgments

Completing this Ph.D. journey has been an incredibly rewarding experience, and I owe a debt of gratitude to many individuals who have supported me along the way.

First and foremost, I would like to express my deepest appreciation to my supervisor, **Prof. Tien Van Do**. His guidance, wisdom, and unwavering belief in my abilities have been instrumental in shaping the direction of my research and helping me navigate the challenges of academia.

I extend my thanks to the dedicated staff and faculty at **Budapest University of Technology and Economics** (BME) for providing a stimulating academic environment and resources essential for conducting my research, and special thanks to my colleague Hai who answers the majority of my questions and notes about the research topic.

My heartfelt appreciation goes out to my family for their endless love, support, and sacrifices. Their encouragement and belief in me have been my driving force, and I am forever grateful for their unwavering support. My gratitude to my father **Eng. Mahmoud Jwaifel** and my mother **Nuha** for their endless support and love, and my siblings and their kids too.

I am also indebted to my friends specially **Rana Ramadan, Bouthaina Bouaziz, Hanan Altous, Hanady Sweity and Roumaissia Onouki** for their camaraderie, encouragement, and stimulating discussions that have enriched my academic journey. My colleagues; Hai, Xiuan, Mohammad, Hassanien and Baseem thank you for the support and the advices, good luck with your coming chapter of your life.

Finally, and above of all, I humbly bow my head with utmost gratitude before mighty **Allah** whose unconditional love and support has made all this possible.

Dedication

Dedicated to my father **Eng. Mahmoud Jwaifel Al Abbadi**, to my lovely mother, to my sisters and brothers and to my best friends, for support and understanding.

Arwa M. Jwaifel Al Abbadi

Contents

Abstract	i
Acknowledgments	iii
Dedication	iv
List of Figures	ix
List of Tables	x
1 Introduction	1
1.1 Motivations	1
1.2 Research Goals	3
1.3 Research Methodology	5
1.4 The organization of this thesis	7
2 Impact of Co-Channel Interference on Performance of Cooperative Wireless Ad-hoc Networks over $\alpha - \mu$ fading channels	9
2.1 Introduction	10
2.2 System Model	12
2.2.1 $\alpha - \mu$ fading model	15
2.2.2 Signal-to-Noise Ratio (SNR)	16
2.2.3 SNR Cumulative Distribution Function (CDF)	18
2.2.4 SNR Moment Generating Function (MGF)	19
2.3 Dual-hop SINR analysis	20
2.3.1 Co-Channel Interference probability density function (PDF)	21
2.3.2 Effective SINR statistical characteristics	24
2.3.3 Dual-Hop Relay SINR PDF	29
2.3.4 Dual-Hop Relay SINR CDF	33
2.3.5 Dual-Hop Relay SINR MGF	37
2.4 Dual-Hop Relay Performance Analysis	38
2.4.1 Outage Probability Analysis	38
2.4.2 Average Error Probability Analysis	41
2.4.2.1 Average error probability for different fading channel links	44
2.5 Numerical results	50
2.5.1 Outage Performance Analysis	51
2.5.2 Error Performance Analysis	52

2.6	Conclusion	56
Glossary — Chapter 2		57
3	Impact of co-channel interference on the performance of cooperative diversity systems	59
3.1	Introduction	60
3.2	System Model	62
3.3	Cooperative diversity SINR analysis	65
3.4	Performance analysis	69
3.4.1	Outage Probability	69
3.4.2	Average Error Probability	72
3.5	Numerical results	75
3.5.1	Outage Probability Performance	75
3.5.2	Effects of Interference on System Performance	75
3.5.3	Error Probability Analysis	76
3.6	Conclusion	80
Glossary — Chapter 3		81
4	Deep Reinforcement Learning for Jointly Resource Allocation and Trajectory Planning in UAV-assisted Networks	83
4.1	Introduction	84
4.2	Related work	86
4.3	An RL-based approach	88
4.4	Simulation and analysis	90
4.4.1	Models used in simulation	90
4.4.1.1	User Mobility	90
4.4.1.2	RB scheduling algorithm	90
4.4.1.3	Energy Consumption Model for Multi-rotor UAV	91
4.4.1.4	Energy model of gNB	96
4.4.1.5	NR frame Frame structure	100
4.4.1.6	5G frame Downlink Link Adaptation	100
4.4.2	Simulation results	105
4.5	Conclusion	114
Glossary — Chapter 4		115
Own Publications		117
Bibliography		117

List of Figures

2.1	Dual-hop relay network with co-channel interference at the relay and destination nodes.	13
2.2	Dual-hop outage probability for $\alpha = 2, \mu = 1, INR = 3dB$	52
2.3	Dual-hop outage probability for $\alpha = 2, \mu = m = 2, INR = 12dB$	53
2.4	Dual-hop outage probability for $\alpha = 2, \mu = m = 2$ and $N = L = 5$	53
2.5	Average error probability for identical number of fading channel with $\alpha = 2$ and $\mu = 1$	54
2.6	Average error probability for identical number of fading channel with $\alpha = 2, \mu = m = 2$ and $N = L = 4$ interferers	55
2.7	Average error probability for identical number of fading channel with $\alpha = 2$, different fading parameters $\mu = m = 1, 2, 3, 4, 5$	55
3.1	Cooperative Diversity Relay Network	62
3.2	Outage probability of identical Fading channels with different coefficients, Selective Combining and without interference. Fading channels coefficients: $\alpha = 2, \mu = 1$	76
3.3	Outage probability of identical Fading channels with different coefficients, Selective Combining and without interference. Fading channels coefficients: $\alpha = 2, \mu = 2$	77
3.4	Outage probability of identical Fading channels with Selective Combining and 5-interferers and $INR = 3dB$. Fading channels coefficients: $\alpha = 2, \mu = 1$	77
3.5	Outage probability of identical Fading channels with Selective Combining and 5-interferers and $INR = 3dB$. Fading channels coefficients: $\alpha = 2, \mu = 1$	78
3.6	Average error probability of identical Fading channels with $SINR = 30 dB$ and SC scheme and various number of interferers (0,5,10). Fading channels coefficients: $\alpha = 2, \mu = 1$	78
3.7	Average error probability of identical Fading channels with $SINR = 30 dB$ and SC scheme and various number of interferers (0,5,10). Fading channels coefficients: $\alpha = 2, \mu = 2$	79
4.1	UAV emergency model.	84
4.2	UAV hovering state forces.	91
4.3	UAV forward state forces.	91
4.4	5G NR Frame structure.	101
4.5	TBS size calculation algorithm flowchart.	105
4.6	Cell grid with UAV trajectory path, for the scenario of 4 UEs positioned at the corners of $750 m^2$ cell grid, $BW=5 MHz$	106

4.7	UAV trajectory and allocated RBs for the scenario of 4 UEs located at the corner of 750 m^2 cell grid, $BW = 5\text{ MHz}$	107
4.8	Cell grid with UAV trajectory path, for the scenario of 10 UEs randomly located and stationary in 1000 m^2 cell grid, $BW=25\text{ MHz}$. .	108
4.9	UAV trajectory and allocated RB, for the scenario of 10 UEs randomly located and stationary in 1000 m^2 cell grid, $BW=25\text{ MHz}$. .	109
4.10	UAV trajectory and allocated RBs for the scenario of 20 UEs randomly located and stationary in 1000 m^2 cell grid, $BW=25\text{ MHz}$. .	110
4.11	Cell grid with UAV trajectory path, for the scenario of 20 UEs randomly located and stationary in 1000 m^2 cell grid, $BW=25\text{ MHz}$. .	110
4.12	Cell grid with UAV trajectory path, 10 UEs with randomwalk model, $BW=10\text{ MHz}$, cell grid size= $1000 \times 1000\text{ m}^2$	111
4.13	UE mobility scenario: 10 UEs with randomwalk model, $BW=10\text{ MHz}$, cell grid size= 1000 m^2	111
4.14	Cell grid with UAV trajectory path, 20 UEs with randomwalk model, $BW=40\text{ MHz}$, cell grid size= $1500 \times 1500\text{ m}^2$	112
4.15	UE mobility scenario: 20 UEs with randomwalk model, $BW=40\text{ MHz}$, cell grid size= $1500 \times 1500\text{ m}^2$	112
4.16	Cell grid with UAV trajectory path, 100 UEs with randomwalk model, $BW=40\text{ MHz}$, cell grid size= $1700 \times 1700\text{ m}^2$	113
4.17	UE mobility scenario: 100 UEs with randomwalk model, $BW=40\text{ MHz}$, cell grid size= $1700 \times 1700\text{ m}^2$	113

List of Tables

4.1	UAV and Motor Simulation Parameters.	97
4.2	UAV Battery Model Simulation Parameters.	97
4.3	gNB Simulation Parameters.	97
4.4	Mobile Network Simulation Parameters.	98
4.5	NR frame slots and subframes based on numerology value.	100

Chapter 1

Introduction

1.1 Motivations

The deployment of 5G and beyond networks represents a transformative leap forward in wireless communication technology, promising unprecedented levels of speed, reliability, and connectivity [1]. However, efficient optimization of network operations is imperative to fully realize the potential of 5G and meet the diverse demands of modern applications and services. This provides the key motivation to drive our research on leveraging machine learning procedures to optimize the operation of 5G and beyond networks, taking advantage of the UAV carrying a gNB to provide mobile services [2], [3], [4], [5], [6], [7] and [8] while in [P1] we dealt with indoor localization. Unmanned Aerial Vehicles (UAVs) have emerged as versatile platforms for a wide range of applications, including surveillance, environmental monitoring, disaster response, and communication relay. As UAVs continue to play an increasingly integral role in various domains, the optimization of their communication capabilities becomes paramount. One of the fundamental challenges in UAV communication systems is the presence of co-channel interference (CCI), which can significantly impact the reliability and performance of wireless links. In this context, the investigation of CCI interference and the application of

advanced communication techniques, such as dual-hop and cooperative diversity, hold immense potential to enhance UAV communication networks.

The presence of CCI in UAV communication systems poses unique challenges that require innovative solutions. CCI occurs when multiple UAVs or ground stations operating on the same frequency interfere with each other, leading to signal degradation and potential communication disruptions. Addressing this interference is critical to ensure reliable and robust communication links for UAVs operating in congested or contested environments.

Dual hop communication, as applied to UAVs, offers a promising approach to mitigate the effects of CCI. By utilizing UAVs as relays between ground stations and remote nodes, dual-hop communication enables the bypassing of direct interference sources and extends the effective communication range. Investigating the integration of dual-hop communication within UAV networks in the context of CCI interference presents an opportunity to assess the potential improvements in link reliability and network coverage. Many studies investigated impact of CCI on amplify-and-forward dual-hop relay network performance such as: [9], [10], [11], [12], [13], [14], [15], [16] and [17].

Furthermore, cooperative diversity techniques, which leverage collaborative signal processing and distributed transmission among UAVs, hold significant potential for combating CCI effects. By forming virtual antenna arrays and coordinating signal reception and transmission, UAVs can enhance the resilience of their communication links in the presence of interference. Investigating the application of cooperative diversity in UAV communication networks provides an avenue to explore the effectiveness of collaborative strategies in mitigating CCI and improving overall system performance. In this thesis, I aimed to explore the intersection of dual-hop

communication, cooperative diversity, and CCI interference mitigation within UAV communication networks. By investigating the effect of CCI on the communication channel, I derived the performance metrics for the network performance such as bit error rate and outage probability. Studies are: [18], [19], [18], [19], [20], [21], [22] and [23].

Integrating machine learning techniques for dynamically optimizing the operation of 5G and beyond networks, addressing the complexity, heterogeneity, and dynamic nature of modern wireless communication systems, can be a promising solution to address these challenges and enhance the quality of service and user experience in next-generation wireless communication systems. By leveraging machine learning (ML) and deploying deep reinforcement learning (DRL) framework, the proposed procedures will enhance network performance, reliability, efficiency, and security, ultimately improving the quality of service and user experience in 5G deployments where I deployed a reinforcement learning (RL) framework to jointly optimize the trajectory of the UAV and the resources allocated by the carried by the UAV. In this approach, we considered the ground user mobility while designing the DRL model in order to solve the optimization problem and reach the optimal solution. Such studies are: [24], [25], [26], [27], [28], [29], [30] and [31].

1.2 Research Goals

Drones are rapidly transforming the landscape of mobile communications, offering unparalleled flexibility and efficiency. These versatile unmanned aerial vehicles (UAVs) serve as dynamic relay nodes or aerial base stations, capable of extending network coverage to remote and under served areas, and enhancing capacity during high-demand events. By operating from elevated vantage points, drones can overcome obstacles that impede terrestrial signals, ensuring robust connectivity

where traditional infrastructure may struggle. Their mobility allows them to adapt in real-time to changing network conditions, optimizing resource allocation, and mitigate interference. As we advance into the 5G era and beyond, the integration of drones into mobile networks promises to redefine connectivity, making it more resilient and expansive, and ultimately, extending the reach of the digital world to new heights.

As UAVs continue to play an increasingly integral role in various domains, the optimization of their communication capabilities becomes paramount. Thus my studies objectives were the following:

- Investigating the integration of dual-hop communication within UAV networks in the context of CCI interference presents an opportunity to assess the potential improvements in link reliability and network coverage. Where I derive the statistical formulas required to analysis the network performance in terms of bit error rate and outage probability. I assumed all links are subjected to α - μ fading channel, [P2].
- Explore the intersection of dual-hop communication, cooperative diversity, and CCI interference mitigation within UAV communication networks. By investigating the effect of CCI on the communication channel, I derived the necessary statistical equations such as the probability density functions and cumulative density functions which are used to build and derive the performance metrics for the network performance such as bit error rate and outage probability, where the fading model is the α - μ fading channel, [P3].
- Deploy deep reinforcement learning (DRL) framework, to optimize the operation of 5G and beyond networks, taking advantage of the UAV carrying a gNB to provide mobile services. The proposed procedures will enhance network performance, reliability, efficiency, and security, optimally improving the quality of service and user experience in 5G deployments where I deployed

an RL framework to jointly optimize the trajectory of the UAV and the resources allocated by the carried by the UAV. In this approach, I considered the mobility of the ground user while designing the DRL model in order to solve the optimization problem and reach the optimal solution, [P4].

1.3 Research Methodology

Digital communication is all about sending information using digital signals through a communication channel. It's fundamental in of modern technology, making it possible to share data quickly and reliably across different platforms, including wireless networks. In this thesis I focused on cooperative systems. The basic setup of cooperative networks is the Dual-hop cooperative systems which are evaluated in this thesis based on performance metrics such as Bit Error Rate (BER), Signal-to-Noise Ratio (SNR), and outage probability (P_{out}).

The first stage involves developing a detailed system model of the dual-hop cooperative network. This includes defining the nodes of the network, which means to identify the source, relay, and destination nodes. The relay node assists in forwarding the signal from the source to the destination and deploying a forwarding algorithm such as amplify-and-forward (AF) or decode-and-forward (DF). The other part is to model the wireless channel characteristics among the network nodes, and this can be done using probabilistic tools. This includes characterizing the fading and noise processes, typically assuming Rayleigh or Rician fading models as in [32] and [33], in addition to assuming α - μ fading channel [34]. The second stage of the approach is probability analysis, which involves utilizing the probabilistic models to evaluate the behavior of the channels and the impact of noise and interference. In this stage, two steps are to be used: define the signal and noise as random variables with specific Probability Density Functions (PDFs) and Cumulative Distribution

Functions (CDFs). Then use Moment-Generating Functions (MGFs) to derive key statistical properties and simplify the calculation of performance metrics such as the Bit Error Rate, the Signal-to-Noise Ratio, and the outage probability (P_{out}) [35].

Comparative analysis can be performed to analyze different relay strategies and adding cooperative diversity to the dual-hop network and analyze the performance for this enhancement and compare it to the dual-hop network, another comparative analysis is to compare different channel conditions such as Rayleigh or Nakagami-m fading models to the α - μ fading model.

Reinforcement learning (RL) is a promising technique for optimizing network resources. It is particularly effective in managing complex and dynamic network environments, making it a valuable tool to address the challenges in modern networking. This involves using RL to make real-time decisions about resource allocation, traffic management, and network configuration to improve performance metrics such as throughput, latency, and energy efficiency. In order to apply RL to solve the problem, I designed our system as a Markov decision problem (MDP). MDP consists of tuple of five elements $\langle S, A, p, r, \gamma \rangle$, where S represents the system state set, A action space set, $p : S \times A \times S \in [0, 1]$ and represents the Transition Probability Matrix between the states, $r : S \times A \times S \rightarrow \mathbb{R}$ denotes the immediate reward between state transitions; finally $\gamma \in [0, 1]$ which represent the discount factor [36]. Different RL algorithms can be deployed to optimize the network resources and the UAV trajectory, specially DRL which is suitable for discrete state space, another RL algorithm that can be deployed is the policy gradient method which is known as Proximal Policy Optimization (PPO) [37].

1.4 The organization of this thesis

In chapter 2, I introduced a comprehensive mathematical and statistical framework to analyze the performance of dual-hop relay networks in the presence of co-channel interference (CCI). Leveraging the α - μ distribution to model interference as the sum of independent but not identically distributed (I.N.I.D) random variables, the framework derives closed-form expressions for the probability density function (PDF), cumulative distribution function (CDF), and moment-generating function (MGF) of the end-to-end signal-to-interference-and-noise ratio (SINR). These expressions enable the computation of key performance metrics, such as outage probability and average error probability, which are critical for assessing the reliability and efficiency of dual-hop relay networks under interference-limited conditions. The analysis highlights the impact of CCI on system performance and provides insights into the design and optimization of dual-hop networks, ensuring robust communication in challenging environments.

In chapter 3, I extended the study to cooperative diversity in relay networks, employing numerical methods to explore the benefits of cooperative diversity in mitigating the effects of CCI in relay ad-hoc networks. By applying advanced statistical modeling techniques, the framework derives the statistical characteristics of the SINR, including its PDF, CDF, and MGF. These derivations facilitate the calculation of critical performance metrics, such as outage probability and average error probability, which are essential for evaluating the effectiveness of cooperative diversity in reducing the impact of CCI. The results demonstrate that cooperative diversity significantly enhances network performance by improving reliability and reducing error rates, providing valuable insights for the design and optimization of interference-resilient relay ad-hoc networks.

Chapter 4, I addressed the challenge of optimizing the trajectory of an unmanned aerial vehicle (UAV) carrying a next-generation NodeB (gNB) while managing resource allocation to ground users. To tackle this complex problem, I formulated it as a Markov Decision Process (MDP), a mathematical framework well-suited for sequential decision-making under uncertainty. By leveraging this MDP framework, I applied reinforcement learning techniques to enable the UAV to autonomously learn optimal policies for trajectory planning and resource allocation, ultimately enhancing network performance and user satisfaction in dynamic environments. This approach provides a robust foundation for addressing the interplay between mobility and resource management in UAV-assisted communication systems.

Chapter 2

Impact of Co-Channel Interference on Performance of Cooperative Wireless Ad-hoc Networks over $\alpha - \mu$ fading channels

2.1 Introduction

Cooperative communication systems play a major role in improving the network coverage and throughput of wireless communication systems. Where a relay node is introduced to the network to create independent paths between both the user and the base-station [38]. Among other relaying schemes which are used in cooperative communication, Amplify-and-Forward (AF) is considered to be the famous one due to its simplicity and low-cost implementation. Using amplify-and-forward relaying scheme, the relay node simply resend a scaled copy of the received noisy signal from the source to the destination node. Another technique for processing at the relay node is to decode the received signal from the source node, re-encode it and finally retransmit it to the receiver node, this relaying technique is termed as Decode-and-Forward (DF) relay scheme.

In light of the increase demand on the wireless communication services, finding a practical strategy to efficiently use the radio spectrum gave a rise to the so called Co-Channel Interference (CCI) due to the frequency reuse in the wireless networks. To enhance the spectrum efficiency, more investigations adopted to understand the limitations at the network performance. Motivated by that, some studies which are investigating the impact of CCI on the performance of amplify-and-forward dual-hop relay systems have been investigated in the literature. For example, [9] and [10] studied the impact of CCI on amplify-and-forward dual-hop relay network performance, assuming Rayleigh fading channels, while both [11] and [12] assumed the Nakagami-m fading channels. In [13], the authors' investigations assumed different fading channels for the interferes' where they considered Rayleigh, Nakagami-m, and Rician fading channels. The authors of [39] investigated the dual-hop relaying system presence of co-channel interference assuming decode-and-forward (DF) relaying scheme and Nakagami-m fading is adopted. Another work that investigated amplify-and-forward dual-hop

relay network performance is represented in [14], where α - μ fading channel is assumed and the performance investigation in terms of the ergodic capacity and ergodic outage probability, however, the interference presence is not considered in this research. Moreover, [15] and [17] derived the outage probability for both amplify-and-forward and decode-and-forward relaying techniques in dual-hop networks in α - μ environment, without considering the interference presence at any of the nodes. In addition, the work in [16] investigated dual-hop amplify-and-forward relay network performance in terms of end-to-end capacity and outage capacity, assuming α - μ environment subject to CCI interference.

Motivated by the preceding, I investigated the error and outage performance of the dual-hop amplify-and-forward relaying network over α - μ fading channels in the presence of CCI affecting both the relay and destination nodes. The α - μ fading channel is considered since it is the general fading model for small-scale fading, and it represents the multipath fading channel model, in which the received signal consists of clusters of multipath waves that propagate in a non-homogeneous environment [34]. The α parameter is used to represent the nonlinear behavior of the propagation medium, while the μ parameter represents the multipath-clusters number. The Nakagami-m and Rayleigh fading can be derived from the α - μ fading. In this chapter, the derived formulas are used to derive other fading channel models such as Rayleigh, Nakagami-m, Chi, and one sided Gaussian where the α value equals 2.

Moreover, I derived the probability density function (PDF) and the cumulative distribution function (CDF) of the signal-to-interference-and-noise ratio (SINR) of dual-hop transmission with amplify-and-forward relaying. The obtained results are used to derive an analytical expression of the error and outage probability for the considered system. The rest of the chapter is organized as follows; In Section 2.2, the

system model is introduced. Then in section 2.3, the SINR analysis is introduced. The system performance in terms of outage and average error probabilities are conducted and derived in section 2.4. Numerical results are presented and discussed in Section 2.5. Finally, conclusions are drawn in Section 2.6.

2.2 System Model

Consider a dual-hop wireless communication system is shown in figure (2.1), where the source node S communicates with a destination node D through a relay node R . The received signals at the relay node R and destination node D are corrupted by CCI signals from N and L co-channel interferer's denoted as $\{x_i\}_{i=1}^N$ for $i \in [1, N]$, with energy of E_i and $\{x_k\}_{k=1}^L$ for $k \in [1, L]$, with energy of E_k , respectively.

The fading coefficients for all links are assumed to be α - μ fading channel. AF relaying scheme is considered due to its simplicity compared to other relaying schemes, where the signal received by the relay node is amplified before being forwarded to the destination node, the amplification factor of AF scheme is proportional to the inverse gain of the channel. The destination node D is assumed to have perfect knowledge of the Channel State Information (CSI), with reference to [9, Eq.1] the received signal at the relay node R is given by

$$y_{sr} = \sqrt{E_S} h_{sr} d_S + \sum_{i=1}^N \sqrt{E_i} h_i d_i + n_{sr} \quad (2.1)$$

where h_{sr} is the α - μ channel flat fading coefficient of the $S \rightarrow R$ link, E_S is the energy of the transmitted signal, d_S is the desired data with unit energy, h_i is the α - μ channel flat fading coefficient of the i -th interfere $\rightarrow R$ link, E_i is the energy

of the i -th interferer at R and d_j is the i -th co-channel interferer's data with unit energy at the relay node. The additive-white-Gaussian-noise (AWGN) at the relay node is denoted as n_{sr} with a zero-mean and N_o variance $\sim CN(0, N_o)$. The signal

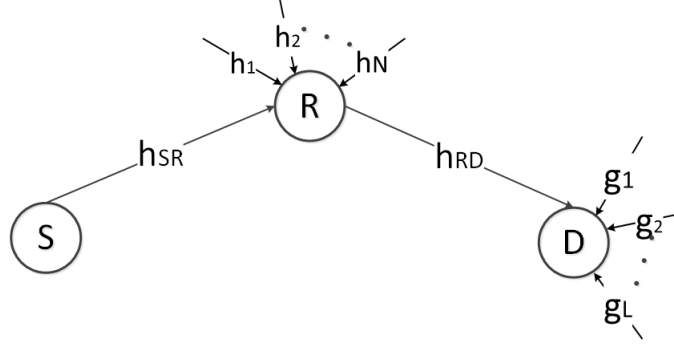


Figure 2.1: Dual-hop relay network with co-channel interference at the relay and destination nodes.

received at the destination node D from the relay node is expressed as

$$y_{rd} = \sqrt{E_R} h_{rd} y_R + \sum_{k=1}^L \sqrt{E_k} g_k d_k + n_{rd}, \quad (2.2)$$

where E_R represents the energy of the relay node transmitted signal, h_{rd} is the α - μ channel flat fading coefficient of the $R \rightarrow D$ link, E_k is the energy of the interference signal at the destination node, g_k is the α - μ flat fading coefficient of the interference channel at the destination, and d_k is the k -th co-channel interferer's data with unit energy at the destination, n_{rd} denotes the AWGN at the destination node with a zero-mean and N_o variance $\sim CN(0, N_o)$. Here $\sim CN(0, N_o)$ represents a complex Gaussian distribution short for "complex normal" with a mean of 0 and a variance of N_o . This is commonly used to model AWGN in communication systems, where the real and imaginary components are independent and identically distributed Gaussian random variables. And y_R is the relayed signal, which can be represented by

$$y_R = G_{AF} y_{sr}, \quad (2.3)$$

The AF gain factor (G_{AF}) is designed to normalized the output energy from the relay node denoted by E_R . The primary target of the relay node energy normalization is to mitigate noise amplification, as the gain factor will scale the signal and noise proportionally, balancing amplification and noise introduction. Additionally, the gain factor G_{AF} ensures the relay's output power does not exceed its maximum allowable transmit power P_R , complying with regulatory and hardware constraints. The gain factor with the presence of CCI is computed as

$$G_{AF} = \sqrt{\frac{E_R}{E_S|h_{sr}|^2 + \sum_{i=1}^N E_i|h_i|^2 + N_o}}, \quad (2.4)$$

After substituting 2.1 and 2.3 into 2.2 then with some algebraic simplifications, the received signal at the destination node D can be expressed as

$$y_{rd} = G_{AF}\sqrt{E_R}h_{rd}\left[\sqrt{E_S}h_{sr}d_S + \sum_{i=1}^N \sqrt{E_i}h_i d_i\right] + \sum_{k=1}^L \sqrt{E_k}g_k d_k + G_{AF}\sqrt{E_R}h_{rd}n_{sr} + n_{rd}. \quad (2.5)$$

Then, (2.5) can be divided into three parts, that is

The signal part:

$$\left\{ \frac{\sqrt{E_R}}{\sqrt{N_o + E_S|h_{sr}|^2 + \sum_{i=1}^N E_i|h_i|^2}} \times h_{rd} \sqrt{E_S} h_{sr} d_S \right\}, \quad (2.6)$$

the noise part:

$$\left\{ \frac{\sqrt{E_R}}{\sqrt{N_o + E_S|h_{sr}|^2 + \sum_{i=1}^N E_i|h_i|^2}} \times h_{rd} n_{sr} + n_{rd} \right\}, \quad (2.7)$$

and the interference part:

$$\left\{ \frac{\sqrt{E_R}}{\sqrt{N_o + E_S|h_{sr}|^2 + \sum_{i=1}^N E_i|h_i|^2}} \times \sum_{i=1}^N \sqrt{E_i}h_i d_i + \sum_{k=1}^L \sqrt{E_k}g_k d_k \right\}. \quad (2.8)$$

In the following subsections, the α - μ fading model will be introduced and the SINR statistical characteristics will be derived in terms of the PDF, CDF, and MGF.

2.2.1 $\alpha - \mu$ fading model

Propagation in the wireless channel is a complicated phenomenon that can affect and fluctuate the envelope and phase of the transmitted signal over time due to the time-varying nature of the wireless channel.

The $\alpha - \mu$ fading channel distribution is adopted in this chapter and is considered the general fading model used for the small-scale variation of the received signal. The α - μ fading channel is known as the multipath fading channel model, in which the received signal consists of multipath clustered waves that are propagating in a non-homogeneous environment [34].

The α - μ model is described by two parameters, (α) and (μ) . The parameter (α) represents the nonlinear behavior of the propagation medium, while the parameter μ represents the number of multipath clusters. The (α) - (μ) fading distribution can derive other distributions as special cases, such as the Nakagami-m and Rayleigh distributions. The α - μ fading model offers a flexible and comprehensive representation of the fading phenomena. It can capture a wide range of fading scenarios and is often compared with other fading models, such as the Rayleigh, Nakagami-m, and Rician models, to assess its accuracy and suitability for specific applications.

The probability density function $f_Z(z)$ of random variable Z which can be used to describe the envelope of the received signal. The $\alpha - \mu$ distributed density function is defined in [34], with parameters $\alpha > 0$, by

$$f_Z(z) = \frac{\alpha \mu^\mu z^{\alpha\mu-1}}{\Gamma(\mu) \hat{z}^{\alpha\mu}} \exp\left(-\mu \frac{z^\alpha}{\hat{z}^\alpha}\right), \quad (2.9)$$

where

- $\hat{z} = \sqrt[\alpha]{\mathbb{E}[Z^\alpha]}$ is the α root mean value,
- $\Gamma(x) = \int_0^\infty t^{x-1} e^{-t} dt$ is the Gamma function,
- $\mu = \frac{(\mathbb{E}[Z^\alpha])^2}{V[Z^\alpha]}$ is the normalized variance of Z^α .

Note that $\mathbb{E}[\cdot]$ and $V[\cdot]$ are the expectation and variance operators, respectively.

2.2.2 Signal-to-Noise Ratio (SNR)

Consider a communication system, where the modulated signal is transmitted over a mobile fading channel, the transmitted signal is given in [35, equation 13.1-1]:

$$s(t) = \text{Re} \{s_l(t) e^{j2\pi f_c t}\} \quad (2.10)$$

where

- $s_l(t)$ is the complex envelope of $s(t)$ with bandwidth B_u .
- f_c is the carrier frequency.
- $j = \sqrt{-1}$;

The received signal through a single path fading channel, that the the received faded signal is from the source node, in addition being corrupted by additive white Gaussian noise (AWGN) can be expressed as in [35, equation 13.1-9], in addition being corrupted by additive white Gaussian noise (AWGN) can be expressed as in [35, equation 13.3-1]

$$r(t) = h(t)e^{j\theta(t)} + n(t) \quad (2.11)$$

where

- $r(t)$ is the received equivalent lowpass signal in one signaling interval.
- $\theta(t) = -2\pi f_c \tau(t)$ is the phase of the received signal from the fading link.
- $h(t)$ is the amplitude of the received signal from the fading link.
- $n(t)$ is the complex envelope Gaussian noise with zero mean and power spectral density N_o .

Let $(\Xi_{|h|})$ be the instantaneous signal-to-noise ratio (SNR) per bit of a received signal as a function of h that represents the envelope (amplitude) of the received signal, with E_b/N_o being the average energy per bit to the noise power spectral density ratio. $(\Xi_{|h|})$ is defined by

$$\Xi_h = |h|^2 \frac{E_b}{N_o}, \quad (2.12)$$

In addition this implies:

- The fading power is $|h|^2$ (i.e., $\alpha = 2$ for the standard power-law relationship).
- For $\alpha = 2$, the α - μ model reduces to the generalized Gamma distribution, which includes Rayleigh ($\mu = 1$) and Nakagami- m ($\mu = m$) as special cases.

with the second moment ($n = 2$) can be derived from the the n -th moment of ($\Xi_{|h|}$), that is denoted by

$$\mathbb{E}[|h|^n] = \hat{r}^n \frac{\Gamma\left(\mu + \frac{n}{\alpha}\right)}{\mu^{n/\alpha} \Gamma(\mu)}, \quad (2.13)$$

setting $n = 2$

$$\mathbb{E}[|h|^2] = \hat{r}^2 \frac{\Gamma\left(\mu + \frac{2}{\alpha}\right)}{\mu^{2/\alpha} \Gamma(\mu)}. \quad (2.14)$$

the PDF can be derived using standard method transformation of R.V's that is developed in [40, chapter 5], the PDF of ($\Xi_{|h|}$) can be expressed as [40, equation 5-18] letting ($\Xi_{|h|} = g(|h|)$).

$$f_{\Xi_{|h|}}(\gamma) = f_{|h|}(g^{-1}(|h|)) \cdot \left| \frac{d}{d\Xi_{|h|}} g^{-1}(|h|) \right| = f_{|h|}(g^{-1}(|h|)) \cdot \left| \frac{1}{2} \sqrt{\frac{N_0}{E_s \Xi_{|h|}}} \right| \quad (2.15)$$

the PDF can be derived using standard method transformation of R.V's that is developed in [40, chapter 5], the PDF of ($\Xi_{|h|}$) can be expressed as

$$f_{\Xi_{|h|}}(\gamma) = \frac{\alpha \mu^\mu \gamma^{\alpha\mu/2-1}}{2\Gamma(\mu) \bar{\beta}_{\Xi_{|h|}}^{\alpha\mu/2}} \exp\left(-\mu \frac{\gamma^{\alpha/2}}{\bar{\beta}_{\Xi_{|h|}}^{\alpha/2}}\right), \quad (2.16)$$

where $\bar{\beta}_{\Xi_{|h|}} = \frac{\mu^{\frac{2}{\alpha}} \Gamma(\mu)}{\Gamma(\mu + \frac{2}{\alpha})} \mathbb{E}[\Xi_{|h|}]$ and $\mathbb{E}[\Xi_{|h|}] = \mathbb{E}\left[\frac{|h|^2 E_b}{N_0}\right] = \frac{E_b}{N_0} \mathbb{E}[|h|^2]$ represents the average SNR.

2.2.3 SNR Cumulative Distribution Function (CDF)

The Cumulative Distribution Function (CDF) is part of the characteristics properties of the SNR distribution. The CDF is defined as [40, equation 4.16]:

$$F_{\Xi_{|h|}}(\gamma) = \int_0^\gamma f_{\Xi_{|h|}}(t) dt. \quad (2.17)$$

Using the PDF of Ξ_Ψ and define the variable $u = \mu \frac{t^{\alpha/2}}{\beta_{\Xi|h}^{\alpha/2}}$ and $dt = \frac{2\bar{\beta}_{\Xi|h}}{\mu^{2/\alpha}} u^{\frac{2}{\alpha}-1} du$, the CDF can be expressed as

$$F_{\Xi|h}(\gamma) = \int_0^{\mu \frac{\gamma^{\alpha/2}}{\beta_{\Xi|h}^{\alpha/2}}} \frac{\alpha \mu^\mu}{2\Gamma(\mu) \bar{\beta}_{\Xi|h}^{\frac{\alpha\mu}{2}}} \left(\frac{\bar{\beta}_{\Xi|h} u^{\frac{2}{\alpha}}}{\mu^{\frac{2}{\alpha}}} \right)^{\frac{\alpha\mu}{2}-1} e^{-u} u^{\frac{2}{\alpha}-1} \left(\frac{2\bar{\beta}_{\Xi|h}}{\mu^{2/\alpha}} \right) du, \quad (2.18)$$

which can be expressed as

$$F_{\Xi|h}(\gamma) = \frac{1}{\Gamma(\mu)} \int_0^{\mu \frac{\gamma^{\alpha/2}}{\beta_{\Xi|h}^{\alpha/2}}} u^{\mu-1} e^{-u} du. \quad (2.19)$$

The integral in (2.19) can be solved with the help of the Lower Incomplete Gamma Function in [41, equation 8.2.1]; $\Gamma^*(a, z) = \int_0^z t^{a-1} e^{-t} dt$, the CDF of the SNR Ξ_Ψ then can be expressed as

$$F_{\Xi|h}(\gamma) = \frac{\Gamma^* \left(\mu, \mu \left(\frac{\gamma}{\beta_{\Xi|h}} \right)^{\frac{\alpha}{2}} \right)}{\Gamma(\mu)}. \quad (2.20)$$

2.2.4 SNR Moment Generating Function (MGF)

The moment generating function is one of the most appropriate and valuable factors of the distribution function it is suitable for calculating the channel capacity as well as the bit-error-rate performance measures of wireless communication systems. The MGF is defined mathematically as [42, equation 3.3-6] and [42, equation 3.3-7]:

$$M_{\Xi|h}(\gamma) = \mathbb{E}[e^{\Xi_\Psi \gamma}] = \int_0^\infty f_{\Xi|h}(x) e^{x\gamma} dx, \quad (2.21)$$

After mathematical manipulation the MGF of Ξ_Ψ is computed as

$$M_{\Xi|h}(\gamma) = \frac{\alpha \mu^\mu}{2\Gamma(\mu) \bar{\beta}_{\Xi|h}^{\frac{\alpha\mu}{2}}} \int_0^\infty x^{\frac{\alpha\mu}{2}-1} e^{-\mu \frac{x^{\alpha/2}}{\beta_{\Xi|h}^{\alpha/2}}} e^{x\gamma} dx \quad (2.22)$$

The Meijer G-Function of the exponential function is given as in [43, equation 8.4.3.1]:

$$e^{-x} = G_{0,1}^{1,0} \left(x \left| \begin{array}{c} - \\ 0 \end{array} \right. \right) \text{ for } \forall x. \quad (2.23)$$

Using (2.23), the MGF of X can be rewritten as

$$M_{\Xi_{|h|}}(\gamma) = \frac{\alpha\mu^\mu}{2\Gamma(\mu)\beta_{\Xi_{|h|}}^{\frac{\alpha\mu}{2}}} \int_0^\infty x^{\frac{\alpha\mu}{2}-1} e^{x\gamma} G_{0,1}^{1,0} \left(\frac{\mu}{\beta_{\Xi_{|h|}}^{\alpha/2}} x^{\alpha/2} \left| \begin{array}{c} - \\ 0 \end{array} \right. \right) dx. \quad (2.24)$$

The integral in (2.24) can be solved using [43, equation 2.24.3.1], after defining the parameters of: ($p = n = 0, q = m = 1, \mu = 1/2$ and $c^* = 1/2$) also a new fraction is to be defined as well $\frac{l}{k}$ such that ($\frac{l}{k} = \frac{\alpha}{2}$) with the ($\gcd(l, k) = 1$) (Great Common Divisor) by this the non integer values of α would be included in the calculations

$$M_{\Xi_{|h|}}(\gamma) = \frac{\alpha\mu^\mu}{2\Gamma(\mu)\beta_{\Xi_{|h|}}^{\frac{\alpha\mu}{2}}} \frac{k^{\frac{1}{2}} l^{\frac{\alpha\mu}{2}-\frac{1}{2}} \gamma^{-\frac{\alpha\mu}{2}}}{(2\pi)^{\frac{l+k-2}{2}}} G_{l,k}^{k,l} \left(\left(\frac{\mu}{\beta_{\Xi_{|h|}}^{\alpha/2}} \right)^k \frac{l^l}{\gamma^l k^k} \left| \begin{array}{c} \Delta(l, 1 - \frac{\alpha\mu}{2}) \\ \Delta(k, 0) \end{array} \right. \right), \quad (2.25)$$

where $\Delta(k, a) = \frac{a}{k}, \frac{a+1}{k}, \dots, \frac{a+k-1}{k}$ (series of numbers).

The MGF of the (α) - (μ) distribution derived in equation 2.25, can be used to derive the MGF of Rayleigh distribution with ($\alpha = 2$) and ($\mu = 1$), and it can be reduced to generate the MGF of the Nakagami-m distribution when ($\alpha = 2$) and ($\mu = m$).

2.3 Dual-hop SINR analysis

In this section, the expression of the signal-interference-and-noise-ratio (SINR) will be derived for the proposed dual-hop relay communication system. The signal-to-noise-ratio at the relay and destinations nodes are expressed as ($\gamma_{sr} = E_S|h_{sr}|^2/N_o$) and ($\gamma_{rd} = E_R|h_{rd}|^2/N_o$), respectively. The SINR at the destination

node D can be written as

$$\gamma_{srd} = \frac{E_S|h_{sr}|^2 E_R|h_{rd}|^2}{\left[G_{AF}^2 E_R|h_{rd}|^2 N_o + G_{AF}^2 E_R|h_{rd}|^2 \sum_{i=1}^N E_i|h_i|^2 + N_o \sum_{k=1}^L E_k|g_k|^2 \right]} \times \frac{1}{\left[N_o + \sum_{i=1}^N E_i|h_i|^2 E_S|h_{sr}|^2 \right]}. \quad (2.26)$$

2.3.1 Co-Channel Interference probability density function (PDF)

Co-channel interference (CCI) occurs when a frequency band is used by multiple users at the same time. For cellular networks CCI occurs by the reuse of frequency in the neighboring cells, which accordingly will affect the performance of the network. CCI may degrade the performance of the system, hence studying its impact is very important and helps in developing mitigation techniques to reduce the performance degradation. In this section the derivation of the formulas will be based under the assumption of CCI that can be modeled as the sum of N independent-identically-distributed (I.I.D) α - μ variates, (i.e., $\sum_{i=1}^N \gamma_{h_i}$). The SNR for a single i -th interferer link can be expressed as

$$\gamma_{h_i} = \frac{E_i|h_i|^2}{N_o}, \quad i = 1, \dots, N. \quad (2.27)$$

The PDF for each single i -th interferer link SNR (γ_{h_i}) is represented by

$$f_{\gamma_{h_i}}(\gamma_i) = \frac{\alpha_i \mu_i^{\mu_i} \gamma_i^{\alpha_i \mu_i / 2 - 1}}{2\Gamma(\mu_i) \beta_i^{\alpha_i \mu_i / 2}} \exp\left(-\mu_i \frac{\gamma_i^{\alpha_i / 2}}{\beta_i^{\alpha_i / 2}}\right), \quad i = 1, \dots, N, \quad (2.28)$$

The joint PDF of $\left(\sum_{i=1}^N \gamma_{h_i}\right)$ is derived by the aid of the moment generating function approach, which is mathematically expressed as

$$f_{\sum_{i=1}^N \gamma_{h_i}}(\gamma) = \mathcal{L}^{-1} \left\{ \prod_{i=1}^N M_{\gamma_{h_i}}(s) \right\}, \quad (2.29)$$

The Laplace transformation is defined as

$$M_{\gamma_{h_i}}(s) = \mathbb{E} [e^{-s\gamma_i}] = \int_0^{\infty} f_{\gamma_{h_i}}(\gamma_i) e^{-s\gamma_i} d\gamma_i. \quad (2.30)$$

The α - μ PDF form represented in equation (2.28) which can then substituted in equation (2.30). The next step is to use and introduce the Meijer G-Function of the exponential function which is given as in [43, equation 8.4.3.1]. Finally, the resulting integral can be solved using [43, equation 2.24.3.1], by setting the parameters: ($p = n = 0, q = m = 1, \mu = 1/2$ and $c^* = 1/2$) also a new fraction is to be defined as well $\frac{l}{k}$ such that $\left(\frac{l}{k} = \frac{a}{2}\right)$ with the $(gcd(l, k) = 1)$, gcd is the Great Common Divisor, by this the non integer values of α would be included in the calculations. The Laplace transformation is formulated as

$$\mathcal{L}_{\gamma_{h_i}}(s) = \frac{\alpha_i \mu_i^{\mu_i}}{2\Gamma(\mu_i) \beta_i^{\frac{\alpha_i \mu_i}{2}}} \frac{k^{\frac{1}{2}} l^{\frac{\alpha_i \mu_i}{2} - \frac{1}{2}} s^{-\frac{\alpha_i \mu_i}{2}}}{(2\pi)^{\frac{l+k-2}{2}}} G_{l,k}^{k,l} \left(\left(\frac{\mu_i}{\beta_i^{\alpha_i/2}} \right)^k \frac{l^l}{s^l k^k} \left| \begin{array}{c} \Delta(l, 1 - \frac{\alpha_i \mu_i}{2}) \\ \Delta(k, 0) \end{array} \right. \right), \quad (2.31)$$

where $\Delta(k, a) = \frac{a}{k}, \frac{a+1}{k}, \dots, \frac{a+k-1}{k}$, and the Meijer G-function is defined generally in [44, equation 07.34.02.0001.01].

The density function of $\left(\sum_{i=1}^N \gamma_{h_i}\right)$ can then be derived and is represented mathematically by

$$f_{\sum_{i=1}^N \gamma_{h_i}}(\gamma_i) = \mathcal{L}^{-1} \left\{ \prod_{i=1}^N \mathcal{L}_{\gamma_{h_i}}(s) \right\} (\gamma_i)$$

$$= \mathcal{L}^{-1} \left\{ \prod_{i=1}^N \frac{\alpha_i \mu_i^{\mu_i}}{2\Gamma(\mu_i) \bar{\beta}_i^{\frac{\alpha_i \mu_i}{2}}} \frac{k^{\frac{1}{2}} l^{\frac{\alpha_i \mu_i}{2} - \frac{1}{2}} s^{-\frac{\alpha_i \mu_i}{2}}}{(2\pi)^{\frac{l+k-2}{2}}} G_{l,k}^{k,l} \left(\left(\frac{\mu_i}{\bar{\beta}_i^{\alpha_i/2}} \right)^k \frac{l^l}{s^l k^k} \middle| \begin{array}{c} \Delta(l, 1 - \frac{\alpha_i \mu_i}{2}) \\ \Delta(k, 0) \end{array} \right) \right\} (\gamma_i), \quad (2.32)$$

where $M_{\gamma_{h_i}}(s)$ represents the Laplace transformation of the i -th link SNR which is expressed in (2.31), and $\mathcal{L}^{-1}\{\cdot\}$ is the inverse Laplace transformation. In the case of N-number of I.I.D interferers, we have $\gamma_i = \gamma$, $\alpha = \alpha_i$, $\mu = \mu_i$, and $\bar{\beta}_I = \bar{\beta}_i$ (which represents the average SNR for the i -th interfere link at the relay node), for $i = 1, \dots, N$. As a consequence, the PDF of the sum of N-number of I.I.D interferers is then can be evaluated as

$$f_{\sum_{i=1}^N \gamma_{h_i}}(\gamma) = \mathcal{L}^{-1} \left\{ \left(\frac{\alpha \mu^\mu}{2\Gamma(\mu) \bar{\beta}_I^{\frac{\alpha \mu}{2}}} \frac{k^{\frac{1}{2}} l^{\frac{\alpha \mu}{2} - \frac{1}{2}} s^{-\frac{\alpha \mu}{2}}}{(2\pi)^{\frac{l+k-2}{2}}} G_{l,k}^{k,l} \left(\left(\frac{\mu}{\bar{\beta}_I^{\alpha/2}} \right)^k \frac{l^l}{s^l k^k} \middle| \begin{array}{c} \Delta(l, 1 - \frac{\alpha \mu}{2}) \\ \Delta(k, 0) \end{array} \right) \right)^N \right\} (\gamma). \quad (2.33)$$

Equation (2.33) is not analytically tractable. However, under some conditions, for example when ($l = k = 1$), this results in ($\alpha = 2$), and then the density function can be analytically expressed as

$$f_{\sum_{i=1}^N \gamma_{h_i}}(\gamma) = \mathcal{L}^{-1} \left\{ \left(\frac{\mu^\mu s^{-\mu}}{\Gamma(\mu) \bar{\beta}_I^\mu} G_{1,1}^{1,1} \left(\frac{\mu}{s \bar{\beta}_I} \middle| \begin{array}{c} 1 - \mu \\ 0 \end{array} \right) \right)^N \right\} (\gamma). \quad (2.34)$$

Using the Meijer G-function expression given by [44, equation 07.34.03.0271.01], and expressed as

$$G_{1,1}^{s1,1} \left(z \middle| \begin{array}{c} a \\ b \end{array} \right) = z^b (z+1)^{a-b-1} \Gamma(1-a+b) \quad (2.35)$$

then substitute equation (2.35) into equation (2.34) will generate

$$f_{\sum_{i=1}^N \gamma_{h_i}}(\gamma) = \mathcal{L}^{-1} \left\{ \left(\frac{\mu^\mu}{\Gamma(\mu)\overline{\beta}_I^\mu} s^{-\mu} \left(\frac{\mu}{s\overline{\beta}_I} + 1 \right)^{-\mu} \Gamma(\mu) \right)^N \right\}, \quad (2.36)$$

finally after some mathematical manipulation, evaluating the inverse Laplace transform (\mathcal{L}^{-1}), the PDF of $\left(\sum_{i=1}^N \gamma_{h_i}\right)$ can be expressed as

$$f_{\sum_{i=1}^N \gamma_{h_i}}(\gamma) = \left(\frac{\mu}{\overline{\beta}_I}\right)^{N\mu} \frac{\gamma^{N\mu-1}}{\Gamma(N\mu)} e^{-\frac{\mu\gamma}{\overline{\beta}_I}}. \quad (2.37)$$

For special cases, equation (2.37) can be reduced to generate different CCI models such as Rayleigh and Nakagami-m. For N-number of I.I.D Rayleigh interferers ($\alpha = 2, \mu = 1$) the PDF of $\sum_{i=1}^N \gamma_{h_i}$ can be expressed as

$$f_{\sum_{i=1}^N \gamma_{h_i}}(\gamma) = \frac{\gamma^{N-1}}{\Gamma(N)\overline{\beta}_I^N} e^{-\frac{\gamma}{\overline{\beta}_I}}. \quad (2.38)$$

this is the same as [9, equation 14], for N-number of I.I.D Nakagami-m Interference, the PDF of $\sum_{i=1}^N \gamma_{h_i}$ which can be reduced from (2.37) and identical to [45, equation 9] with setting ($\alpha = 2, \mu_i = \mu = m$)

$$f_{\sum_{k=1}^N \gamma_{h_i}}(\gamma) = \left(\frac{m}{\overline{\beta}_I}\right)^{Nm} \frac{\gamma^{Nm-1}}{\Gamma(Nm)} e^{-\frac{m\gamma}{\overline{\beta}_I}}. \quad (2.39)$$

where $\Gamma(k)$ is the Complete Gamma function which is given by ($\Gamma(k) = \int_0^\infty t^{k-1} e^{-t} dt$) and can be expressed in terms of factorial operation as $(k-1)!$ for $k = N$ or $k = Nm$.

2.3.2 Effective SINR statistical characteristics

The interference affecting the destination node are denoted as $\gamma_{g_k} = E_k |g_k|^2 / N_o$ for $k = 1, 2, \dots, L$. Let $\gamma_{sr}^{eff} = \gamma_{sr} / \left(1 + \sum_{i=1}^N \gamma_{h_i}\right)$, with $f_{\gamma_{sr}}$ is the PDF of the source-relay SNR and $f_{\sum_{i=1}^N \gamma_{h_i}}$ is the PDF of the sum of N-number I.I.D channel

gains. In addition; $\gamma_{rd}^{eff} = \gamma_{rd} / \left(1 + \sum_{k=1}^L \gamma_{gk}\right)$, with $f_{\gamma_{rd}}$ is the PDF of the relay-destination SNR and $f_{\sum_{k=1}^L \gamma_{gk}}$. Both of γ_{sr}^{eff} and γ_{rd}^{eff} represent the effective SINRs at the relay and the destination node, respectively.

As a consequence, eq. (2.26) can be expressed as

$$\gamma_{srd} = \frac{\gamma_{sr}^{eff} \gamma_{rd}^{eff}}{\gamma_{sr}^{eff} + \gamma_{rd}^{eff} + 1}. \quad (2.40)$$

In this section, I will derive the statistical characteristics of the effective SINR γ_{sr}^{eff} and γ_{rd}^{eff} of the links $S \rightarrow R$ and $R \rightarrow D$, respectively, in terms of the PDF and the CDF when both links are subject to α - μ fading channel. The PDF of γ_{sr}^{eff} can be derived using [40, equation 6-60] while the equality holds through the substitution $z = y + 1$ which is $z = 1 + \sum_{i=1}^N \gamma_{h_i}$, the PDF can be expressed as

$$f_{\gamma_{sr}^{eff}}(\gamma) = \int_0^\infty y f_{\gamma_{sr}}(y\gamma) f_{1+\sum_{i=1}^N \gamma_{h_i}}(y) dy = \int_0^\infty (y+1) f_{\gamma_{sr}}((y+1)\gamma) f_{\sum_{i=1}^N \gamma_{h_i}}(y) dy, \quad (2.41)$$

Using eq. (2.32) we obtain

$$\begin{aligned} f_{\gamma_{sr}^{eff}}(\gamma) &= \int_0^\infty (y+1) \frac{\alpha_{sr} \mu_{sr}^{\mu_{sr}} ((y+1)\gamma)^{\frac{\alpha_{sr} \mu_{sr}}{2} - 1}}{2\Gamma(\mu_{sr}) d_{\mu_{sr}}^{\frac{\alpha_{sr} \mu_{sr}}{2}} \bar{\beta}_{sr}^{\frac{\alpha_{sr} \mu_{sr}}{2}}} \exp\left(-\mu_{sr} \frac{((y+1)\gamma)^{\alpha_{sr}/2}}{d_{\mu_{sr}}^{\alpha_{sr}/2} \bar{\beta}_{sr}^{\alpha_{sr}/2}}\right) \\ &\quad \left[\mathcal{L}^{-1} \left\{ \prod_{i=1}^N \frac{\alpha_i \mu_i^{\mu_i}}{2\Gamma(\mu_i) d_{\mu_i}^{\frac{\alpha_i \mu_i}{2}} \bar{\beta}_i^{\frac{\alpha_i \mu_i}{2}}} \frac{k_i^{\frac{1}{2}} l_i^{\frac{\alpha_i \mu_i}{2} - \frac{1}{2}} s^{-\frac{\alpha_i \mu_i}{2}}}{(2\pi)^{\frac{l_i + k_i - 2}{2}}} \right. \right. \\ &\quad \left. \left. G_{l_i, k_i}^{k_i, l_i} \left(\left(\frac{\mu_i}{d_{\mu_i}^{\alpha_i/2} \bar{\beta}_i^{\alpha_i/2}} \right)^{k_i} \frac{l_i^{l_i}}{s^{l_i} k_i^{k_i}} \left| \begin{array}{c} \Delta(l_i, 1 - \frac{\alpha_i \mu_i}{2}) \\ \Delta(k_i, 0) \end{array} \right. \right) \right\} \right]_{\gamma_{h_i}=y} dy, \end{aligned} \quad (2.42)$$

Under some conditions where $l_i = k_i = 1$, $\alpha_{sr} = \alpha_{rd} = \alpha_i = 2$ and $\mu_i = \mu_I$ and $\bar{\beta}_i = \bar{\beta}_I$ since the interferes links at the relay node assumed to be I.I.D links and all

the parameters are identical for each interfere link, the PDF is reduced to

$$f_{\gamma_{sr}^{eff}}(\gamma) = \frac{\mu_{sr}^{\mu_{sr}}(\gamma)^{\mu_{sr}-1}}{\Gamma(\mu_{sr})\bar{\beta}_{sr}^{\mu_{sr}}\Gamma(N\mu_I)} \left(\frac{\mu_I}{\beta_I}\right)^{N\mu_I} \int_0^\infty (y+1)^{\mu_{sr}} e^{-\frac{\mu_{sr}(\gamma)}{\beta_{sr}}(y+1)} e^{-y\left(\frac{\mu_I}{\beta_I}\right)} y^{\mu_I N-1} dy, \quad (2.43)$$

after mathematical manipulation, the PDF of γ_{sr}^{eff} can then be expressed:

$$f_{\gamma_{sr}^{eff}}(\gamma) = \frac{\mu_{sr}^{\mu_{sr}}(\gamma)^{\mu_{sr}-1} \left(\mu_I^{\mu_I} \bar{\beta}_I^{-\mu_I}\right)^N e^{\left(\frac{\mu_I}{\beta_I}\right)}}{\Gamma(\mu_{sr})\bar{\beta}_{sr}^{\mu_{sr}}\Gamma(N\mu_I)} \int_1^\infty u^{\mu_{sr}} (u-1)^{\mu_I N-1} e^{-u\left(\frac{\mu_{sr}(\gamma)}{\beta_{sr}} + \frac{\mu_I}{\beta_I}\right)} du, \quad (2.44)$$

then using [46, equation 3.383.4], the effective SINR can be evaluated as

$$f_{\gamma_{sr}^{eff}}(\gamma) = \frac{\mu_{sr}^{\mu_{sr}} \left(\mu_I^{\mu_I} \bar{\beta}_I^{-\mu_I}\right)^N e^{\left(\frac{\mu_I}{\beta_I}\right)}}{\Gamma(\mu_{sr})\bar{\beta}_{sr}^{\mu_{sr}}} \left(\frac{\mu_{sr}}{\beta_{sr}}\gamma + \frac{\mu_I}{\beta_I}\right)^{-\frac{\mu_I N + \mu_{sr} + 1}{2}} \gamma^{\mu_{sr}-1} e^{-\left(\frac{\mu_{sr}}{2\beta_{sr}}\gamma + \frac{\mu_I}{2\beta_I}\right)} W_{\frac{\mu_{sr}-\mu_I N+1}{2}, \frac{-\mu_I N - \mu_{sr}}{2}} \left(\frac{\mu_{sr}}{\beta_{sr}}\gamma + \frac{\mu_I}{\beta_I}\right), \quad (2.45)$$

for $\text{Re}(\mu_I N) > 0 \wedge \text{Re}\left(\frac{\mu_I}{\beta_I} + \frac{\gamma\mu_{sr}}{\beta_{sr}}\right) > 0 \wedge \text{Re}(\mu_I) \in \mathbb{Z}$. and the function $W_{v,\mu}(z)$ is the Whittaker Function which is defined in [44, equation 07.45.02.0001.01].

Since the PDF of γ_{sr}^{eff} is assumed to be identical for both the SR and the RD links, with $l_i = k_i = 1$, $\alpha_{sr} = \alpha_{rd} = \alpha_k = 2$ and $\mu_k = \mu_K$ and $\bar{\beta}_k = \bar{\beta}_K$ since the interferes links at the relay node assumed to be I.I.D links, the effective SINR for RD link $\gamma_{rd}^{eff}(\gamma)$ can be evaluated as

$$f_{\gamma_{rd}^{eff}}(\gamma) = \frac{\mu_{rd}^{\mu_{rd}} \left(\mu_K^{\mu_K} \bar{\beta}_K^{-\mu_K}\right)^L e^{\left(\frac{\mu_K}{\beta_K}\right)}}{\Gamma(\mu_{rd})\bar{\beta}_{rd}^{\mu_{rd}}} \left(\frac{\mu_{rd}}{\beta_{rd}}\gamma + \frac{\mu_K}{\beta_K}\right)^{-\frac{\mu_K L + \mu_{rd} + 1}{2}} \gamma^{\mu_{rd}-1} e^{-\left(\frac{\mu_{rd}}{2\beta_{rd}}\gamma + \frac{\mu_K}{2\beta_K}\right)} W_{\frac{\mu_{rd}-\mu_K L+1}{2}, \frac{-\mu_K L - \mu_{rd}}{2}} \left(\frac{\mu_{rd}}{\beta_{rd}}\gamma + \frac{\mu_K}{\beta_K}\right), \quad (2.46)$$

for $\text{Re}(\mu_K L) > 0 \wedge \text{Re}\left(\frac{\mu_K}{\beta_K} + \frac{\gamma\mu_{rd}}{\beta_{rd}}\right) > 0 \wedge \text{Re}(\mu_K) \in \mathbb{Z}$.

Special cases for different values of μ_{sr} :

A. For ($\mu_{sr} = 1$), the PDF of γ_{sr}^{eff} can be evaluated as

$$f_{\gamma_{sr}^{eff}}(\gamma) = \exp\left(-\frac{\gamma}{\beta_{sr}}\right) \left[\frac{N\Lambda^N}{(\gamma + \Lambda)^{N+1}} + \frac{1}{\beta_{sr}} \left(\frac{\Lambda}{\gamma + \Lambda}\right)^N \right] , \quad (2.47)$$

where ($\Lambda = \frac{\beta_{sr}}{\beta_I}$), is the average Signal to Interference Ratio (SIR) at the Relay node. (2.47) is identical to [9, equation 16], and this result is identical to [9, equation 18] when ($\mu_{sr} = \mu_{rd}$).

B. For ($\mu_{sr} = m_{sr}$) and ($\mu_I = m_I$) the PDF of γ_{sr}^{eff} can be written as

$$f_{\gamma_{sr}^{eff}}(\gamma) = \frac{1}{\Gamma(m_{sr})} \gamma^{m_{sr}-1} \left(\frac{m_{sr}}{\beta_{sr}}\right)^{m_{sr}} \left(\frac{m_I}{\beta_I}\right)^l \exp\left(-\frac{\gamma m_{sr}}{\beta_{sr}}\right) \sum_{m=0}^{m_{sr}} \binom{m_{sr}}{m} (lm_I)_m \left(\frac{m_I}{\beta_I} + \frac{m_{sr}\gamma}{\beta_{sr}}\right)^{-lm_I-m} , \quad (2.48)$$

which is identical to [45, equation 10].

Cumulative Distribution Function ($F_{\gamma_{sr}^{eff}}(\gamma)$) is defined as the probability in which the random variable (γ_{sr}^{eff}) takes a value less than or equal to (γ), which is expressed as

$$F_{\gamma_{sr}^{eff}}(\gamma) = Pr \{ \gamma_{sr}^{eff} \leq \gamma \} . \quad (2.49)$$

CDF can be mathematically presented by

$$F_{\gamma_{sr}^{eff}}(\gamma) = \int_0^\gamma f_{\gamma_{sr}^{eff}}(t) dt , \quad (2.50)$$

substituting (2.45) in (2.50), the CDF of the SR link can be expressed as

$$F_{\gamma_{sr}^{eff}}(\gamma) = \int_0^\gamma \frac{\mu_{sr}^{\mu_{sr}}}{\Gamma(\mu_{sr}) \beta_{sr}^{\mu_{sr}}} e^{\left(\frac{\mu_I}{\beta_I}\right)} \left(\frac{\mu_I}{\beta_I}\right)^{N\mu_I} \left(\frac{\mu_{sr}}{\beta_{sr}} t + \frac{\mu_I}{\beta_I}\right)^{-\frac{\mu_I N + \mu_{sr} + 1}{2}} t^{\mu_{sr}-1} e^{-\left(\frac{\mu_{sr}}{2\beta_{sr}} t + \frac{\mu_I}{2\beta_I}\right)} W_{\frac{\mu_{sr}-\mu_I N+1}{2}, \frac{-\mu_I N - \mu_{sr}}{2}} \left(\frac{\mu_{sr}}{\beta_{sr}} t + \frac{\mu_I}{\beta_I}\right) dt , \quad (2.51)$$

by using [40, equation 4.6] and [40, equation 4.6], the CDF can then be written after mathematical manipulation as

$$F_{\gamma_{sr}^{eff}}(\gamma) = 1 - \frac{1}{\Gamma(\mu_{sr})} e^{\left(\frac{\mu_I}{\beta_I}\right)} \left(\frac{\mu_I}{\beta_I}\right)^{N\mu_I} \sum_{v=0}^{\mu_{sr}-1} \left(\frac{\mu_{sr}}{\beta_{sr}}\gamma\right)^v \int_{\frac{\mu_{sr}}{\beta_{sr}}\gamma + \frac{\mu_I}{\beta_I}}^{\infty} (z)^{\frac{-\mu_I N - \mu_{sr} + 1}{2}} \left(z - \left(\frac{\mu_I}{\beta_I} + \frac{\mu_{sr}}{\beta_{sr}}\gamma\right)\right)^{\mu_{sr}-v-1} e^{-\left(\frac{z}{2}\right)} W_{\frac{\mu_{sr}-\mu_I N+1}{2}, \frac{-\mu_I N - \mu_{sr}}{2}}(z) dz, \quad (2.52)$$

applying [43, equation 2.19.5.12], therefore the CDF of γ_{sr}^{eff} can be evaluated as

$$F_{\gamma_{sr}^{eff}}(\gamma) = 1 - \frac{1}{\Gamma(\mu_{sr})} e^{\left(\frac{\mu_I}{\beta_I}\right)} \left(\frac{\mu_I}{\beta_I}\right)^{N\mu_I} \sum_{v=0}^{\mu_{sr}-1} \left(\frac{\mu_{sr}}{\beta_{sr}}\gamma\right)^v \Gamma(\mu_{sr} - v) e^{-\frac{1}{2}\left(\frac{\mu_I}{\beta_I} + \frac{\mu_{sr}}{\beta_{sr}}\gamma\right)} \left(\frac{\mu_I}{\beta_I} + \frac{\mu_{sr}}{\beta_{sr}}\gamma\right)^{\frac{-\mu_I N - v - 1}{2}} W_{-\frac{\mu_I N + v + 1}{2}, \frac{-\mu_I N - v}{2}}\left(\frac{\mu_I}{\beta_I} + \frac{\mu_{sr}}{\beta_{sr}}\gamma\right). \quad (2.53)$$

Hence; the CDF of the RD link γ_{rd}^{eff} is evaluated as

$$F_{\gamma_{rd}^{eff}}(\gamma) = 1 - \frac{1}{\Gamma(\mu_{rd})} e^{\left(\frac{\mu_k}{\beta_k}\right)} \left(\frac{\mu_k}{\beta_k}\right)^{L\mu_k} \sum_{v=0}^{\mu_{rd}-1} \left(\frac{\mu_{rd}}{\beta_{rd}}\gamma\right)^v \Gamma(\mu_{rd} - v) e^{-\frac{1}{2}\left(\frac{\mu_K}{\beta_K} + \frac{\mu_{rd}}{\beta_{rd}}\gamma\right)} \left(\frac{\mu_K}{\beta_K} + \frac{\mu_{rd}}{\beta_{rd}}\gamma\right)^{\frac{-\mu_K L - v - 1}{2}} W_{-\frac{\mu_K L + v + 1}{2}, \frac{-\mu_K L - v}{2}}\left(\frac{\mu_K}{\beta_K} + \frac{\mu_{rd}}{\beta_{rd}}\gamma\right). \quad (2.54)$$

This result can be reduced to special cases, such as

A. For $(\mu_{sr} = 1)$ and $(\mu_I = 1)$, the CDF of γ_{sr}^{eff} is evaluated as

$$F_{\gamma_{sr}^{eff}}(\gamma) = 1 - e^{-\frac{\gamma}{\beta_{sr}}} \left[\frac{\Lambda}{\gamma + \Lambda} \right]^N. \quad (2.55)$$

This result is identical to [9, equation 17], where $(\Lambda = \frac{\bar{\beta}_{sr}}{\beta_I})$, is the average SIR at the Relay node. Since the RD is identical to the SR link, [9, equation 19] can be evaluated by setting $(\mu_{rd} = 1)$ and $(\mu_K = 1)$ in (2.55)

B. For $(\mu_{sr} = m_{sr})$ and $\mu_I = m_I$, the CDF of γ_{sr}^{eff} can be evaluated as

$$F_{\gamma_{sr}^{eff}}(\gamma) = 1 - \frac{1}{\Gamma(m_{sr})} e^{\left(\frac{m_I}{\beta_I}\right)} \left(\frac{m_I}{\beta_I}\right)^{N m_I} \sum_{v=0}^{m_{sr}-1} \left(\frac{m_{sr}}{\beta_{sr}} \gamma\right)^v \Gamma(m_{sr} - v) e^{-\frac{1}{2} \left(\frac{m_I}{\beta_I} + \frac{m_{sr}}{\beta_{sr}} \gamma\right)} \left(\frac{m_I}{\beta_I} + \frac{m_{sr}}{\beta_{sr}} \gamma\right)^{\frac{-m_I N - v - 1}{2}} W_{\frac{-m_I N + v + 1}{2}, \frac{-m_I N - v}{2}} \left(\frac{m_I}{\beta_I} + \frac{m_{rd}}{\beta_{sr}} \gamma\right). \quad (2.56)$$

(2.56) can be used to express the CDF of the γ_{sr}^{eff} by setting $(\mu_{sr} = m_{sr})$

2.3.3 Dual-Hop Relay SINR PDF

To derive the SINR for the relay link in (2.40), I have used a tight upper bound to simplify the analysis of the network performance, i.e.,

$$\gamma_{srd} \leq \gamma_{up} = \min \left(\gamma_{sr}^{eff}, \gamma_{rd}^{eff} \right), \quad (2.57)$$

hence, $f_{\gamma_{up}}(\gamma)$ can be expressed as

$$f_{\gamma_{up}}(\gamma) = f_{\gamma_{sr}^{eff}}(\gamma) \left[1 - F_{\gamma_{rd}^{eff}}(\gamma) \right] + f_{\gamma_{rd}^{eff}}(\gamma) \left[1 - F_{\gamma_{sr}^{eff}}(\gamma) \right], \quad (2.58)$$

after substituting equations: (2.53), (2.45), (2.54) and (2.46), which represent the SR link CDF and PDF, and the RD link CDF and PDF, then the PDF of γ_{up} can be expressed after mathematical manipulation as

$$f_{\gamma_{up}}(\gamma) = \frac{\mu_{sr}^{\mu_{sr}} e^{\left(\frac{\mu_I}{\beta_I} + \frac{\mu_K}{\beta_k}\right)}}{\Gamma(\mu_{sr}) \Gamma(\mu_{rd}) \beta_{sr}^{\mu_{sr}}} \gamma^{\mu_{sr}-1} \left(\frac{\mu_I}{\beta_I}\right)^{N \mu_I} \left(\frac{\mu_K}{\beta_k}\right)^L \left(\frac{\mu_{sr}}{\beta_{sr}} \gamma + \frac{\mu_I}{\beta_I}\right)^{-\frac{\mu_I N + \mu_{sr} + 1}{2}} e^{-\left(\frac{\mu_{sr}}{2\beta_{sr}} \gamma + \frac{\mu_I}{2\beta_I}\right)} e^{-\left(\frac{\mu_{rd}}{2\beta_{rd}} \gamma + \frac{\mu_K}{2\beta_k}\right)} W_{\frac{\mu_{sr} - \mu_I N + 1}{2}, \frac{-\mu_I N - \mu_{sr}}{2}} \left(\frac{\mu_{sr}}{\beta_{sr}} \gamma + \frac{\mu_I}{\beta_I}\right)^{\mu_{rd}-1} \sum_{j=0}^{\mu_{rd}-1} \left(\frac{\mu_{rd}}{\beta_{rd}} \gamma\right)^j \Gamma(\mu_{rd} - j) \left(\frac{\mu_{rd}}{\beta_{rd}} \gamma + \frac{\mu_K}{\beta_k}\right)^{\frac{-\mu_K L - j - 1}{2}} W_{\frac{-\mu_K L + j + 1}{2}, \frac{-\mu_K L - j}{2}} \left(\frac{\mu_{rd}}{\beta_{rd}} \gamma + \frac{\mu_K}{\beta_k}\right)$$

$$\begin{aligned}
& + \frac{\mu_{rd}^{\mu_{rd}} e^{\left(\frac{\mu_K + \mu_I}{\bar{\beta}_k + \bar{\beta}_I}\right)}}{\Gamma(\mu_{rd}) \Gamma(\mu_{sr}) \bar{\beta}_{rd}^{\mu_{rd}}} \gamma^{\mu_{rd}-1} \left(\frac{\mu_K}{\bar{\beta}_k}\right)^{L\mu_K} \left(\frac{\mu_I}{\bar{\beta}_I}\right)^{N\mu_I} \left(\frac{\mu_{rd}}{\bar{\beta}_{rd}} \gamma + \frac{\mu_K}{\bar{\beta}_k}\right)^{-\frac{\mu_K L + \mu_{rd} + 1}{2}} \\
& e^{-\left(\frac{\mu_{rd}}{2\bar{\beta}_{rd}} \gamma + \frac{\mu_K}{2\bar{\beta}_k}\right)} e^{-\left(\frac{\mu_{sr}}{2\bar{\beta}_{sr}} \gamma + \frac{\mu_I}{2\bar{\beta}_I}\right)} W_{\frac{\mu_{rd} - \mu_K L + 1}{2}, \frac{-\mu_K L - \mu_{rd}}{2}} \left(\frac{\mu_{rd}}{\bar{\beta}_{rd}} \gamma + \frac{\mu_K}{\bar{\beta}_k}\right)^{\mu_{sr}-1} \sum_{v=0}^{\mu_{sr}-1} \left(\frac{\mu_{sr}}{\bar{\beta}_{sr}} \gamma\right)^v \\
& \Gamma(\mu_{sr} - v) \left(\frac{\mu_{sr}}{\bar{\beta}_{sr}} \gamma + \frac{\mu_I}{\bar{\beta}_I}\right)^{-\frac{-\mu_I N - v - 1}{2}} W_{\frac{-\mu_I N + v + 1}{2}, \frac{-\mu_I N - v}{2}} \left(\frac{\mu_{sr}}{\bar{\beta}_{sr}} \gamma + \frac{\mu_I}{\bar{\beta}_I}\right) \quad , \quad (2.59)
\end{aligned}$$

Assuming identical number of fading links $N = L = M$ with identical coefficients $\mu_I = \mu_I$, $\mu_{sr} = \mu_{rd} = \mu$, and the average SNRs are identical for all links as $\bar{\beta}_i = \bar{\beta}_k = \bar{\beta}_I$, and $\bar{\beta}_{rd} = \bar{\beta}_{sr} = \bar{\beta}$, the CDF of the Dual-Hop Relay network which represented by (2.59) can be reduced to

$$\begin{aligned}
f_{\gamma_{up}}(\gamma) &= \frac{2\gamma^{\mu-1}}{\Gamma(\mu)^2} \left(\frac{\mu}{\bar{\beta}}\right)^{\mu} \left(\frac{\mu_I}{\bar{\beta}_I}\right)^{2M\mu_I} e^{\left(\frac{\mu_I}{\bar{\beta}_I} - \frac{\gamma\mu}{\bar{\beta}}\right)} \left(\frac{\mu_I}{\bar{\beta}_I} + \frac{\gamma\mu}{\bar{\beta}}\right)^{-\frac{1}{2}(M\mu_I + \mu + 1)} \\
& W_{\frac{1}{2}(\mu - M\mu_I + 1), \frac{1}{2}(-\mu - M\mu_I)} \left(\frac{\mu_I}{\bar{\beta}_I} + \frac{\mu\gamma}{\bar{\beta}}\right) \sum_{v=0}^{\mu-1} \Gamma(\mu - v) \left(\frac{\gamma\mu}{\bar{\beta}}\right)^v \\
& \left(\frac{\mu_I}{\bar{\beta}_I} + \frac{\gamma\mu}{\bar{\beta}}\right)^{-\frac{1}{2}(v + M\mu_I + 1)} W_{\frac{1}{2}(v - M\mu_I + 1), \frac{1}{2}(-v - M\mu_I)} \left(\frac{\mu_I}{\bar{\beta}_I} + \frac{\mu\gamma}{\bar{\beta}}\right) \quad , \quad (2.60)
\end{aligned}$$

applying the Whittaker properties, as in [41, equation 13.14.31] such that ($W_{\kappa, \mu}(z) = W_{\kappa, -\mu}(z)$), the PDF can be rewritten as

$$\begin{aligned}
f_{\gamma_{up}}(\gamma) &= \frac{2\gamma^{\mu-1}}{\Gamma(\mu)^2} \left(\frac{\mu}{\bar{\beta}}\right)^{\mu} \left(\frac{\mu_I}{\bar{\beta}_I}\right)^{2l\mu_I} e^{\left(\frac{\mu_I}{\bar{\beta}_I} - \frac{\gamma\mu}{\bar{\beta}}\right)} \left(\frac{\mu_I}{\bar{\beta}_I} + \frac{\gamma\mu}{\bar{\beta}}\right)^{-\frac{1}{2}(M\mu_I + \mu + 1)} \\
& W_{\frac{1}{2}(\mu - M\mu_I + 1), \frac{1}{2}(\mu + N\mu_I)} \left(\frac{\mu_I}{\bar{\beta}_I} + \frac{\mu\gamma}{\bar{\beta}}\right) \sum_{v=0}^{\mu-1} \Gamma(\mu - v) \left(\frac{\gamma\mu}{\bar{\beta}}\right)^v \\
& \left(\frac{\mu_I}{\bar{\beta}_I} + \frac{\gamma\mu}{\bar{\beta}}\right)^{-\frac{1}{2}(v + M\mu_I + 1)} W_{\frac{1}{2}(v - M\mu_I + 1), \frac{1}{2}(v + M\mu_I)} \left(\frac{\mu_I}{\bar{\beta}_I} + \frac{\mu\gamma}{\bar{\beta}}\right) \quad , \quad (2.61)
\end{aligned}$$

by using Whittaker W function in [41, equation 13.14.3], the PDF can be written as

$$W_{\kappa, \mu}(z) = e^{-\frac{1}{2}z} z^{\frac{1}{2} + \mu} U\left(\frac{1}{2} + \mu - \kappa, 1 + 2\mu, z\right) \quad , \quad (2.62)$$

where $U(a, b, x)$ is the Confluent Hypergeometric Function of the Second Kind or also known as the Kummer's function, and is defined as

$$U(a, b; z) = \frac{\Gamma(1-b)}{\Gamma(1+a-b)} {}_1F_1(a, b, z) + \frac{\Gamma(b-1)}{\Gamma(a)} z^{1-b} {}_1F_1(1+a-b, 2-b, z) \quad , \quad (2.63)$$

it can be related to the Whittaker Function by relationship [41, equation 13.14.5] which is;

$$U(a, b; z) = z^{-\frac{b}{2}} e^{\frac{z}{2}} W_{\frac{b-a}{2}, \frac{b-1}{2}}(z) \quad , \quad (2.64)$$

Confluent Hypergeometric Function can be expanded as [41, equation 13.2.8]:

$$U(a, a+n+1, z) = z^{-a} \sum_{j=0}^n \binom{n}{j} (a)_j z^{-j} \quad , \quad (2.65)$$

using identities in (2.64) and (2.65), the PDF of γ_{up} can be mathematically manipulated as

$$\begin{aligned} f_{\gamma_{up}}(\gamma) &= \frac{2\gamma^{\mu-1}}{\Gamma(\mu)^2} \left(\frac{\mu}{\beta}\right)^\mu \left(\frac{\mu_I}{\beta_I}\right)^{2l\mu_I} e^{\frac{1}{2}\left(\frac{\mu_I}{\beta_I} - \frac{3\mu}{\beta}\gamma\right)} \sum_{j=0}^{\mu} \binom{\mu}{j} (M\mu_I)_j \left(\frac{\mu_I}{\beta_i} + \frac{\mu\gamma}{\beta}\right)^{-M\mu_I-j} \\ &\sum_{v=0}^{\mu-1} \Gamma(\mu-k) \left(\frac{\gamma\mu}{\beta}\right)^v \left(\frac{\mu_I}{\beta_i} + \frac{\gamma\mu}{\beta}\right)^{-\frac{1}{2}(v+M\mu_I+1)} W_{\frac{1}{2}(v-M\mu_I+1), \frac{1}{2}(v+M\mu_I)} \left(\frac{\mu_I}{\beta_i} + \frac{\mu\gamma}{\beta}\right) \quad , \end{aligned} \quad (2.66)$$

where $(a)_j$ is the Pochhammer symbol and is defined as $\left(\frac{\Gamma(a+j)}{\Gamma(a)}\right)$.

applying identities in (2.62) and (2.65), then the PDF of γ_{up} in (2.66) can be evaluated as

$$f_{\gamma_{up}}(\gamma) = \frac{2\gamma^{\mu-1}}{\Gamma(\mu)^2} \left(\frac{\mu}{\beta}\right)^\mu \left(\frac{\mu_I}{\beta_I}\right)^{2l\mu_I} e^{\frac{1}{2}\left(\frac{\mu_I}{\beta_I} - \frac{3\mu}{\beta}\gamma\right)} \sum_{j=0}^{\mu} \binom{\mu}{j} (M\mu_I)_j \left(\frac{\mu_I}{\beta_I} + \frac{\mu\gamma}{\beta}\right)^{-M\mu_I-j}$$

$$\sum_{v=0}^{\mu-1} \Gamma(\mu-v) \left(\frac{\gamma\mu}{\beta}\right)^v \left(\frac{\mu_I}{\beta_I} + \frac{\gamma\mu}{\beta}\right)^{-\frac{1}{2}(v+M\mu_I+1)} e^{-\frac{1}{2}\left(\frac{\mu_I}{\beta_I} + \frac{\mu\gamma}{\beta}\right)} \left(\frac{\mu_I}{\beta_I} + \frac{\mu\gamma}{\beta}\right)^{\frac{1}{2} + \frac{1}{2}(v+M\mu_I)} \left(\frac{\mu_I}{\beta_I} + \frac{\mu\gamma}{\beta}\right)^{-M\mu_I} \sum_{n=0}^v \binom{v}{n} (M\mu_I)_n \left(\frac{\mu_I}{\beta_I} + \frac{\mu\gamma}{\beta}\right)^{-n}, \quad (2.67)$$

the series index k is shifted by (1), which yield to express the PDF after mathematical manipulation as

$$f_{\gamma_{up}}(\gamma) = \frac{2}{\Gamma(\mu)^2} \left(\frac{\mu}{\beta}\right)^\mu \left(\frac{\mu_I}{\beta_i}\right)^{2M\mu_I} \sum_{j=0}^{\mu} \sum_{v=1}^{\mu} \sum_{n=0}^{v-1} \binom{\mu}{j} \binom{v-1}{n} (l\mu_I)_j (l\mu_I)_n \Gamma(\mu-v+1) \left(\frac{\mu}{\beta}\right)^{v-1} \gamma^{\mu+v-2} e^{-2\frac{\mu}{\beta}\gamma} \left(\frac{\mu_I}{\beta_i} + \frac{\mu\gamma}{\beta}\right)^{-2M\mu_I-j-n}. \quad (2.68)$$

This result can be reduced to give other PDF expressions for values such that:

- A. For identical links: $L=N$, $\mu = \mu_I = 1$, ($\gamma_i = \gamma_k = \gamma_I$) and ($\gamma_h = \gamma_g = \gamma$), the PDF $f_{\gamma_{up}}(\gamma)$ can be expressed after mathematical manipulation as

$$f_{\gamma_{up}}(\gamma) = 2 \left[\frac{N\Lambda^{2N}}{(\gamma + \Lambda)^{2N+1}} + \frac{1}{\beta} \left(\frac{\Lambda}{\gamma + \Lambda}\right)^{2N} \right] e^{-\frac{2\gamma}{\beta}}. \quad (2.69)$$

and this is identical to [9, equation 20], which corresponds to the Rayleigh fading channel model.

- B. For non-identical links, (2.68) can be reduced to be identical to [9, equation 21], where the PDF $f_{\gamma_{up}}(\gamma)$ can be expressed as

$$f_{\gamma_{up}}(\gamma) = e^{-\gamma\left(\frac{1}{\beta_{rd}} + \frac{1}{\beta_{sr}}\right)} \left(\left[\frac{N\Lambda^N}{(\gamma + \Lambda)^{N+1}} + \frac{1}{\beta_{sr}} \left(\frac{\Lambda}{\gamma + \Lambda}\right)^N \right] \left(\frac{\Upsilon}{\gamma + \Upsilon}\right)^L + \left[\frac{L\Upsilon^L}{(\gamma + \Upsilon)^{L+1}} + \frac{1}{\beta_{rd}} \left(\frac{\Upsilon}{\gamma + \Upsilon}\right)^L \right] \left(\frac{\Lambda}{\gamma + \Lambda}\right)^N \right), \quad (2.70)$$

where $(\Lambda = \frac{\bar{\beta}_{sr}}{\bar{\beta}_i})$, is the average Signal to Interference Ratio (SIR) at the Relay node, and $(\Upsilon = \frac{\bar{\beta}_{rd}}{\bar{\beta}_{gI}})$, is the average Signal to Interference Ratio (SIR) at the Destination node.

C. For identical fading channels, $\mu = m, \mu_I = m_I$, and $(\gamma_i = \gamma_k = \gamma_I)$, the PDF of γ_{up} can be evaluated as

$$f_{\gamma_{up}}(\gamma) = \frac{2}{\Gamma(m)^2} \left(\frac{m}{\bar{\beta}}\right)^m \left(\frac{m_I}{\bar{\beta}_I}\right)^{2lm_I} \sum_{j=0}^m \sum_{v=1}^m \sum_{n=0}^{v-1} \binom{m}{j} \binom{v-1}{n} (lm_I)_j (lm_I)_n \Gamma(m-v+1) \left(\frac{m}{\bar{\beta}}\right)^{v-1} \gamma^{m+v-2} e^{-2\frac{m}{\bar{\beta}}\gamma} \left(\frac{m_I}{\bar{\beta}_I} + \frac{m\gamma}{\bar{\beta}}\right)^{-2lm_I-j-n} . \quad (2.71)$$

2.3.4 Dual-Hop Relay SINR CDF

The density function for the Dual-Hop Relay network is expressed in (2.59), the next step is to derive the Cumulative Distribution Function of the Dual-Hop Relay network, starting from the definition of CDF:

$$F_{\gamma_{up}}(\gamma) = \int_0^{\gamma} f_{\gamma_{up}}(t) dt , \quad (2.72)$$

The CDF of the Dual-Hop network is derived for the upper bound; i.e. the minimum of two random variables as

$$F_{\gamma_{up}}(\gamma) = F_{\gamma_{sr}}(\gamma) + F_{\gamma_{rd}}(\gamma) - F_{\gamma_{sr}}(\gamma)F_{\gamma_{rd}}(\gamma), \quad (2.73)$$

Substituting both (2.53) and (2.54) into (2.73) will result in the Dual-Hop Relay network CDF to be expressed as

$$F_{\gamma_{up}}(\gamma) = 2 - \frac{\left(\mu_I^{\mu_I} \bar{\beta}_I^{-\mu_I}\right)^N e^{\left(\frac{\mu_I}{\bar{\beta}_I}\right)} e^{-\frac{\mu_{sr}}{2\bar{\beta}_{sr}}\gamma - \frac{\mu_I}{2\bar{\beta}_I}} \sum_{v=0}^{\mu_{sr}-1} \left(\frac{\mu_{sr}}{\bar{\beta}_{sr}}\gamma\right)^v \Gamma(\mu_{sr} - v)}{\Gamma(\mu_{sr})}$$

$$\begin{aligned}
& \left(\frac{\mu_{sr}}{\beta_{sr}} \gamma + \frac{\mu_I}{\beta_I} \right)^{\frac{-\mu_I N - v - 1}{2}} W_{\frac{-\mu_I N + v + 1}{2}, \frac{-\mu_I N - v}{2}} \left(\frac{\mu_{sr}}{\beta_{sr}} \gamma + \frac{\mu_I}{\beta_I} \right) \\
& - \frac{\left(\mu_K^{\mu_K} \bar{\beta}_K^{-\mu_K} \right)^L e^{\left(\frac{\mu_K}{\beta_K} \right)} e^{-\frac{\mu_{rd}}{2\beta_{rd}} \gamma - \frac{\mu_K}{2\beta_K}} \sum_{u=0}^{\mu_{rd}-1} \left(\frac{\mu_{rd}}{\beta_{rd}} \gamma \right)^u \Gamma(\mu_{rd} - u)}{\Gamma(\mu_{rd})} \\
& \left(\frac{\mu_{rd}}{\beta_{rd}} \gamma + \frac{\mu_K}{\beta_K} \right)^{\frac{-\mu_K L - u - 1}{2}} W_{\frac{-\mu_K L + u + 1}{2}, \frac{-\mu_K L - u}{2}} \left(\frac{\mu_{rd}}{\beta_{rd}} \gamma + \frac{\mu_K}{\beta_K} \right) \\
& - \left[1 - \frac{\left(\mu_I^{\mu_I} \bar{\beta}_I^{-\mu_I} \right)^N e^{\left(\frac{\mu_I}{\beta_I} \right)} e^{-\frac{\mu_{sr}}{2\beta_{sr}} \gamma - \frac{\mu_I}{2\beta_I}} \sum_{v=0}^{\mu_{sr}-1} \left(\frac{\mu_{sr}}{\beta_{sr}} \gamma \right)^v \Gamma(\mu_{sr} - v)}{\Gamma(\mu_{sr})} \right. \\
& \left. \left(\frac{\mu_{sr}}{\beta_{sr}} \gamma + \frac{\mu_I}{\beta_I} \right)^{\frac{-\mu_I N - v - 1}{2}} W_{\frac{-\mu_I N + v + 1}{2}, \frac{-\mu_I N - v}{2}} \left(\frac{\mu_{sr}}{\beta_{sr}} \gamma + \frac{\mu_I}{\beta_I} \right) \right] \\
& \times \left[1 - \frac{\left(\mu_K^{\mu_K} \bar{\beta}_K^{-\mu_K} \right)^L e^{\left(\frac{\mu_K}{\beta_K} \right)} e^{-\frac{\mu_{rd}}{2\beta_{rd}} \gamma - \frac{\mu_K}{2\beta_K}} \sum_{u=0}^{\mu_{rd}-1} \left(\frac{\mu_{rd}}{\beta_{rd}} \gamma \right)^u \Gamma(\mu_{rd} - u)}{\Gamma(\mu_{rd})} \right. \\
& \left. \left(\frac{\mu_{rd}}{\beta_{rd}} \gamma + \frac{\mu_K}{\beta_K} \right)^{\frac{-\mu_K L - u - 1}{2}} W_{\frac{-\mu_K L + u + 1}{2}, \frac{-\mu_K L - u}{2}} \left(\frac{\mu_{rd}}{\beta_{rd}} \gamma + \frac{\mu_K}{\beta_K} \right) \right] , \quad (2.74)
\end{aligned}$$

after mathematical manipulation, the CDF can be evaluated to yield:

$$\begin{aligned}
F_{\gamma_{up}}(\gamma) &= 1 - \frac{\left(\mu_I^{\mu_I} \bar{\beta}_I^{-\mu_I} \right)^N \left(\mu_k^{\mu_k} \bar{\beta}_k^{-\mu_k} \right)^L e^{\left(\frac{\mu_I}{\beta_I} + \frac{\mu_k}{\beta_k} \right)} e^{-\frac{1}{2} \left(\left(\frac{\mu_{sr}}{\beta_{sr}} + \frac{\mu_{rd}}{\beta_{rd}} \right) \gamma + \left(\frac{\mu_I}{\beta_I} + \frac{\mu_k}{\beta_k} \right) \right)}}{\Gamma(\mu_{sr}) \Gamma(\mu_{rd})} \\
& \sum_{v=0}^{\mu_{sr}-1} \left(\frac{\mu_{sr}}{\beta_{sr}} \gamma \right)^v \Gamma(\mu_{sr} - v) \left(\frac{\mu_{sr}}{\beta_{sr}} \gamma + \frac{\mu_I}{\beta_I} \right)^{\frac{-\mu_I N - v - 1}{2}} W_{\frac{-\mu_I N + v + 1}{2}, \frac{-\mu_I N - v}{2}} \left(\frac{\mu_{sr}}{\beta_{sr}} \gamma + \frac{\mu_I}{\beta_I} \right) \\
& \sum_{u=0}^{\mu_{rd}-1} \left(\frac{\mu_{rd}}{\beta_{rd}} \gamma \right)^u \Gamma(\mu_{rd} - u) \left(\frac{\mu_{rd}}{\beta_{rd}} \gamma + \frac{\mu_k}{\beta_k} \right)^{\frac{-\mu_k L - u - 1}{2}} W_{\frac{-\mu_k L + u + 1}{2}, \frac{-\mu_k L - u}{2}} \left(\frac{\mu_{rd}}{\beta_{rd}} \gamma + \frac{\mu_k}{\beta_k} \right). \quad (2.75)
\end{aligned}$$

for identical fading channel links, with $N = L = l, \mu_I = \mu_K = \mu_I, \bar{\beta}_I = \bar{\beta}_K = \bar{\beta}_I$ and $\bar{\beta}_{sr} = \bar{\beta}_{rd} = \bar{\beta}$, the CDF can be evaluated as

$$\begin{aligned}
F_{\gamma_{up}}(\gamma) = & 1 - \frac{1}{\Gamma(\mu)^2} \left(\frac{\mu_I}{\beta_I}\right)^{2l\mu_I} e^{\frac{\mu_I}{\beta_I} - \frac{\gamma\mu}{\beta}} \left(\frac{\mu_I}{\beta_I} + \frac{\gamma\mu}{\beta}\right)^{-l\mu_I} \left(\sum_{v=0}^{\mu-1} \Gamma(\mu-v) \left(\frac{\gamma\mu}{\beta}\right)^v\right. \\
& \left. \left(\frac{\mu_I}{\beta_I} + \frac{\gamma\mu}{\beta}\right)^{\frac{-v-1}{2}} \times W_{\frac{v-l\mu_I+1}{2}, \frac{-v-l\mu_I}{2}} \left(\frac{\mu_I}{\beta_I} + \frac{\gamma\mu}{\beta}\right)\right)^2, \tag{2.76}
\end{aligned}$$

the Lagrange's identity, which is identified by

$$\left(\sum_{k=1}^n a_k b_k\right)^2 = \sum_{k=1}^n a_k^2 b_k^2 + 2 \sum_{i=1}^{n-1} \sum_{j=i+1}^n a_i b_i a_j b_j, \tag{2.77}$$

is applied to (2.76), the CDF can be evaluated after shifting the index k by (1) as

$$\begin{aligned}
F_{\gamma_{up}}(\gamma) = & 1 - \frac{1}{\Gamma(\mu)^2} \left(\frac{\mu_I}{\beta_I}\right)^{2l\mu_I} e^{\frac{\mu_I}{\beta_I} - \frac{\gamma\mu}{\beta}} \left(\frac{\mu_I}{\beta_I} + \frac{\gamma\mu}{\beta}\right)^{-l\mu_I} \\
& \times \left(\sum_{v=1}^{\mu} \Gamma(\mu-v+1)^2 \left(\frac{\gamma\mu}{\beta}\right)^{2k-2} \left(\frac{\mu_I}{\beta_I} + \frac{\gamma\mu}{\beta}\right)^{-v}\right. \\
& \times W_{\frac{v-l\mu_I}{2}, \frac{-v-l\mu_I+1}{2}}^2 \left(\frac{\mu_I}{\beta_I} + \frac{\gamma\mu}{\beta}\right) \\
& + 2 \sum_{i=1}^{\mu-1} \sum_{j=i+1}^{\mu} \Gamma(\mu-i+1) \left(\frac{\gamma\mu}{\beta}\right)^{i-1} \left(\frac{\mu_I}{\beta_I} + \frac{\gamma\mu}{\beta}\right)^{-\frac{i}{2}} \\
& \times W_{\frac{i-l\mu_I}{2}, \frac{-i-l\mu_I+1}{2}} \left(\frac{\mu_I}{\beta_I} + \frac{\gamma\mu}{\beta}\right) \Gamma(\mu-j+1) \\
& \left. \times \left(\frac{\gamma\mu}{\beta}\right)^{j-1} \left(\frac{\mu_I}{\beta_I} + \frac{\gamma\mu}{\beta}\right)^{-\frac{j}{2}} \times W_{\frac{j-l\mu_I}{2}, \frac{-j-l\mu_I+1}{2}} \left(\frac{\mu_I}{\beta_I} + \frac{\gamma\mu}{\beta}\right)\right), \tag{2.78}
\end{aligned}$$

the CDF can be manipulated to be expressed in a tractable form by shifting the series indexes (j) and (i) by (1), then applying the Whittaker W-function property in [41, equation 13.14.31], as

$$\begin{aligned}
F_{\gamma_{up}}(\gamma) &= 1 - \frac{1}{\Gamma(\mu)^2} \left(\frac{\mu_I}{\beta_I}\right)^{2l\mu_I} e^{\frac{\mu_I}{\beta_I} - \frac{\gamma\mu}{\beta}} \left(\frac{\mu_I}{\beta_I} + \frac{\gamma\mu}{\beta}\right)^{-l\mu_I} \\
&\quad \times \sum_{v=1}^{\mu} \Gamma(\mu - v + 1)^2 \left(\frac{\gamma\mu}{\beta}\right)^{2k-2} \left(\frac{\mu_I}{\beta_I} + \frac{\gamma\mu}{\beta}\right)^{-v} \\
&\quad \times W_{\frac{v-l\mu_I}{2}, \frac{-v-l\mu_I+1}{2}}^2 \left(\frac{\mu_I}{\beta_I} + \frac{\gamma\mu}{\beta}\right) \\
&\quad - \frac{2}{\Gamma(\mu)^2} \left(\frac{\mu_I}{\beta_I}\right)^{2l\mu_I} e^{\frac{\mu_I}{\beta_I} - \frac{\gamma\mu}{\beta}} \left(\frac{\mu_I}{\beta_I} + \frac{\gamma\mu}{\beta}\right)^{-l\mu_I} \\
&\quad \times \sum_{i=0}^{\mu-2} \sum_{j=i+1}^{\mu-1} \Gamma(\mu - i)\Gamma(\mu - j) \left(\frac{\gamma\mu}{\beta}\right)^{i+j} \left(\frac{\mu_I}{\beta_I} + \frac{\gamma\mu}{\beta}\right)^{-\frac{i}{2}-\frac{j}{2}-1} \\
&\quad \times W_{\frac{i-l\mu_I+1}{2}, \frac{i+l\mu_I}{2}} \left(\frac{\mu_I}{\beta_I} + \frac{\gamma\mu}{\beta}\right) \times W_{\frac{j-l\mu_I+1}{2}, \frac{j+l\mu_I}{2}} \left(\frac{\mu_I}{\beta_I} + \frac{\gamma\mu}{\beta}\right), \tag{2.79}
\end{aligned}$$

substituting the alternative expression of the Whittaker W-function in terms of the Confluent Hypergeometric Function presented in (2.62), then applying the identity as in (2.65), where the Confluent Hypergeometric Function is represented in Series expression, the CDF is expressed after mathematical manipulation as

$$\begin{aligned}
F_{\gamma_{up}}(\gamma) &= 1 - \frac{1}{\Gamma(\mu)^2} \left(\frac{\mu_I}{\beta_I}\right)^{2l\mu_I} e^{\frac{\mu_I}{\beta_I} - \frac{\gamma\mu}{\beta}} \left(\frac{\mu_I}{\beta_I} + \frac{\gamma\mu}{\beta}\right)^{-l\mu_I} \sum_{v=1}^{\mu} \Gamma(\mu - v + 1)^2 \left(\frac{\gamma\mu}{\beta}\right)^{2v-2} \\
&\quad \left(\frac{\mu_I}{\beta_I} + \frac{\gamma\mu}{\beta}\right)^{-v} \times W_{\frac{v-l\mu_I}{2}, \frac{-v-l\mu_I+1}{2}}^2 \left(\frac{\mu_I}{\beta_I} + \frac{\gamma\mu}{\beta}\right) - \frac{2}{\Gamma(\mu)^2} \left(\frac{\mu_I}{\beta_I}\right)^{2l\mu_I} \\
&\quad \sum_{i=0}^{\mu-2} \sum_{j=i+1}^{\mu-1} \sum_{n=0}^i \sum_{t=0}^j \Gamma(\mu - i)\Gamma(\mu - j) \binom{i}{n} (l\mu_I)_n \binom{j}{t} (l\mu_I)_t \left(\frac{\gamma\mu}{\beta}\right)^{i+j} \\
&\quad e^{-\frac{2\mu}{\beta}\gamma} \left(\frac{\mu_I}{\beta_I} + \frac{\gamma\mu}{\beta}\right)^{-2l\mu_I - n - t}. \tag{2.80}
\end{aligned}$$

This result can be reduced to special cases for the CDF of γ_{up} , such that:

A. For identical fading links with $\mu = 1$, which corresponds to identical Rayleigh fading channel, the CDF in (2.80) can be reduced to

$$F_{\gamma_{up}}(\gamma) = 1 - e^{-\frac{2\gamma}{\beta}} \left(\frac{\Lambda}{\gamma + \Lambda} \right)^{2l}. \quad (2.81)$$

where $(\Lambda = \frac{\bar{\beta}_{sr}}{\beta_I})$, is the average SIR at the Relay node.

B. For non-identical fading links with $\mu = 1$ the CDF can be expressed as

$$F_{\gamma_{up}}(\gamma) = 1 - e^{-\gamma \left(\frac{1}{\beta_{sr}} + \frac{1}{\beta_{rd}} \right)} \left(\frac{\Lambda}{\gamma + \Lambda} \right)^N \left(\frac{\Upsilon}{\gamma + \Upsilon} \right)^L, \quad (2.82)$$

where $(\Lambda = \frac{\bar{\beta}_{sr}}{\beta_I})$, is the average SIR at the Relay node, and $(\Upsilon = \frac{\bar{\beta}_{rd}}{\beta_k})$, is the average SIR at the Destination node.

C. For identical Fading links with $\mu = m$ which corresponds to the Nakagami-m fading channel, the CDF can be expressed as

$$\begin{aligned} F_{\gamma_{up}}(\gamma) = & 1 - \frac{1}{\Gamma(m)^2} \left(\frac{m_I}{\beta_I} \right)^{2lm_I} e^{\frac{m_I}{\beta_I} - \frac{\gamma m}{\beta}} \left(\frac{m_I}{\beta_I} + \frac{\gamma m}{\beta} \right)^{-lm_I} \sum_{v=1}^m \Gamma(m-v+1)^2 \\ & \left(\frac{\gamma m}{\beta} \right)^{2v-2} \left(\frac{m_I}{\beta_I} + \frac{\gamma m}{\beta} \right)^{-v} \times W_{\frac{v-lm_I}{2}, \frac{-v-lm_I+1}{2}}^2 \left(\frac{m_I}{\beta_I} + \frac{\gamma m}{\beta} \right) - \frac{2}{\Gamma(m)^2} \\ & \left(\frac{m_I}{\beta_I} \right)^{2lm_I} \sum_{i=0}^{m-2} \sum_{j=i+1}^{m-1} \sum_{n=0}^i \sum_{s=0}^j \Gamma(m-i)\Gamma(m-j) \binom{i}{n} (lm_I)_n \binom{j}{s} (lm_I)_s \\ & \left(\frac{\gamma m}{\beta} \right)^{i+j} e^{-\frac{2m}{\beta}\gamma} \left(\frac{m_I}{\beta_I} + \frac{\gamma m}{\beta} \right)^{-2lm_I-n-s}. \end{aligned} \quad (2.83)$$

2.3.5 Dual-Hop Relay SINR MGF

The Moment Generating function (MGF) is very useful for deriving the performance metrics of the network, which is given as

$$M_{\gamma_{up}}(s) = \int_0^{\infty} f_{\gamma_{up}}(\gamma) e^{-s\gamma} d\gamma, \quad (2.84)$$

substituting the PDF of the dual-hop given in (2.60) while assuming identical number of fading links such that $N = L = l$, and using [47, equation 2.3.6.9], the MGF can be expressed as

$$M_{\gamma_{up}}(s) = \frac{2}{\Gamma(\mu)^2} \left(\frac{\mu}{\beta}\right)^\mu \left(\frac{\mu_I}{\beta_i}\right)^{2l\mu_I} \sum_{j=0}^{\mu} \sum_{v=1}^{\mu} \sum_{n=0}^{v-1} \Gamma(\mu - v + 1) \binom{\mu}{j} \binom{v-1}{n} (l\mu_I)_j (l\mu_I)_n \left(\frac{\mu}{\beta}\right)^{v-2l\mu_I-j-n-1} \int_0^\infty \gamma^{\mu+v-2} e^{-\gamma(2\frac{\mu}{\beta}+s)} \left(\gamma + \frac{\mu_I\bar{\beta}}{\mu\beta_I}\right)^{-2l\mu_I-j-n} d\gamma, \quad (2.85)$$

using application in [47, equation 2.3.6.9], MGF can be evaluated as

$$M_{\gamma_{up}}(s) = \frac{2}{\Gamma(\mu)^2} \sum_{j=0}^{\mu} \sum_{v=1}^{\mu} \sum_{n=0}^{v-1} \Gamma(\mu - v + 1) \Gamma(\mu + v - 1) \binom{\mu}{j} \binom{v-1}{n} (l\mu_I)_j (l\mu_I)_n \left(\frac{\mu_I}{\beta_I}\right)^{\mu+v-j-n-1} U\left(\mu + v - 1, \mu + v - 2l\mu_I - j - n; \frac{\mu_I\bar{\beta}}{\mu\beta_I} \left(2\frac{\mu}{\beta} + s\right)\right), \quad (2.86)$$

where the $U(a, b, x)$ is the Confluent Hypergeometric Function of the Second Kind and is defined generally as in [44, equation 07.33.02.0001.01].

2.4 Dual-Hop Relay Performance Analysis

2.4.1 Outage Probability Analysis

Outage probability (P_{out}) is a fundamental performance metric in wireless communication systems that measures the likelihood of a communication link becoming temporarily unusable due to severe channel degradation. It occurs when the instantaneous SNR falls below a critical threshold (γ_{th}) that is required to maintain reliable communication. This threshold depends on factors such as the modulation scheme, target bit error rate, and coding techniques being used. The concept is particularly important in fading environments where signal strength can

vary dramatically due to multipath propagation, shadowing, and interference.

Physically, outage probability reflects how often users at the edge of a cell or in challenging propagation conditions might experience dropped connections or unacceptable service quality. In practical system design, it helps engineers determine the required transmit power, cell coverage areas, and the need for diversity techniques to ensure adequate service reliability. For instance, a system designed for voice calls might tolerate a higher outage probability than one designed for critical emergency communications.

Mathematically, outage probability is derived from the cumulative distribution function of the received SNR, representing the probability that the SNR remains below the minimum threshold (γ_{th}) needed for proper signal detection. From a system perspective, outage probability is closely related to other key performance indicators like coverage probability and capacity. It plays a crucial role in network planning, particularly for emerging technologies like 5G and IoT networks where reliability requirements are stringent. Techniques such as transmit diversity, adaptive modulation, and cooperative communications are often employed to reduce outage probability and enhance overall system robustness in challenging wireless environments. In this section the Outage Probability of the dual-hop relay network will be analyzed. The outage probability is defined as

$$P_{out} = \Pr(\gamma_{up} \leq \gamma_{th}) = P_{\gamma_{up}}(\gamma_{th}) = \int_0^{\gamma_{th}} f_{\gamma_{up}}(\gamma) d\gamma, \quad (2.87)$$

which can be evaluated after substituting the PDF as

$$\begin{aligned}
P_{out} &= \int_0^{\gamma_{th}} \frac{\mu_{sr}^{\mu_{sr}} e^{\left(\frac{\mu_I}{\beta_I} + \frac{\mu_K}{\beta_K}\right)}}{\Gamma(\mu_{sr})\Gamma(\mu_{rd})\bar{\beta}_{sr}^{\mu_{sr}}} \gamma^{\mu_{sr}-1} \left(\frac{\mu_I}{\beta_I}\right)^{N\mu_I} \left(\frac{\mu_K}{\beta_K}\right)^L \left(\frac{\mu_{sr}}{\beta_{sr}}\gamma + \frac{\mu_I}{\beta_I}\right)^{-\frac{\mu_I N + \mu_{sr} + 1}{2}} \\
&e^{-\left(\frac{\mu_{sr}}{2\beta_{sr}}\gamma + \frac{\mu_I}{2\beta_I}\right)} e^{-\left(\frac{\mu_{rd}}{2\beta_{rd}}\gamma + \frac{\mu_K}{2\beta_K}\right)} W_{\frac{\mu_{sr} - \mu_I N + 1}{2}, \frac{-\mu_I N - \mu_{sr}}{2}} \left(\frac{\mu_{sr}}{\beta_{sr}}\gamma + \frac{\mu_I}{\beta_I}\right)^{\mu_{rd}-1} \sum_{u=0}^{\mu_{rd}-1} \left(\frac{\mu_{rd}}{\beta_{rd}}\gamma\right)^u \\
&\Gamma(\mu_{rd} - u) \left(\frac{\mu_{rd}}{\beta_{rd}}\gamma + \frac{\mu_K}{\beta_K}\right)^{\frac{-\mu_K L - u - 1}{2}} W_{\frac{-\mu_K L + u + 1}{2}, \frac{-\mu_K L - u}{2}} \left(\frac{\mu_{rd}}{\beta_{rd}}\gamma + \frac{\mu_K}{\beta_K}\right) \\
&+ \frac{\mu_{rd}^{\mu_{rd}} e^{\left(\frac{\mu_K}{\beta_K} + \frac{\mu_I}{\beta_I}\right)}}{\Gamma(\mu_{rd})\Gamma(\mu_{sr})\bar{\beta}_{rd}^{\mu_{rd}}} \gamma^{\mu_{rd}-1} \left(\frac{\mu_K}{\beta_K}\right)^{L\mu_K} \left(\frac{\mu_I}{\beta_I}\right)^{N\mu_I} \left(\frac{\mu_{rd}}{\beta_{rd}}\gamma + \frac{\mu_K}{\beta_K}\right)^{-\frac{\mu_K L + \mu_{rd} + 1}{2}} \\
&e^{-\left(\frac{\mu_{rd}}{2\beta_{rd}}\gamma + \frac{\mu_K}{2\beta_K}\right)} e^{-\left(\frac{\mu_{sr}}{2\beta_{sr}}\gamma + \frac{\mu_I}{2\beta_I}\right)} W_{\frac{\mu_{rd} - \mu_K L + 1}{2}, \frac{-\mu_K L - \mu_{rd}}{2}} \left(\frac{\mu_{rd}}{\beta_{rd}}\gamma + \frac{\mu_K}{\beta_K}\right)^{\mu_{sr}-1} \sum_{v=0}^{\mu_{sr}-1} \left(\frac{\mu_{sr}}{\beta_{sr}}\gamma\right)^v \\
&\Gamma(\mu_{sr} - v) \left(\frac{\mu_{sr}}{\beta_{sr}}\gamma + \frac{\mu_I}{\beta_I}\right)^{\frac{-\mu_I N - v - 1}{2}} W_{\frac{-\mu_I N + v + 1}{2}, \frac{-\mu_I N - v}{2}} \left(\frac{\mu_{sr}}{\beta_{sr}}\gamma + \frac{\mu_I}{\beta_I}\right)
\end{aligned} \tag{2.88}$$

Thus; the outage probability can be computed as

$$\begin{aligned}
P_{out} &= 1 - \frac{\left(\mu_I \bar{\beta}_I^{-\mu_I}\right)^{N h_I} \left(\mu_K \bar{\beta}_K^{-\mu_K}\right)^L e^{\left(\frac{\mu_I}{\beta_I} + \frac{\mu_K}{\beta_K}\right)}}{\Gamma(\mu_{sr})\Gamma(\mu_{rd})} e^{-\frac{1}{2}\left(\left(\frac{\mu_{sr}}{\beta_{sr}} + \frac{\mu_{rd}}{\beta_{rd}}\right)\gamma_{th} + \left(\frac{\mu_I}{\beta_I} + \frac{\mu_K}{\beta_K}\right)\right)} \\
&\times \sum_{v=0}^{\mu_{sr}-1} \left(\frac{\mu_{sr}}{\beta_{sr}}\gamma_{th}\right)^v \Gamma(\mu_{sr} - v) \left(\frac{\mu_{sr}}{\beta_{sr}}\gamma_{th} + \frac{\mu_I}{\beta_I}\right)^{\frac{-\mu_I N - v - 1}{2}} \\
&W_{\frac{-\mu_I N h_I + v + 1}{2}, \frac{-\mu_I N - v}{2}} \left(\frac{\mu_{sr}}{\beta_{sr}}\gamma_{th} + \frac{\mu_I}{\beta_I}\right)^{\mu_{rd}-1} \sum_{u=0}^{\mu_{rd}-1} \left(\frac{\mu_{rd}}{\beta_{rd}}\gamma_{th}\right)^u \Gamma(\mu_{rd} - u) \\
&\left(\frac{\mu_{rd}}{\beta_{rd}}\gamma_{th} + \frac{\mu_K}{\beta_K}\right)^{\frac{-\mu_K L - u - 1}{2}} W_{\frac{-\mu_K L + u + 1}{2}, \frac{-\mu_K L - u}{2}} \left(\frac{\mu_{rd}}{\beta_{rd}}\gamma_{th} + \frac{\mu_K}{\beta_K}\right).
\end{aligned} \tag{2.89}$$

This result can be reduced to different special cases such as

A. For identical fading channel with $\mu = 1$ that corresponds to the Rayleigh fading channel, the outage probability is:

$$P_{out} = 1 - \left(\frac{\Lambda}{\Lambda + \gamma_{th}} \right)^{2N} e^{-\frac{2\gamma_{th}}{\bar{\beta}}}. \quad (2.90)$$

where $(\Lambda = \frac{\bar{\beta}_{sr}}{\bar{\beta}_I})$, is the average SIR at the Relay node. This result is identical to [9, equation 22].

B. For non-identical fading channel with $\mu = 1$, outage probability is expressed as

$$P_{out} = 1 - \left(\frac{\Lambda}{\Lambda + \gamma_{th}} \right)^L \left(\frac{\Upsilon}{\Upsilon + \gamma_{th}} \right)^N e^{-\gamma_{th} \left(\frac{1}{\bar{\beta}_{sr}} + \frac{1}{\bar{\beta}_{rd}} \right)}. \quad (2.91)$$

where $(\Lambda = \frac{\bar{\beta}_{sr}}{\bar{\beta}_I})$, is the average SIR at the Relay node, and $(\Upsilon = \frac{\bar{\beta}_{rd}}{\bar{\beta}_k})$, is the average SIR at the Destination node. This is identical to [9, equation 23].

C. For identical fading channel with $\mu = m = 2$;(2.89) can be reduced to:

$$P_{out} = 1 - \left(\frac{\Lambda}{\Lambda + \gamma_{th}} \right)^{4N} \frac{(\bar{\beta}_I \gamma_{th} (2N\bar{\beta} + 2\gamma_{th} + \bar{\beta}) + \bar{\beta} (2\gamma_{th} + \bar{\beta}))^2}{\bar{\beta}^2 (\bar{\beta}_I \gamma_{th} + \bar{\beta})^2} e^{-\frac{4\gamma_{th}}{\bar{\beta}}}. \quad (2.92)$$

equation (2.89) can be used to generate many different formulas such as [9, equation 22] which represents identical number of fading channel with $\mu = 1$, and as in [9, equation 23] for non-identical number of fading channel with $\mu = 1$, and many other formulas for other fading channels such that with $\mu = m$ which corresponds to the Nakagami-m fading model.

2.4.2 Average Error Probability Analysis

In wireless communication systems, the error probability P_e for a given given signal-to-noise ratio γ , often measured as the bit error rate (BER), serves as a critical performance metric that quantifies the likelihood of incorrect symbol or bit detection at the receiver. The physical meaning of P_e is deeply rooted in

the impairments introduced by the wireless channel, including AWGN, multipath fading, interference, and distortions caused by bandwidth limitations. When a signal propagates through a wireless medium, it is subject to random fluctuations in amplitude and phase, particularly in fading environments such as $\alpha - \mu$ fading channel, where the signal strength varies unpredictably. These variations degrade the SNR, leading to an increased probability that the receiver misinterprets a transmitted bit.

For instance, in an AWGN channel with binary phase-shift keying (BPSK) modulation, the theoretical P_e is given by the Gaussian Q -function of the square root of the bit energy-to-noise power spectral density ratio [35, 4.3-13]

$$P_e = Q\left(\sqrt{2\gamma}\right) = Q\left(\sqrt{\frac{2E_b}{N_0}}\right) \quad (2.93)$$

where (E_b) is the energy per bit and (N_0) is the noise power spectral density. This equation illustrates how higher SNR reduces error probability. However, in practical scenarios, factors like inter-symbol interference (ISI), CCI, and Doppler spread further exacerbate $(\overline{P_e})$, particularly in high-mobility or dense multipath environments.

Advanced techniques such as error-correcting codes (ECC), adaptive modulation and coding (AMC), and diversity combining are employed to mitigate these effects and improve system reliability. Thus, (E_b) not only reflects the quality of the communication link but also guides the design of robust wireless systems, balancing trade-offs between data rate, power efficiency, and spectral efficiency.

The error probability P_e denoted by 2.93 is considered as the conditional error probability where the channel gain is considered fixed, in order to obtain the error

probability for random channel gain, the P_e should be averaged over the probability density function of the end-to-end SNR $f_{\gamma_{SRD}}(\gamma)$ the "Source-Relay-Destination" link. And that can be achieved by evaluating the integral given by [35]

$$\bar{P}_e = \int_0^\infty P_e f_{\gamma_{SRD}}(\gamma) d\gamma, \quad (2.94)$$

where P_e is the conditional error probability for a given signal-to-noise ratio γ . For Binary-Phase-Shift-Keying (BPSK) modulation, the average error roadability and known as the average BER is expressed as

$$\bar{P}_e = \int_0^\infty Q(\sqrt{2\gamma}) f_{\gamma_{SRD}}(\gamma) d\gamma, \quad (2.95)$$

substituting (2.59) into (2.95) will yield to express the average bit error probability as

$$\begin{aligned} \bar{P}_e = & \int_0^\infty Q(\sqrt{2\gamma}) \left[\frac{\mu_{sr}^{\mu_{sr}} \left(\mu_I^{\mu_I} \bar{\beta}_I^{-\mu_I} \right)^N \left(\mu_K^{\mu_K} \bar{\beta}_K^{-\mu_K} \right)^L e^{\left(\frac{\mu_I}{\beta_I} \right)} e^{\left(\frac{\mu_K}{\beta_K} \right)}}{\Gamma(\mu_{sr}) \Gamma(\mu_{rd}) \bar{\beta}_{sr}^{\mu_{sr}}} \right. \\ & \left(\frac{\mu_{sr}}{\beta_{sr}} \gamma + \frac{\mu_I}{\beta_I} \right)^{-\frac{\mu_I N + \mu_{sr} + 1}{2}} e^{-\left(\frac{\mu_{sr}}{2\beta_{sr}} \gamma + \frac{\mu_I}{2\beta_I} \right)} e^{-\left(\frac{\mu_{rd}}{2\beta_{rd}} \gamma + \frac{\mu_K}{2\beta_K} \right)} \gamma^{\mu_{sr} - 1} \\ & W_{\frac{\mu_{sr} - \mu_I N + 1}{2}, \frac{-\mu_I N - \mu_{sr}}{2}} \left(\frac{\mu_{sr}}{\beta_{sr}} \gamma + \frac{\mu_I}{\beta_I} \right)^{\mu_{rd} - 1} \left(\frac{\mu_{rd}}{\beta_{rd}} \gamma \right)^u \Gamma(\mu_{rd} - u) \\ & \left(\frac{\mu_{rd}}{\beta_{rd}} \gamma + \frac{\mu_K}{\beta_K} \right)^{-\frac{\mu_K L - u - 1}{2}} W_{\frac{-\mu_K L + u + 1}{2}, \frac{-\mu_K L - u}{2}} \left(\frac{\mu_{rd}}{\beta_{rd}} \gamma + \frac{\mu_K}{\beta_K} \right) \\ & + \frac{\mu_{rd}^{\mu_{rd}} \left(\mu_K^{\mu_K} \bar{\beta}_K^{-\mu_K} \right)^L \left(\mu_I^{\mu_I} \bar{\beta}_I^{-\mu_I} \right)^N e^{\left(\frac{\mu_K}{\beta_K} \right)} e^{\left(\frac{\mu_I}{\beta_I} \right)}}{\Gamma(\mu_{rd}) \Gamma(\mu_{sr}) \bar{\beta}_{rd}^{\mu_{rd}}} \gamma^{\mu_{rd} - 1} \\ & \left(\frac{\mu_{rd}}{\beta_{rd}} \gamma + \frac{\mu_K}{\beta_K} \right)^{-\frac{\mu_K L + \mu_{rd} + 1}{2}} e^{-\left(\frac{\mu_{rd}}{2\beta_{rd}} \gamma + \frac{\mu_K}{2\beta_K} \right)} e^{-\left(\frac{\mu_{sr}}{2\beta_{sr}} \gamma + \frac{\mu_I}{2\beta_I} \right)} \\ & W_{\frac{\mu_{rd} - \mu_K L + 1}{2}, \frac{-\mu_K L - \mu_{rd}}{2}} \left(\frac{\mu_{rd}}{\beta_{rd}} \gamma + \frac{\mu_K}{\beta_K} \right)^{\mu_{sr} - 1} \left(\frac{\mu_{sr}}{\beta_{sr}} \gamma \right)^v \Gamma(\mu_{sr} - v) \\ & \left. \left(\frac{\mu_{sr}}{\beta_{sr}} \gamma + \frac{\mu_I}{\beta_I} \right)^{-\frac{\mu_I N - v - 1}{2}} W_{\frac{-\mu_I N + v + 1}{2}, \frac{-\mu_I N - v}{2}} \left(\frac{\mu_{sr}}{\beta_{sr}} \gamma + \frac{\mu_I}{\beta_I} \right) \right] d\gamma \Bigg|_{s=1}, \quad (2.96) \end{aligned}$$

using the alternative form of the Q-function expressed in terms of the MGF as in [33, equation 6.44],

$$\begin{aligned}
\overline{P}_e = & \frac{1}{2} \int_0^\infty e^{-s\gamma} \left[\frac{\mu_{sr}^{\mu_{sr}} \left(\mu_i^{\mu_i} \overline{\beta}_i^{-\mu_i} \right)^N \left(\mu_K^{\mu_K} \overline{\beta}_K^{-\mu_K} \right)^L e^{\left(\frac{\mu_i}{\overline{\beta}_i} \right)} e^{\left(\frac{\mu_K}{\overline{\beta}_K} \right)}}{\Gamma(\mu_{sr}) \Gamma(\mu_{rd}) \overline{\beta}_{sr}^{\mu_{sr}}} \right. \\
& \left(\frac{\mu_{sr}}{\overline{\beta}_{sr}} \gamma + \frac{\mu_i}{\overline{\beta}_i} \right)^{-\frac{\mu_i N + \mu_{sr} + 1}{2}} e^{-\left(\frac{\mu_{sr}}{2\overline{\beta}_{sr}} \gamma + \frac{\mu_i}{2\overline{\beta}_i} \right)} e^{-\left(\frac{\mu_{rd}}{2\overline{\beta}_{rd}} \gamma + \frac{\mu_K}{2\overline{\beta}_K} \right)} \gamma^{\mu_{sr}-1} \\
& W_{\frac{\mu_{sr}-\mu_i N+1}{2}, \frac{-\mu_i N-\mu_{sr}}{2}} \left(\frac{\mu_{sr}}{\overline{\beta}_{sr}} \gamma + \frac{\mu_i}{\overline{\beta}_i} \right) \sum_{u=0}^{\mu_{rd}-1} \left(\frac{\mu_{rd}}{\overline{\beta}_{rd}} \gamma \right)^u \Gamma(\mu_{rd}-u) \\
& \left(\frac{\mu_{rd}}{\overline{\beta}_{rd}} \gamma + \frac{\mu_K}{\overline{\beta}_K} \right)^{-\frac{\mu_K L-u-1}{2}} W_{\frac{-\mu_K L+u+1}{2}, \frac{-\mu_K L-u}{2}} \left(\frac{\mu_{rd}}{\overline{\beta}_{rd}} \gamma + \frac{\mu_K}{\overline{\beta}_K} \right) \\
& + \frac{\mu_{rd}^{\mu_{rd}} \left(\mu_K^{\mu_K} \overline{\beta}_K^{-\mu_K} \right)^L \left(\mu_i^{\mu_i} \overline{\beta}_i^{-\mu_i} \right)^N e^{\left(\frac{\mu_K}{\overline{\beta}_K} \right)} e^{\left(\frac{\mu_i}{\overline{\beta}_i} \right)}}{\Gamma(\mu_{rd}) \Gamma(\mu_{sr}) \overline{\beta}_{rd}^{\mu_{rd}}} \gamma^{\mu_{rd}-1} \\
& \left(\frac{\mu_{rd}}{\overline{\beta}_{rd}} \gamma + \frac{\mu_K}{\overline{\beta}_K} \right)^{-\frac{\mu_K L+\mu_{rd}+1}{2}} e^{-\left(\frac{\mu_{rd}}{2\overline{\beta}_{rd}} \gamma + \frac{\mu_K}{2\overline{\beta}_K} \right)} e^{-\left(\frac{\mu_{sr}}{2\overline{\beta}_{sr}} \gamma + \frac{\mu_i}{2\overline{\beta}_i} \right)} \\
& W_{\frac{\mu_{rd}-\mu_K L+1}{2}, \frac{-\mu_K L-\mu_{rd}}{2}} \left(\frac{\mu_{rd}}{\overline{\beta}_{rd}} \gamma + \frac{\mu_K}{\overline{\beta}_K} \right) \sum_{v=0}^{\mu_{sr}-1} \left(\frac{\mu_{sr}}{\overline{\beta}_{sr}} \gamma \right)^v \Gamma(\mu_{sr}-v) \\
& \left. \left(\frac{\mu_{sr}}{\overline{\beta}_{sr}} \gamma + \frac{\mu_i}{\overline{\beta}_i} \right)^{-\frac{\mu_i N-v-1}{2}} W_{\frac{-\mu_i N+v+1}{2}, \frac{-\mu_i N-v}{2}} \left(\frac{\mu_{sr}}{\overline{\beta}_{sr}} \gamma + \frac{\mu_i}{\overline{\beta}_i} \right) \right] d\gamma \Big|_{s=1}, \quad (2.97)
\end{aligned}$$

2.4.2.1 Average error probability for different fading channel links

Result in (2.97) can be reduced to special cases of the error probability by setting different values of the fading channel coefficients.

2.4.2.1.1 Average error probability for identical fading channel links with

$$\mu = 1$$

Average error probability using BPSK modulation for identical links reduced from (2.97) with assumptions as $\alpha = 2$ and $\mu = 1$, ($L = N = M$), ($\mu_{sr} = \mu_{rd} = \mu_I = \mu_K = 1$), ($\overline{\beta}_{sr} = \overline{\beta}_{rd} = \overline{\beta}$) and ($\overline{\beta}_I = \overline{\beta}_K = \overline{\beta}_I$), can be expressed after mathematical manipulation as

$$\overline{P_e} = \frac{2}{\pi} \int_0^{\frac{\pi}{2}} \int_0^{\infty} e^{-\gamma s} \left[\frac{M\Lambda^{2M}}{(\gamma + \Lambda)^{2M+1}} + \frac{1}{\beta} \left(\frac{\Lambda}{\gamma + \Lambda} \right)^{2M} \right] e^{-\frac{2\gamma}{\beta}} d\gamma d\phi \quad , \quad (2.98)$$

where $(\Lambda = \frac{\overline{\beta}_{sr}}{\beta_I})$, is the average SIR at the Relay node.

the inner integration can be solved using application [47, equation 2.3.4.2], average error probability can then be evaluated as

$$\begin{aligned} \overline{P_e} = \frac{2}{\pi} \int_0^{\frac{\pi}{2}} \left[N\Lambda^{2M} \left(s + \frac{2}{\beta} \right)^{2M} \Gamma \left(-2M, \left(s + \frac{2}{\beta} \right) \Lambda \right) e^{(s+\frac{2}{\beta})\Lambda} \right. \\ \left. + \frac{\Lambda^{2M}}{\beta} \left(s + \frac{2}{\beta} \right)^{2M-1} \Gamma \left(1 - 2M, \left(s + \frac{2}{\beta} \right) \Lambda \right) e^{(s+\frac{2}{\beta})\Lambda} \right] d\phi \quad , \end{aligned} \quad (2.99)$$

using the exponential integral in [48, equation 5.1.45]; i.e $(E_n(x) = x^{n-1}\Gamma(1-n, x))$, the average error probability for identical fading channel coefficient $\mu = 1$ links can be evaluated as

$$\overline{P_e} = \frac{2}{\pi} \int_0^{\frac{\pi}{2}} \left[M E_{2M+1} \left(\Lambda s + \frac{2\Lambda}{\beta} \right) e^{(\Lambda s + \frac{2\Lambda}{\beta})} + \frac{\Lambda}{\beta} E_{2M} \left(\Lambda s + \frac{2\Lambda}{\beta} \right) e^{(\Lambda s + \frac{2\Lambda}{\beta})} \right] d\phi \quad , \quad (2.100)$$

where $E_n(x)$ is the generalized exponential integral, which is defined as in [48, equation 5.1.4]; $(E_n(x) = \int_1^{\infty} \frac{e^{-xt}}{t^n} dt)$.

For BPSK modulation technique, the average error probability is upper bounded as [49, equation 9.27]:

$$\overline{P_e} = M E_{2M+1} \left(\Lambda + \frac{2\Lambda}{\beta} \right) e^{(\Lambda + \frac{2\Lambda}{\beta})} + \frac{\Lambda}{\beta} E_{2M} \left(\Lambda + \frac{2\Lambda}{\beta} \right) e^{(\Lambda + \frac{2\Lambda}{\beta})} \quad , \quad (2.101)$$

2.4.2.1.2 Average error probability for non-identical fading channel links with $\mu = 1$

For non-identical fading channel links with $(L \neq N)$, $(\mu_{sr} = \mu_{rd} = \mu_i = \mu_k = 1)$, $(\bar{\beta}_{sr} \neq \bar{\beta}_{rd})$ and $(\bar{\beta}_i \neq \bar{\beta}_k)$, then the error probability can then be expressed as

$$\begin{aligned} \bar{P}_e = & \int_0^\infty Q(\sqrt{2\gamma}) \left[e^{-\gamma\left(\frac{1}{\bar{\beta}_{rd}} + \frac{1}{\bar{\beta}_{sr}}\right)} \left(\left[\frac{N\Lambda^N}{(\gamma + \Lambda)^{N+1}} + \frac{1}{\bar{\beta}_{sr}} \left(\frac{\Lambda}{\gamma + \Lambda} \right)^N \right] \left(\frac{\Upsilon}{\gamma + \Upsilon} \right)^L \right. \right. \\ & \left. \left. + \left[\frac{L\Upsilon^L}{(\gamma + \Upsilon)^{L+1}} + \frac{1}{\bar{\beta}_{rd}} \left(\frac{\Upsilon}{\gamma + \Upsilon} \right)^L \right] \left(\frac{\Lambda}{\gamma + \Lambda} \right)^N \right) \right] d\gamma \quad , \end{aligned} \quad (2.102)$$

where $(\Lambda = \frac{\bar{\beta}_{sr}}{\bar{\beta}_i})$, is the average SIR at the Relay node, and $(\Upsilon = \frac{\bar{\beta}_{rd}}{\bar{\beta}_k})$, is the average Signal to Interference Ratio (SIR) at the Destination node.

for BPSK modulation scheme , the Error Probability has an upper bound in [49, equation 9.27] is evaluated and mathematically manipulated as

$$\begin{aligned} \bar{P}_e = & \frac{N\Lambda^N\Upsilon^L}{4} \int_0^\infty \frac{e^{-\gamma\left(\frac{1}{\bar{\beta}_{rd}} + \frac{1}{\bar{\beta}_{sr}} + s\right)}}{(\gamma + \Upsilon)^L (\gamma + \Lambda)^{N+1}} d\gamma + \frac{L\Lambda^N\Upsilon^L}{2} \int_0^\infty \frac{e^{-\gamma\left(\frac{1}{\bar{\beta}_{rd}} + \frac{1}{\bar{\beta}_{sr}} + s\right)}}{(\gamma + \Lambda)^N (\gamma + \Upsilon)^{L+1}} d\gamma \\ & + \frac{\Lambda^N\Upsilon^L}{2} \left(\frac{1}{\bar{\beta}_{sr}} + \frac{1}{\bar{\beta}_{rd}} \right) \int_0^\infty \frac{e^{-\gamma\left(\frac{1}{\bar{\beta}_{rd}} + \frac{1}{\bar{\beta}_{sr}} + s\right)}}{(\gamma + \Upsilon)^L (\gamma + \Lambda)^N} d\gamma \Bigg|_{s=1} \quad , \end{aligned} \quad (2.103)$$

using partial fraction, error probability can then be evaluated as

$$\begin{aligned} \bar{P}_e = & \frac{N\Lambda^N\Upsilon^L}{4} \int_0^\infty e^{-\gamma\left(\frac{1}{\bar{\beta}_{rd}} + \frac{1}{\bar{\beta}_{sr}} + s\right)} \left[\frac{a_1}{(\gamma + \Upsilon)^L} + \frac{b_1}{(\gamma + \Lambda)^{N+1}} \right] d\gamma \\ & + \frac{L\Lambda^N\Upsilon^L}{2} \int_0^\infty e^{-\gamma\left(\frac{1}{\bar{\beta}_{rd}} + \frac{1}{\bar{\beta}_{sr}} + s\right)} \left[\frac{a_2}{(\gamma + \Upsilon)^{L+1}} + \frac{b_2}{(\gamma + \Lambda)^N} \right] d\gamma \\ & + \frac{\Lambda^N\Upsilon^L}{2} \left(\frac{1}{\bar{\beta}_{sr}} + \frac{1}{\bar{\beta}_{rd}} \right) \int_0^\infty e^{-\gamma\left(\frac{1}{\bar{\beta}_{rd}} + \frac{1}{\bar{\beta}_{sr}} + s\right)} \left[\frac{a_3}{(\gamma + \Upsilon)^L} + \frac{b_3}{(\gamma + \Lambda)^N} \right] d\gamma \Bigg|_{s=1} \quad , \end{aligned} \quad (2.104)$$

applying the Partial fraction decomposition (2.104) is evaluated as

$$\begin{aligned}
\overline{P}_e = & \frac{N\Lambda^N\Upsilon^L}{4} \int_0^\infty e^{-\gamma\left(\frac{1}{\beta_{rd}} + \frac{1}{\beta_{sr}} + s\right)} \left[\sum_{i_1=1}^L \frac{a_{i_1}}{(\gamma + \Upsilon)^{i_1}} + \sum_{i_2=1}^{N+1} \frac{b_{i_2}}{(\gamma + \Lambda)^{i_2}} \right] d\gamma \\
& + \frac{L\Lambda^N\Upsilon^L}{2} \int_0^\infty e^{-\gamma\left(\frac{1}{\beta_{rd}} + \frac{1}{\beta_{sr}} + s\right)} \left[\sum_{i_3=1}^{L+1} \frac{a_{i_3}}{(\gamma + \Upsilon)^{i_3}} + \sum_{i_4=1}^N \frac{b_{i_4}}{(\gamma + \Lambda)^{i_4}} \right] d\gamma \\
& + \frac{\Lambda^N\Upsilon^L}{2} \left(\frac{1}{\beta_{sr}} + \frac{1}{\beta_{rd}} \right) \int_0^\infty e^{-\gamma\left(\frac{1}{\beta_{rd}} + \frac{1}{\beta_{sr}} + s\right)} \left[\sum_{i_5=1}^L \frac{a_{i_5}}{(\gamma + \Upsilon)^{i_5}} \right. \\
& \left. + \sum_{i_6=1}^N \frac{b_{i_6}}{(\gamma + \Lambda)^{i_6}} \right] d\gamma \Big|_{s=1}, \tag{2.105}
\end{aligned}$$

where the coefficient can be determined as ($a_{ij} = \frac{1}{(k_i-j)!} \lim_{x \rightarrow x_i} \frac{d^{k_i-j}}{dx^{k_i-j}} ((x - x_i)^{k_i})$), which can be expressed as

$$a_{i_1} = \frac{1}{(L - i_1)!} \frac{\partial^{L-i_1}}{\partial \gamma^{L-i_1}} \left[\frac{1}{(\gamma + \Lambda)^{N+1}} \right] \Big|_{\gamma=-\Upsilon}, \tag{2.106a}$$

$$b_{i_2} = \frac{1}{(N - i_2 + 1)!} \frac{\partial^{N-i_2+1}}{\partial \gamma^{N-i_2+1}} \left[\frac{1}{(\gamma + \Upsilon)^L} \right] \Big|_{\gamma=-\Lambda}, \tag{2.106b}$$

$$a_{i_3} = \frac{1}{(L - i_3 + 1)!} \frac{\partial^{L-i_3+1}}{\partial \gamma^{L-i_3+1}} \left[\frac{1}{(\gamma + \Lambda)^N} \right] \Big|_{\gamma=-\Upsilon}, \tag{2.106c}$$

$$b_{i_4} = \frac{1}{(N - i_4)!} \frac{\partial^{N-i_4}}{\partial \gamma^{N-i_4}} \left[\frac{1}{(\gamma + \Upsilon)^{L+1}} \right] \Big|_{\gamma=-\Lambda}, \tag{2.106d}$$

$$a_{i_5} = \frac{1}{(L - i_5)!} \frac{\partial^{L-i_5}}{\partial \gamma^{L-i_5}} \left[\frac{1}{(\gamma + \Lambda)^N} \right] \Big|_{\gamma=-\Upsilon}, \tag{2.106e}$$

$$b_{i_6} = \frac{1}{(N - i_6)!} \frac{\partial^{N-i_6}}{\partial \gamma^{N-i_6}} \left[\frac{1}{(\gamma + \Upsilon)^L} \right] \Big|_{\gamma=-\Lambda}, \tag{2.106f}$$

using application in [47, equation 2.3.4.2] after applying the exponential integral expression in [48, equation 5.1.45], the error probability can then be evaluated after mathematically rearranged as

$$\begin{aligned}
\bar{P}_e = & \frac{\Lambda^N \Upsilon^L}{4} e^{(\Upsilon + \Lambda) \left(\frac{1}{\bar{\beta}_{rd}} + \frac{1}{\bar{\beta}_{sr}} + 1 \right)} \left[\sum_{i_1=1}^L N a_{i_1} E_{i_1} \left(\Upsilon \left(\frac{1}{\bar{\beta}_{rd}} + \frac{1}{\bar{\beta}_{sr}} + 1 \right) \right) \right. \\
& + \sum_{i_2=1}^{N+1} N b_{i_2} E_{i_2} \left(\Lambda \left(\frac{1}{\bar{\beta}_{rd}} + \frac{1}{\bar{\beta}_{sr}} + 1 \right) \right) + \sum_{i_3=1}^{L+1} L a_{i_3} E_{i_3} \left(\Upsilon \left(\frac{1}{\bar{\beta}_{rd}} + \frac{1}{\bar{\beta}_{sr}} + 1 \right) \right) \\
& + \sum_{i_4=1}^N L b_{i_4} E_{i_4} \left(\Lambda \left(\frac{1}{\bar{\beta}_{rd}} + \frac{1}{\bar{\beta}_{sr}} + 1 \right) \right) + \left(\frac{1}{\bar{\beta}_{sr}} + \frac{1}{\bar{\beta}_{rd}} \right) \\
& \times \sum_{i_5=1}^L a_{i_5} E_{i_5} \left(\Upsilon \left(\frac{1}{\bar{\beta}_{rd}} + \frac{1}{\bar{\beta}_{sr}} + 1 \right) \right) + \left(\frac{1}{\bar{\beta}_{sr}} + \frac{1}{\bar{\beta}_{rd}} \right) \\
& \left. \times \sum_{i_6=1}^N b_{i_6} E_{i_6} \left(\Lambda \left(\frac{1}{\bar{\beta}_{rd}} + \frac{1}{\bar{\beta}_{sr}} + 1 \right) \right) \right] .
\end{aligned} \tag{2.107}$$

where the coefficients are defined in (2.106).

2.4.2.1.3 Average error probability for identical fading channel links with $\mu = m$

For identical fading channel links with ($L = N$), ($\mu_{sr} = \mu_{rd} = m$), ($\mu_I = \mu_K = m_I$), ($\bar{\beta}_{sr} = \bar{\beta}_{rd} = \bar{\beta}$) and ($\bar{\beta}_I = \bar{\beta}_K = \bar{\beta}_I$), the error probability for BPSK modulation is given by

$$\begin{aligned}
\bar{P}_e \approx & \frac{1}{\Gamma(m)^2} \left(\frac{m}{\bar{\beta}} \right)^m \left(\frac{m_I}{\bar{\beta}_I} \right)^{2m_I} \sum_{j=0}^m \sum_{v=1}^m \sum_{n=0}^{v-1} \binom{m}{j} \binom{v-1}{n} (lm_I)_j (lm_I)_n \Gamma(m-v+1) \\
& \left(\frac{m}{\bar{\beta}} \right)^{v-1} \int_0^\infty \gamma^{m+v-2} e^{-\gamma \left(s + \frac{2m}{\bar{\beta}} \right)} \left(\frac{m_I}{\bar{\beta}_I} + \frac{m\gamma}{\bar{\beta}} \right)^{-2lm_I-j-n} d\gamma \Big|_{s=1} ,
\end{aligned} \tag{2.108}$$

using application in [47, equation 2.3.6.9], the average error probability can be expressed as

$$\begin{aligned} \bar{P}_e \approx & \frac{1}{\Gamma(m)^2} \sum_{j=0}^m \sum_{v=1}^m \sum_{n=0}^{v-1} \binom{m}{j} \binom{v-1}{n} (lm_I)_j (lm_I)_n \Gamma(m-v+1) \Gamma(m+v-1) \\ & \left(\frac{m_I}{\bar{\beta}_I} \right)^{m+v-1-j-n} U \left(m+v-1, m+v-2lm_I-j-n; \left(\frac{m_I \bar{\beta}}{m \bar{\beta}_I} + \frac{2m_I}{\bar{\beta}_I} \right) \right) \end{aligned} \quad (2.109)$$

2.4.2.1.4 Average error probability for non-identical fading links with

$\mu = m$

The average error probability for non-identical fading links with $\mu_{sr} = m_{sr}, \mu_{rd} = m_{rd}, \mu_i = m_I, \mu_k = m_K, \bar{\beta}_i = \bar{\beta}_I$ and $\bar{\beta}_k = \bar{\beta}_K$ can be expressed after mathematical manipulation as

$$\begin{aligned} \bar{P}_e = & \frac{m_{sr}^{m_{sr}}}{2\Gamma(m_{sr})\Gamma(m_{rd})\bar{\beta}_{sr}^{m_{sr}}} \left(\frac{m_I}{\bar{\beta}_I} \right)^{Nm_I} \left(\frac{m_K}{\bar{\beta}_K} \right)^{Lm_K} \sum_{v=1}^{m_{rd}} \left(\frac{m_{rd}}{\bar{\beta}_{rd}} \right)^{v-1} \Gamma(m_{rd}-v+1) \\ & \sum_{j=0}^{m_{sr}} \sum_{p=0}^{v-1} \binom{m_{sr}}{j} \binom{v-1}{p} (m_I N)_j (m_K L)_p \left(\frac{m_{rd}}{\bar{\beta}_{rd}} \right)^{-p-m_K L} \left(\frac{m_{sr}}{\bar{\beta}_{sr}} \right)^{-j-m_I N} \\ & \sum_{f=0}^{\infty} \sum_{t=0}^{\infty} \left(-\frac{m_K \bar{\beta}_{rd}}{m_{rd} \bar{\beta}_K} \right)^f \left(-\frac{m_I \bar{\beta}_{sr}}{m_{sr} \bar{\beta}_I} \right)^t \int_0^{\infty} e^{-s\gamma} \gamma^{m_{sr}+v-2} e^{-\left(\frac{m_{sr}}{\bar{\beta}_{sr}} + \frac{m_{rd}}{\bar{\beta}_{rd}}\right)\gamma} \\ & \left(\gamma + \frac{m_K \bar{\beta}_{rd}}{m_{rd} \bar{\beta}_K} + \frac{m_I \bar{\beta}_{sr}}{m_{sr} \bar{\beta}_I} \right)^{-s-m_K L-j-m_I N-f-t} d\gamma + \frac{m_{rd}^{m_{rd}}}{2\Gamma(m_{rd})\Gamma(m_{sr})\bar{\beta}_{sr}^{m_{rd}}} \\ & \left(\frac{m_K}{\bar{\beta}_K} \right)^{Lm_K} \left(\frac{m_I}{\bar{\beta}_I} \right)^{Nm_I} \sum_{v=1}^{m_{sr}} \left(\frac{m_{sr}}{\bar{\beta}_{rd}} \right)^{v-1} \Gamma(m_{sr}-v+1) \sum_{j=0}^{m_{rd}} \sum_{p=0}^{v-1} \binom{m_{rd}}{j} \binom{v-1}{p} \\ & (m_K L)_j (m_I N)_p \left(\frac{m_{sr}}{\bar{\beta}_{rd}} \right)^{-p-m_I N} \left(\frac{m_{rd}}{\bar{\beta}_{sr}} \right)^{-j-m_K L} \sum_{f=0}^{\infty} \sum_{t=0}^{\infty} \left(-\frac{m_I \bar{\beta}_{rd}}{m_{sr} \bar{\beta}_I} \right)^f \left(-\frac{m_K \bar{\beta}_{sr}}{m_{rd} \bar{\beta}_K} \right)^t \\ & \int_0^{\infty} e^{-s\gamma} \gamma^{m_{rd}+k-2} e^{-\left(\frac{m_{rd}}{\bar{\beta}_{sr}} + \frac{m_{sr}}{\bar{\beta}_{rd}}\right)\gamma} \left(\gamma + \frac{m_I \bar{\beta}_{rd}}{m_{sr} \bar{\beta}_I} + \frac{m_K \bar{\beta}_{sr}}{m_{rd} \bar{\beta}_K} \right)^{-s-m_I N-j-m_K L-f-t} d\gamma, \end{aligned} \quad (2.110)$$

using application in in [47, equation 2.3.6.9], the error probability function can be expressed as

$$\begin{aligned}
\bar{P}_e &= \frac{m_{sr}^{m_{sr}}}{2\Gamma(m_{sr})\Gamma(m_{rd})\bar{\beta}_{sr}^{m_{sr}}} \left(\frac{m_I}{\bar{\beta}_I}\right)^{Nm_I} \left(\frac{m_K}{\bar{\beta}_K}\right)^{Lm_K} \sum_{v=1}^{m_{rd}} \left(\frac{m_{rd}}{\bar{\beta}_{rd}}\right)^{v-1} \Gamma(m_{rd} - v + 1) \\
&\sum_{j=0}^{m_{sr}} \sum_{p=0}^{v-1} \binom{m_{sr}}{j} \binom{v-1}{p} (m_I N)_j (m_K L)_p \left(\frac{m_{rd}}{\bar{\beta}_{rd}}\right)^{-p-m_K L} \left(\frac{m_{sr}}{\bar{\beta}_{sr}}\right)^{-j-m_I N} \sum_{f=0}^{\infty} \sum_{t=0}^{\infty} \\
&\left(-\frac{m_K \bar{\beta}_{rd}}{m_{rd} \bar{\beta}_K}\right)^f \left(-\frac{m_I \bar{\beta}_{sr}}{m_{sr} \bar{\beta}_I}\right)^t \Gamma(m_{sr} + v - 1) \left(\frac{m_K \bar{\beta}_{rd}}{m_{rd} \bar{\beta}_K} + \frac{m_I \bar{\beta}_{sr}}{m_{sr} \bar{\beta}_I}\right)^{m_{sr} + \rho} \\
U &\left(m_{sr} + vu - 1, m_{sr} + \alpha; \left(\frac{m_{sr}}{\bar{\beta}_{sr}} + \frac{m_{rd}}{\bar{\beta}_{rd}} + 1\right) \left(\frac{m_K \bar{\beta}_{rd}}{m_{rd} \bar{\beta}_K} + \frac{m_I \bar{\beta}_{sr}}{m_{sr} \bar{\beta}_I}\right)\right) \\
&+ \frac{m_{rd}^{m_{rd}}}{2\Gamma(m_{rd})\Gamma(m_{sr})\bar{\beta}_{sr}^{m_{rd}}} \left(\frac{m_K}{\bar{\beta}_K}\right)^{Lm_K} \left(\frac{m_I}{\bar{\beta}_I}\right)^{Nm_I} \sum_{v=1}^{m_{sr}} \left(\frac{m_{sr}}{\bar{\beta}_{rd}}\right)^{v-1} \Gamma(m_{sr} - v + 1) \\
&\sum_{j=0}^{m_{rd}} \sum_{p=0}^{v-1} \binom{m_{rd}}{j} \binom{v-1}{p} (m_K L)_j (m_I N)_p \left(\frac{m_{sr}}{\bar{\beta}_{rd}}\right)^{-p-m_I N} \left(\frac{m_{rd}}{\bar{\beta}_{sr}}\right)^{-j-m_K L} \\
&\sum_{f=0}^{\infty} \sum_{t=0}^{\infty} \left(-\frac{m_I \bar{\beta}_{rd}}{m_{sr} \bar{\beta}_I}\right)^f \left(-\frac{m_K \bar{\beta}_{sr}}{m_{rd} \bar{\beta}_K}\right)^t \Gamma(m_{rd} + v - 1) \left(\frac{m_I \bar{\beta}_{rd}}{m_{sr} \bar{\beta}_I} + \frac{m_K \bar{\beta}_{sr}}{m_{rd} \bar{\beta}_K}\right)^{m_{rd} + \rho} \\
U &\left(m_{rd} + \rho, m_{rd} + \alpha; \left(\frac{m_{sr}}{\bar{\beta}_{sr}} + \frac{m_{rd}}{\bar{\beta}_{rd}} + 1\right) \left(\frac{m_I \bar{\beta}_{rd}}{m_{sr} \bar{\beta}_I} + \frac{m_K \bar{\beta}_{sr}}{m_{rd} \bar{\beta}_K}\right)\right). \tag{2.111}
\end{aligned}$$

where $(\rho = v - 1 - p - m_K L - j - m_I N - f - t)$, $(\alpha = v - p - m_K L - j - m_I N - f - t)$.

2.5 Numerical results

In this section, we present numerical results to validate the analytical expressions derived in Section 2.4 for the outage and error performance of the dual-hop AF relaying system under α - μ fading with co-channel interference at both the relay and destination nodes. The results highlight the impact of key system parameters — fading severity (μ), interference power (INR), and the number of interferers — on the overall system performance. For consistency, the nonlinearity parameter (α) is fixed at ($\alpha = 2$) which corresponds to Rayleigh fading when ($\mu = 1$) and Nakagami- m

fading when ($\mu = m$), while (μ) is varied to examine different fading conditions. All links (dual-hop and interferers) are assumed to experience statistically independent and identical fading channels.

2.5.1 Outage Performance Analysis

The outage probability, defined as the probability that the end-to-end SNR falls below a predefined threshold (γ_{th}), is evaluated for varying average SNR (dB). The results are categorized as follows:

- **Light Fading ($\mu = 1$) with Moderate Interference ($INR = 3dB$):**

Figure 2.2 illustrates the outage performance when $\alpha = 2$ and $\mu = 1$ (Rayleigh fading), and equal-power interferers with $IN = 3dB$. The curves demonstrate how the outage probability degrades as the number of interferers ($N = L$) increases at both the relay and destination nodes. For instance, with $N = L = 2$, the system achieves an outage probability of almost 10^{-1} at $SNR = 20dB$, whereas for $N = L = 10$, the same performance requires $SNR > 25dB$. This confirms that CCI induces a *multiplicative degradation effect*, as the interference power scales with number of interferes links N and L number of interferes at the relay and destination nodes respectively.

- **Moderate Fading ($\mu = 2$) with Strong Interference ($INR = 12dB$):**

Figure 2.3 examines a more favorable fading scenario ($\mu = 2$) but under stronger interference power with value of ($INR = 12dB$). Here, the diversity gain from higher μ mitigates fading severity, but the elevated interference power dominates at high SNR, leading to an *error floor*. For example, with $N = L = 4$, the outage probability value of 10^{-1} for $SNR > 25dB$.

- **Impact of Interference Power Disparity:**

Figure 2.4 investigates the case where interferers have unequal power levels (e.g., INR values of 3 dB, 6 dB, 9 dB, and 12 dB) for $\alpha = 2$, $\mu = 2$. The results

reveal that the high-power interferer (e.g., 6 interferers with $INR = 12$ dB) can degrade performance more severely than multiple low-power interferers (e.g., 5 interferers with $INR = 12$ dB each). This emphasizes how crucial the role of *dominant interferers* are in system design

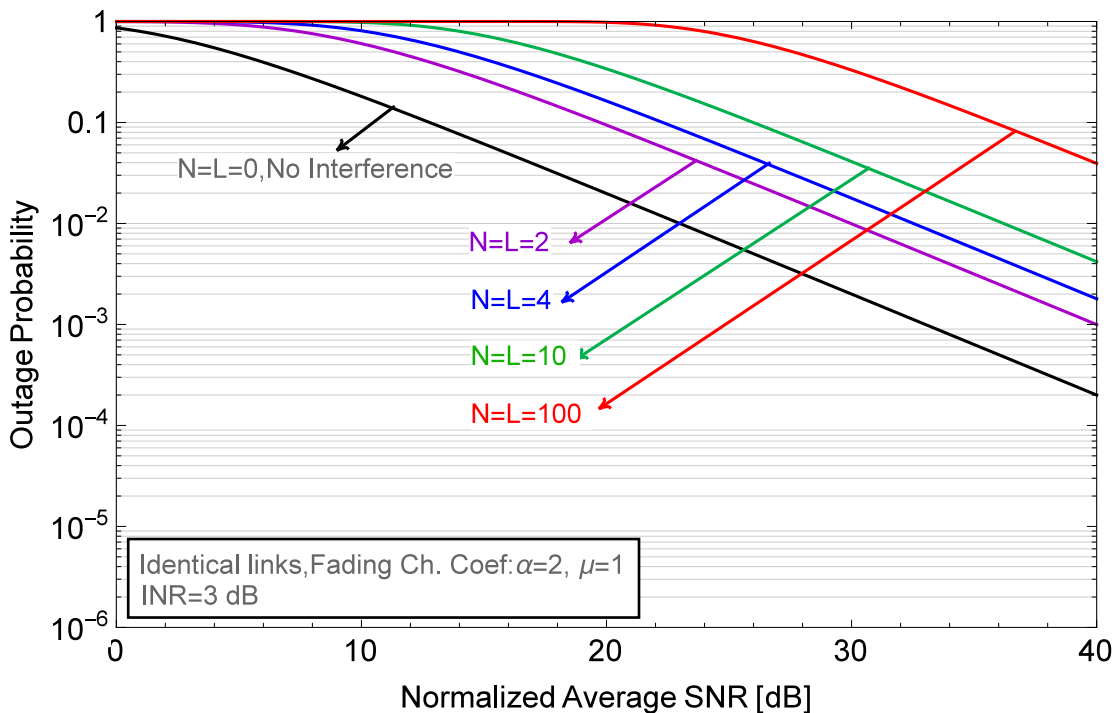


Figure 2.2: Dual-hop outage probability for $\alpha = 2$, $\mu = 1$, $INR = 3$ dB .

2.5.2 Error Performance Analysis

The bit error rate (BER) for coherent BPSK modulation is evaluated to further quantify the system's reliability. Key observations include:

- **BER Floor Due to CCI:**

Figures 2.5 and 2.6 demonstrate that the BER curves exhibit an irreducible floor at high SNR. For $\mu = 1$ and $INR = 30$ dB presented in (Figure 2.5), the BER floor rises from 10^{-3} to 10^{-2} as $N = L$ increases from 1 to 10. This aligns with the outage results, emphasizing that interference—not noise—governs performance at practical SNR levels.

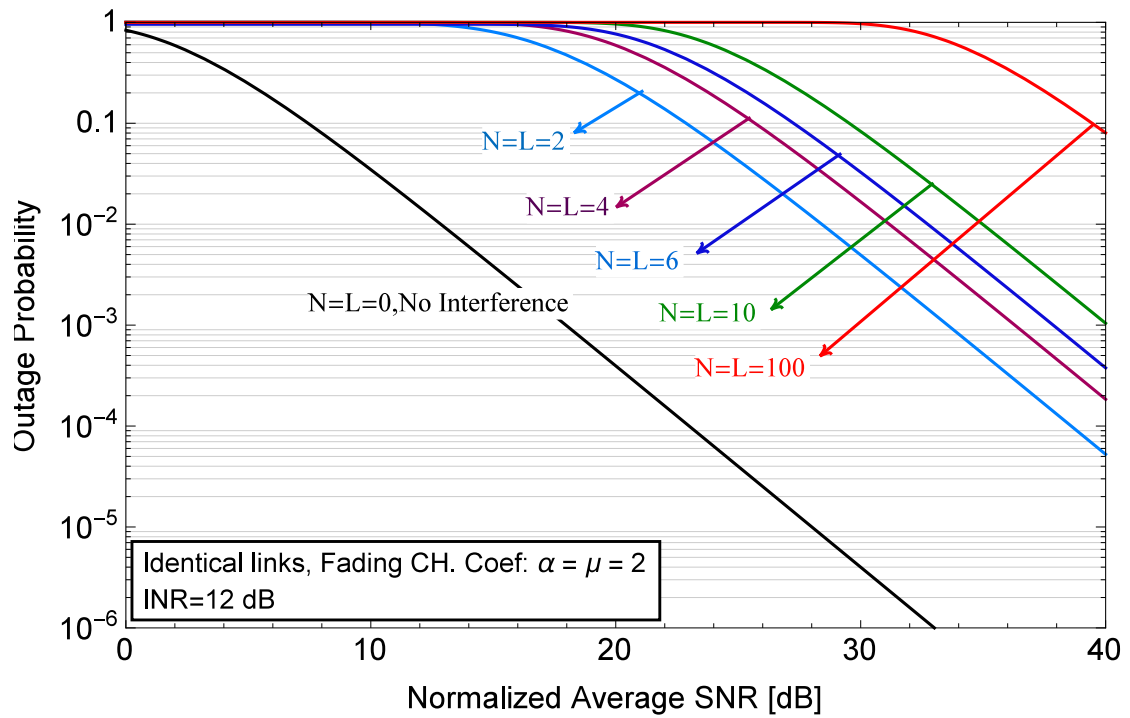


Figure 2.3: Dual-hop outage probability for $\alpha = 2$, $\mu = m = 2$, $INR = 12$ dB .

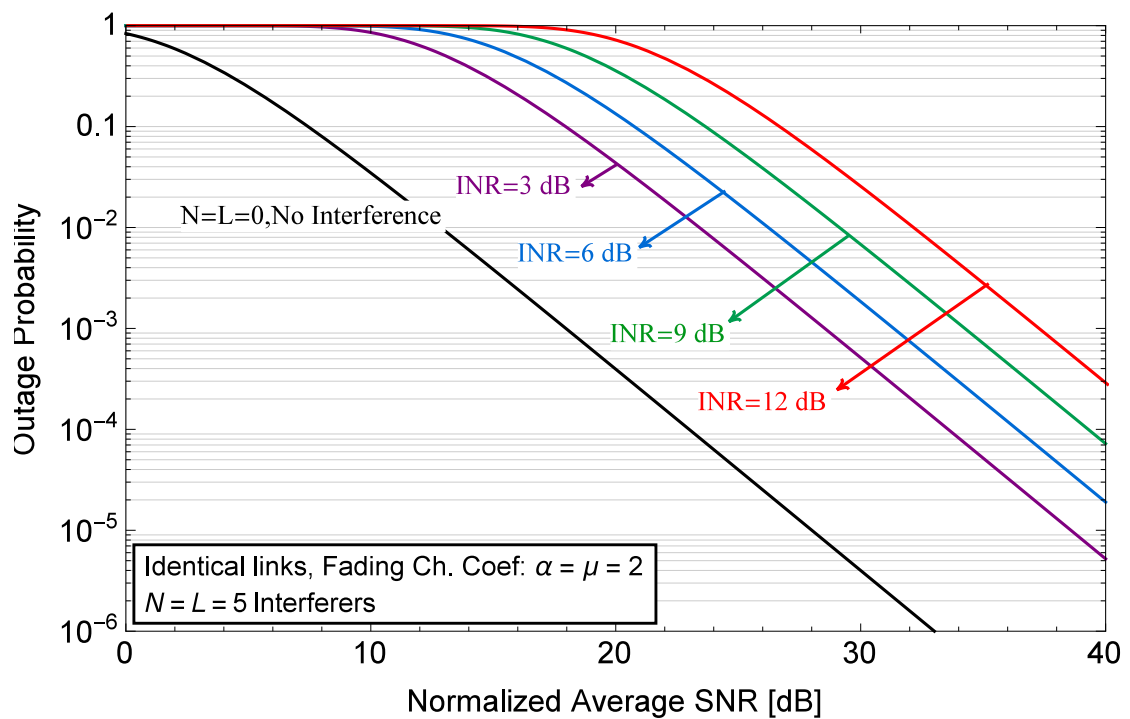


Figure 2.4: Dual-hop outage probability for $\alpha = 2$, $\mu = m = 2$ and $N = L = 5$

- **Fading Severity Trade-offs:**

Figure 2.6 ($\mu = 2$) shows improved BER compared to Figure 2.5 ($\mu = 1$) due to reduced fading depth. However, the interference-limited floor persists, suggesting that while fading mitigation helps, CCI remains the primary bottleneck.

- **Interferer Fading Sensitivity:**

Figure 2.7 highlights the impact of interferers fading parameters (α, μ) on BER. When the interferers experience severe fading (e.g. $\mu = 1$), the system performance degrades significantly compared to milder fading ($\mu = 2$). This is because lower μ increases the likelihood of deep fades in interferer links, causing severe interference effect.

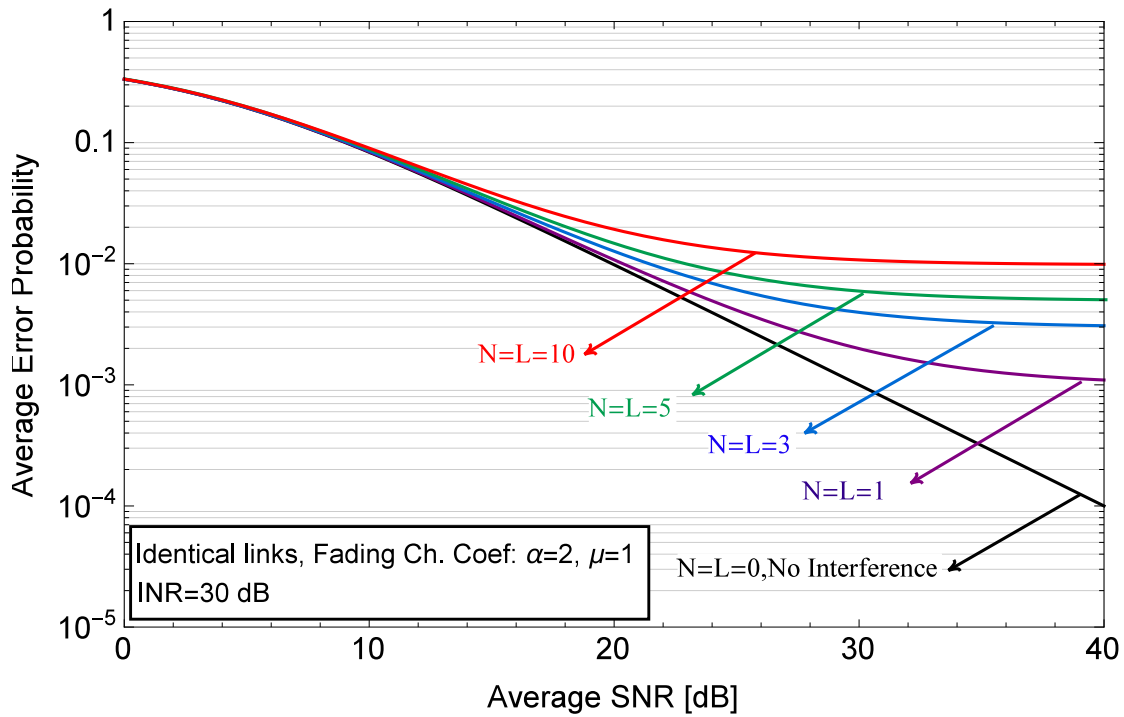


Figure 2.5: Average error probability for identical number of fading channel with $\alpha = 2$ and $\mu = 1$.

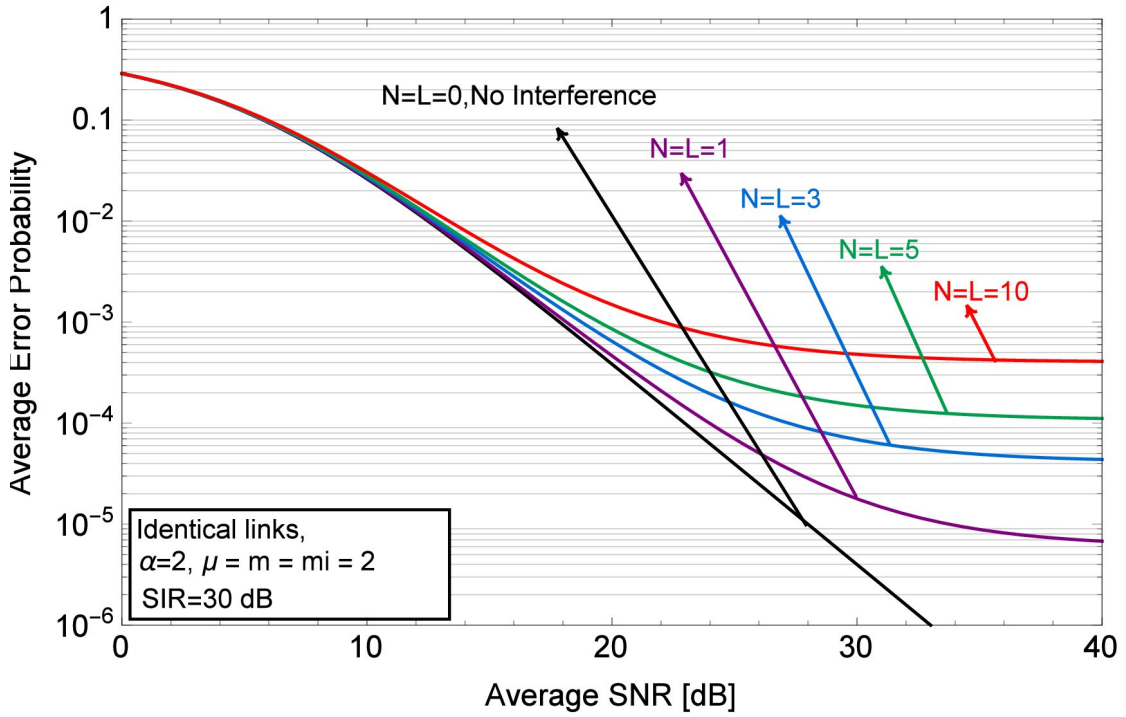


Figure 2.6: Average error probability for identical number of fading channel with $\alpha = 2$, $\mu = m = 2$ and $N = L = 4$ interferers

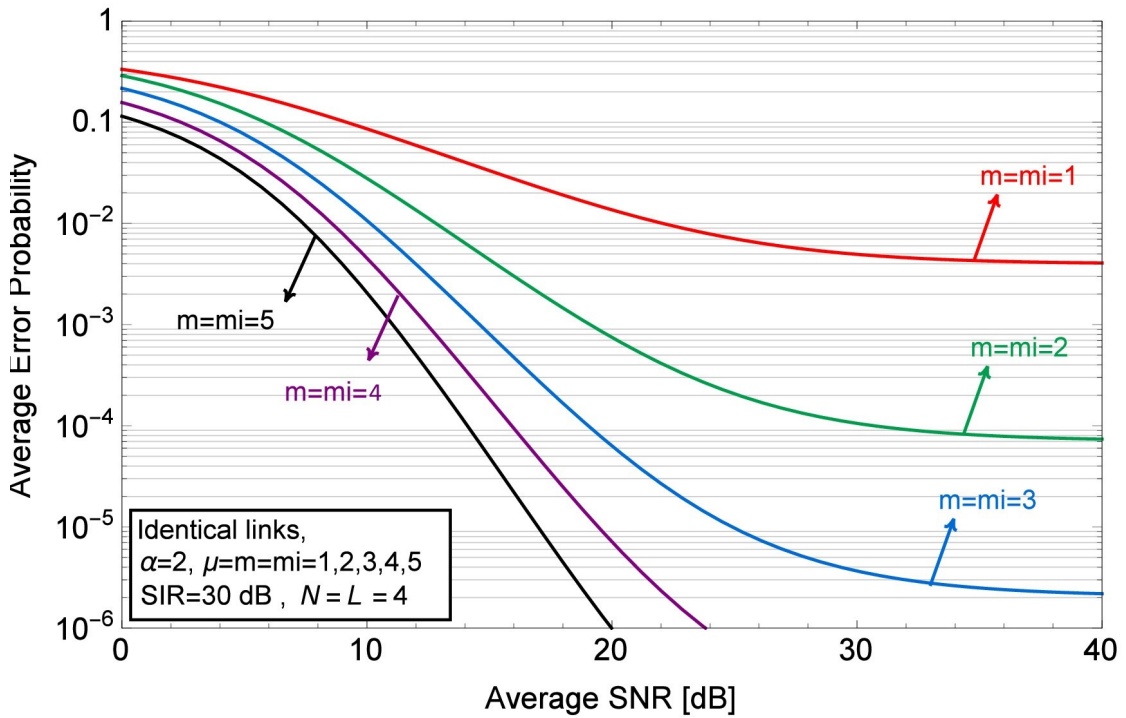


Figure 2.7: Average error probability for identical number of fading channel with $\alpha = 2$, different fading parameters $\mu = m = 1, 2, 3, 4, 5$

2.6 Conclusion

This chapter has presented a comprehensive analytical framework for evaluating the performance of dual-hop amplify-and-forward (AF) relaying systems operating in generalized α - μ fading channels with co-channel interference (CCI). The key contributions and findings include the derivation of novel analytical expressions, specifically exact closed-form expressions for the PDF and CDF of the upper-bound SINR, which enable efficient computation of outage and error probabilities using the moment generating function (MGF) approach to characterize aggregate interference from N IID interferers. The generality of the α - μ model was demonstrated, as the derived results encompass classical fading scenarios such as Rayleigh fading ($\alpha = 2$, $\mu = 1$) and Nakagami- m fading ($\alpha = 2$, $\mu = m$), with numerical validation confirming exact alignment with prior literature for these special cases. The study also examined the impact of interference, revealing significant performance degradation with increasing interferers (N), including higher outage probabilities due to reduced SINR and the formation of error floors in interference-limited regimes. Additionally, the results provide practical insights by quantifying the fundamental trade-off between diversity gain (determined by α - μ fading parameters) and interference-induced degradation, offering valuable guidelines for system design in interference-heavy environments. Overall, the proposed framework serves as a foundation for analyzing next-generation relaying systems in generalized fading environments with practical interference conditions.

Glossary — Chapter 2

Term	Description	Page
E_b	The bit energy.	17
P_{out}	The Outage Probability of the dual-hop relay network	39
f_c	The carrier frequency of the transmitted signal.	16
g_k	The α - μ flat fading coefficient of the k-th interference channel at the destination node	13
$h(t)$	The amplitude of the received signal from the fading link.	16
h_i	The α - μ flat fading coefficient of the i -th interference channel at the relay node	12
h_{rd}	The channel flat fading coefficient of $R \rightarrow D$ link	13
h_{sr}	The channel flat fading coefficient of $S \rightarrow R$ link	12
$n(t)$	The complex envelope Gaussian noise with zero mean and power spectral density N_o .	16
$r(t)$	The received equivalent lowpass signal in one signaling interval.	16
$s_l(t)$	The complex envelope of the transmitted signal $s(t)$	16
$u(t)$	The transmitted signal $s(t)$	16
E_R	The energy of the transmitted signal from the Relay node	13
E_S	The energy of the transmitted signal from the Source node	12
E_i	The i -th interference channel energy received at the relay node	12
E_k	The k-th interference channel energy received at the destination node	13

Term	Description	Page
d_S	The desired transmitted data from the source node with unit energy	12
d_i	The transmitted data from relay node with unit energy	12
d_k	The k-th co-channel interferer's data with unit energy at the destination	13
n_{rd}	The Additive White Gaussian Noise at the destination node	13
n_{sr}	The Additive White Gaussian Noise at the relay node	12
x_i	The α - μ flat fading coefficient of the i -th interference channel at the relay node	12
$\bar{\beta}_I$	The average SNR for each of the i.i.d interferers links at relay node.	23
$\bar{\beta}_K$	The average SNR for each of the i.i.d interferers links at destination node.	26
γ_{h_i}	The SNR for a single i -th interferer link.	21
$\Gamma(z)$	The Gamma function	15
$M_{\gamma_{h_i}}(s)$	The MGF for each single i -th interferer link SNR (γ_{h_i}).	21
μ	The normalized variance of ψ^α	15
$P_b(\gamma)$	The error probability for a given given signal-to-noise ratio γ .	42
$f_{\gamma_{h_i}}(\gamma)$	The PDF for each single i -th interferer link SNR (γ_{h_i}).	21
$\sum_{i=1}^N \gamma_{h_i}$	The PDF of joint sum of (γ_{h_i}) SNR.	21
$\theta(t)$	The phase of the received signal from the fading link ($\theta = -2\pi f_c \tau(t)$).	16
$\hat{\psi}$	The α root mean value	15

Chapter 3

Impact of co-channel interference on the performance of cooperative diversity systems

3.1 Introduction

Wireless communication has undergone a tremendous revolution in the recent years, where cooperative diversity is a promising means to enhance the network coverage and data throughput. Moreover, it can cope with the effect of the Small Scale Fading where unpredictable and rapid fluctuations of the received signal levels can cause the degradation of throughput.

Many researches targeted the cooperative diversity of the relay networks in their investigations, such as the study in [18] where the authors investigated the performance of cooperative diversity networks with amplify-and-forward (AF) relaying and equal gain combining (EGC) techniques, which is used to combine the signal from the source and the relay nodes at the destination node. The results in [18] were extended to investigate the Nakagami-m Fading Channels case except that several relay nodes were introduced to the cooperative diversity network under investigation as in [19]. The authors of [18] and [19], focused on the cooperative relay network without the presence of the co-channel interference (CCI) at either node of the network under investigation, and they assumed that the source and destination nodes are connected through direct link. In [20], best-relay selection scheme was introduced, where the destination receives two copies of the source signal; one from the source node (direct link), and the other from the best relay node. Then the authors employed the maximum ratio combining (MRC) at the destination node to combine the both signal copies received, the fading channel is assumed to be Rayleigh model and the researches did not consider the effect of CCI in their investigation.

The effect of the presence of CCI on the performance of cooperative diversity networks was investigated in [21], assuming Optimum Combining (OC) technique over Rayleigh fading channels and the authors employed the decode-and-forward

relaying schema in the network settings. Additional investigation of CCI was considered in work [22], where the authors analyzed the performance of the DF cooperative relaying systems over Nakagami fading channels in terms of the outage probability, and implementing Maximal Ratio combining (MRC). Moreover, the authors of [23], derived the exact-form expressions for the outage probability of the cooperative diversity network over Nakagami-m fading channels while implementing DF relaying schema. They studied the effect of CCI presence at both the relay and destination nodes.

In this chapter, we extended the investigation in chapter 2 and represented in paper [P2] by introducing cooperative diversity to the proposed network, we added multiple relay nodes between the source and destination nodes. The impact of the presence of CCI at the network was investigated by deriving the error and outage probabilities of the network over α - μ fading channels, while using the selective combining schema to get the signal from the best relay link assuming that there is no direct link between the source and destination nodes. In addition, we develop the mathematical formulas of the probability density function in addition to the cumulative distribution function of the signal-to-interference-and-noise ratio of the cooperative diversity network.

The rest of this chapter is organized as follows. Section 3.2 describes the system and channel models. Section 3.3 presents the analysis of the cooperative diversity SINR. Section 3.4 presents the system performance analysis. Numerical results are given in Section 3.5. Finally, Section 3.6 concludes this chapter.

3.2 System Model

In this letter, we propose a cooperative network which consists of a source node S , a destination node D and M -number active relay nodes R_j for $j = 1, \dots, M$, shown in figure (3.1). It is assumed that the j -th relay node is subjected to N -number interferers, and the destination node is subject to L interferers, respectively. For the proposed cooperative network, the transmission occurs in two stages as follows.

- The first stage represent broadcasting the signal from the source node, which accordingly is received by the active relay nodes that are willing to participate in the transmission.
- The second stage, each relay node perform amplification of the received signal then forwards it to the destination node. Correspondingly the relaying technique used in this stage is the Amplify-and-Forward relaying schema.

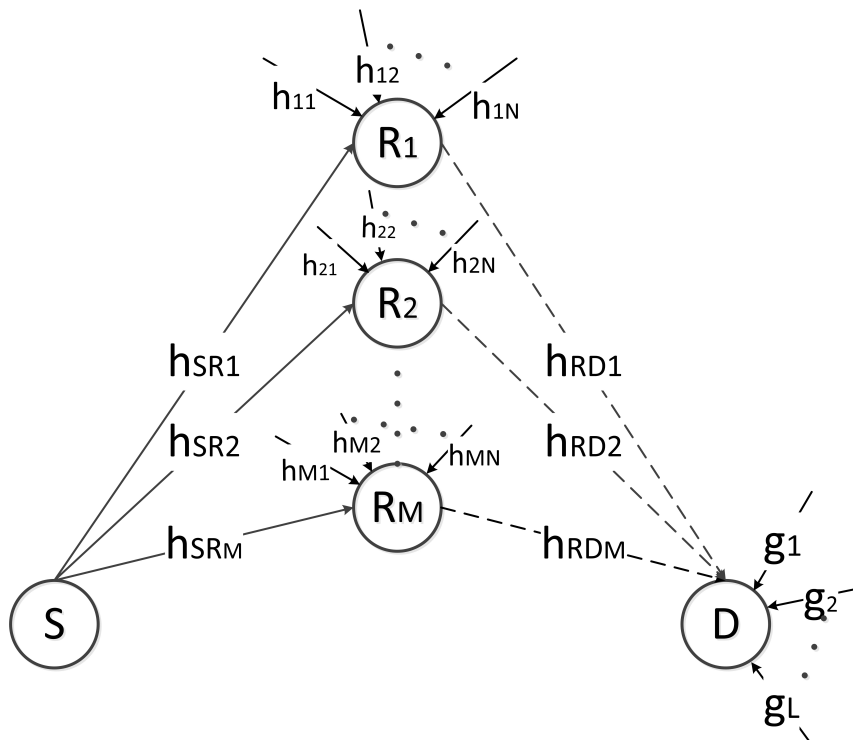


Figure 3.1: Cooperative Diversity Relay Network

The received signal at the j -th relay in the first stage of the transmission, assuming that the relay and destination nodes are both corrupted by

interference, is denoted by

$$y_{sr_j}(t) = \sqrt{E_{sr_j}} h_{sr_j} d_{sr_j}(t) + \sum_{i=1}^{N_j} \sqrt{E_{ji}} h_{ji} d_{ji}(t) + n_{r_j}(t) \quad (3.1)$$

where h_{sr_j} is the channel fading coefficient of the transmitted data $d_{sr_j}(t)$ from the source to the j -th relay node and with average transmitted energy of E_{sr_j} . $d_{ji}(t)$ is the received data from the j -th interferer of the j -th relay node with average transmitted energy of E_{ji} . h_{ji} is the channel gain of the Co-Channel Interference link. Finally, the n_{r_j} represents the AWGN at the j -th relay node, and is considered to have zero-mean and variance $N_o \sim CN(0, N_o)$.

The received signal at the destination node from the j -th relay is denoted by

$$y_{r_jd}(t) = G_{AF_j} \sqrt{E_{r_j}} h_{r_jd} d_{r_j}(t) \times y_{sr_j}(t) + \sum_{k=1}^L \sqrt{E_k} g_k d_k(t) + n_d(t), \quad (3.2)$$

where h_{r_jd} is the channel fading coefficient from the j -th relay to the destination link, $d_{r_j}(t)$ is the transmitted data from the j -th relay node and has average transmitted energy of E_{r_j} . And g_k is the channel gain of the Co-Channel interference link at the destination node, $d_k(t)$ is the k -th interferer's data at the destination with average energy of E_k . The AWGN is represented as $n_d(t)$, and is modeled as zero-mean and variance $N_o \sim CN(0, N_o)$. G_{AF_j} is the amplification gain of the j -th relay, and is chosen to normalized the transmitted signal energy at the j -th relay node denoted by E_{r_j} , the amplification gain and known as the scaling factor is given by

$$G_{AF_j} = \sqrt{\frac{E_{r_j}}{E_{sr_j} \|h_{sr_j}\|^2 + \sum_{j,i=1}^{N_j} E_{ji} \|h_{ji}\|^2 + N_o}}, \quad (3.3)$$

The $\|h_{sr_j}\|^2$ and $\|h_{ji}\|^2$ represent the channel gain of the S-R and the j -th interference links respectively.

Substituting equation (3.1) into equation (3.2) the signal received at the destination is expressed by

$$y_{r_j d}(t) = G_{AF_j} \sqrt{E_{r_j d}} h_{r_j d} d_{r_j}(t) \left(\sqrt{E_{sr_j}} h_{sr_j} d_{sr_j}(t) + \sum_{i=1}^{N_j} \sqrt{E_{ji}} h_{ji} d_{ji}(t) + n_{r_j}(t) \right) + \sum_{k=1}^L \sqrt{E_k} g_k d_k(t) + n_d(t), \quad (3.4)$$

In (3.4) by defining $I_{r_j}(t)$ to represent interference at the j -th relay node, and denoted by

$$I_{r_j}(t) = \sum_{i=1}^{N_j} \sqrt{E_{ji}} h_{ji} d_{ji}(t), \quad \text{for } i = 1, 2, \dots, M \quad (3.5)$$

By defining the interferences, equation 3.4 can be rewritten as

$$y_{r_j d}(t) = G_{AF_j} \sqrt{E_{r_j d}} h_{r_j d} d_{r_j}(t) \left(\sqrt{E_{sr_j}} h_{sr_j} d_{sr_j}(t) + I_{r_j}(t) + n_{r_j}(t) \right) + \sum_{k=1}^L \sqrt{E_k} g_k d_k(t) + n_d(t), \quad (3.6)$$

and after some mathematical manipulation, the received signal at the destination node D from the j -th relay node r_j can be expressed as

$$y_{r_j d}(t) = G_{AF_j} \sqrt{E_{r_j d}} h_{r_j d} h_{sr_j} d_{r_j}(t) d_{sr_j}(t) + G_{AF_j} h_{r_j D} d_{r_j}(t) \sum_{i=1}^{N_j} \sqrt{E_{ji}} d_{ji}(t) h_{ji} + G_{AF_j} \sqrt{E_{r_j d}} h_{r_j d} d_{r_j}(t) n_{r_j}(t) + \sum_{k=1}^L g_k d_k(t) + n_{r_j D}(t). \quad (3.7)$$

The interference $I_D(t)$ can be denoted by

$$I_D(t) = G_{AF_j} h_{r_j D} d_{r_j}(t) \sum_{i=1}^{N_j} \sqrt{E_{ji}} d_{ji}(t) h_{ji} + \sum_{k=1}^L \sqrt{E_k} g_k d_k(t), \quad (3.8)$$

Finally, equation (3.7), can be represented by

$$y_{r_j d}(t) = G_{AF_j} h_{r_j d} h_{sr_j} \sqrt{E_{r_j}} d_{r_j}(t) d_{sr_j}(t) + G_{AF_j} h_{r_j d} \sqrt{E_{r_j}} d_{r_j}(t) n_{r_j}(t) + I_D(t) + n_{r_j D}(t). \quad (3.9)$$

The best-relay and direct link statistical properties (PDF, CDF) will be derived in the following section.

3.3 Cooperative diversity SINR analysis

In this chapter, I will introduce the Selective Combining (SC) technique at the destination node D , where the branch with the highest SINR is chosen as the output SINR to be used in the next stage of calculations. In this section I will derive the end-to-end Signal-to-noise ratio which is mathematically defined as the ratio of signal power to the noise power, measured within the same receiver bandwidth. The SINR at the combiner output of the destination node is a result of the best-relay SINR, and can be expressed as

$$\gamma_d = \max_j (\gamma_{sr_j d}), \quad (3.10)$$

where $\gamma_{sr_j d}$ is the received SINR from the j -th indirect path ($S \rightarrow R_j \rightarrow D$), and it can be derived after substituting the value of the amplification gain G_{AF_j} which is given in (3.3), then dividing both the nominator and denominator by N_o^2 then by $(1 + \sum_{j=1}^{N_i} \gamma_{ji}) \times (1 + \sum_{k=1}^L \gamma_k)$, the SINR can be derived and simplified as

$$\gamma_{sr_j d} = \frac{\gamma_{sr_j}^{eff} \gamma_{r_j d}^{eff}}{\gamma_{sr_j}^{eff} + \gamma_{r_j d}^{eff} + 1}. \quad (3.11)$$

where the effective SINR for the $S \rightarrow R_j$ and the $R_j \rightarrow D$ links are defined as

$$\gamma_{sr_j}^{eff} = \frac{\gamma_{sr_j}}{1 + \sum_{i=1}^{N_j} \gamma_{ji}}, \quad (3.12a)$$

$$\gamma_{r_jd}^{eff} = \frac{\gamma_{r_jd}}{1 + \sum_{k=1}^L \gamma_k}, \quad (3.12b)$$

To have an attractable mathematical for of the performance metrics as the outage and error probability for the network, tight upper bound for γ_d was adopted such that:

$$\gamma_d \leq \max_j \left(\min_j \left(\gamma_{sr_j}^{eff}, \gamma_{r_jd}^{eff} \right) \right) . \quad (3.13)$$

The PDF of the relay link SINR $\left(\min_j \left(\gamma_{sr_j}^{eff}, \gamma_{r_jd}^{eff} \right) \right)$ is evaluated and given by equation 2.68. Moreover, the CDF is derived and expressed in equation 2.80. The next step is to derive the statistical characteristics (CDF) of the best-relay node SINR (γ_d). The CDF of γ_d is mathematically represented as

$$F_{\gamma_d}(\gamma) = \prod_j^M F_{\gamma_j}(\gamma) , \quad (3.14)$$

the $S \rightarrow R \rightarrow D$ link CDF derived in section 2.3.4 and the formula computed in equation 2.75,, then the best-relay CDF can be derived as

$$\begin{aligned}
F_{\gamma_d}(\gamma) &= \prod_j^M \left(1 - \frac{\left(\frac{\mu_{I_j}}{\beta_{I_j}} \bar{\beta}_{I_j}^{-\mu_{I_j}} \right)^{N_j} \left(\frac{\mu_K^{\mu_K} \bar{\beta}_K^{-\mu_K} \right)^L e^{\left(\frac{\mu_{I_j}}{\beta_{I_j}} + \frac{\mu_K}{\beta_K} \right) \gamma}}{\Gamma(\mu_{sr_j}) \Gamma(\mu_{r_j d})} e^{-\frac{1}{2} \left(\left(\frac{\mu_{sr_j}}{\beta_{sr_j}} + \frac{\mu_{r_j d}}{\beta_{r_j d}} \right) \gamma + \left(\frac{\mu_{I_j}}{\beta_{I_j}} + \frac{\mu_K}{\beta_K} \right) \right)} \right) \\
&\times \left(\frac{\mu_{sr_j}}{\beta_{sr_j}} \gamma + \frac{\mu_{I_j}}{\beta_{I_j}} \right)^{\frac{-\mu_{I_j} N_j - v - 1}{2}} \sum_{v=0}^{\mu_{sr_j} - 1} \sum_{u=0}^{\mu_{r_j d} - 1} \left(\frac{\mu_{sr_j}}{\beta_{sr_j}} \gamma \right)^v \left(\frac{\mu_{r_j d}}{\beta_{r_j d}} \gamma \right)^u \Gamma(\mu_{sr_j} - v) \\
&\times \Gamma(\mu_{r_j d} - u) \left(\frac{\mu_{r_j d}}{\beta_{r_j d}} \gamma + \frac{\mu_K}{\beta_K} \right)^{\frac{-\mu_K L - u - 1}{2}} W_{\frac{-\mu_{I_j} N_j + v + 1}{2}, \frac{-\mu_{I_j} N_j - k}{2}} \left(\frac{\mu_{sr_j}}{\beta_{sr_j}} \gamma + \frac{\mu_{I_j}}{\beta_{I_j}} \right) \\
&\times W_{\frac{-\mu_K L + u + 1}{2}, \frac{-\mu_K L - u}{2}} \left(\frac{\mu_{r_j d}}{\beta_{r_j d}} \gamma + \frac{\mu_K}{\beta_K} \right) \Big) \Big) \tag{3.15}
\end{aligned}$$

equation (3.15) can be expressed after substituting the definition of Whittaker function in (2.62) as

$$\begin{aligned}
F_{\gamma_d}(\gamma) &= \prod_j^M \left[1 - \frac{\left(\frac{\mu_j^{\mu_j} \bar{\beta}_j^{-\mu_j}} \right)^{N_j} \left(\frac{\mu_K^{\mu_K} \bar{\beta}_K^{-\mu_K} \right)^L m^{-\left(\frac{\mu_{sr_j}}{\beta_{sr_j}} + \frac{\mu_{r_j d}}{\beta_{r_j d}} \right) \gamma}}{\Gamma(\mu_{sr_j}) \Gamma(\mu_{r_j d})} e^{-\left(\frac{\mu_{sr_j}}{\beta_{sr_j}} + \frac{\mu_{r_j d}}{\beta_{r_j d}} \right) \gamma} \sum_{u=0}^{\mu_{sr_j} - 1} \sum_{v=0}^{\mu_{r_j d} - 1} \right. \\
&\left. \left(\frac{\mu_{sr_j}}{\beta_{sr_j}} \gamma \right)^u \left(\frac{\mu_{r_j d}}{\beta_{r_j d}} \gamma \right)^v U \left(\mu_j N_j, 1 + \mu_j N_j + u, \left(\frac{\mu_{sr_j}}{\beta_{sr_j}} \gamma + \frac{\mu_j}{\beta_j} \right) \right) \right. \\
&\left. \Gamma(\mu_{sr_j} - u) \Gamma(\mu_{r_j d} - v) U \left(\mu_K L, 1 + \mu_K L + v, \left(\frac{\mu_{r_j d}}{\beta_{r_j d}} \gamma + \frac{\mu_K}{\beta_K} \right) \right) \right] \tag{3.16}
\end{aligned}$$

using the series representation of the Confluent Hypergeometric function in (2.65), the CDF can be evaluated as

$$\begin{aligned}
F_{\gamma_d}(\gamma) &= \prod_j^M \left[1 - \frac{\left(\frac{\mu_j^{\mu_j} \bar{\beta}_j^{-\mu_j}} \right)^{N_j} \left(\frac{\mu_K^{\mu_K} \bar{\beta}_K^{-\mu_K} \right)^L}{\Gamma(\mu_{sr_j}) \Gamma(\mu_{r_j d})} \sum_{v=1}^{\mu_{sr_j}} \sum_{u=1}^{\mu_{r_j d}} \sum_{q=0}^{v-1} \sum_{t=0}^{u-1} \binom{v-1}{q} \right. \\
&\left. \binom{u-1}{t} (\mu_j N_j)_q (\mu_K L)_t \Gamma(\mu_{sr_j} - v + 1) \Gamma(\mu_{r_j d} - u + 1) \left(\frac{\mu_{sr_j}}{\beta_{sr_j}} \right)^{v-1} \left(\frac{\mu_{r_j d}}{\beta_{r_j d}} \right)^{u-1} \right. \\
&\left. \gamma^{v+u-2} e^{-\left(\frac{\mu_{sr_j}}{\beta_{sr_j}} + \frac{\mu_{r_j d}}{\beta_{r_j d}} \right) \gamma} \left(\frac{\mu_{sr_j}}{\beta_{sr_j}} \gamma + \frac{\mu_j}{\beta_j} \right)^{-q - \mu_j N_j} \left(\frac{\mu_{r_j d}}{\beta_{r_j d}} \gamma + \frac{\mu_K}{\beta_K} \right)^{-t - \mu_K L} \right] \tag{3.17}
\end{aligned}$$

using the binomial expansion, the CDF is computed and manipulated as

$$\begin{aligned}
F_{\gamma_d}(\gamma) = & \prod_j^M \left[1 - \frac{1}{\Gamma(\mu_{cf})\Gamma(\mu_{r_j d})} \sum_{v=1}^{\mu_{sr_j}} \sum_{u=1}^{\mu_{r_j d}} \sum_{q=0}^{v-1} \sum_{t=0}^{u-1} \sum_{p=0}^{\infty} \sum_{r=0}^{\infty} \binom{v-1}{q} \binom{u-1}{t} \right. \\
& \binom{-q - \mu_j N_j}{p} \binom{-t - \mu_K L}{r} (\mu_J N_j)_v (\mu_K L)_t \Gamma(\mu_{sr_j} - v + 1) \Gamma(\mu_{r_j d} - u + 1) \\
& \left. \left(\frac{\mu_{sr_j}}{\beta_{sr_j}} \right)^{v+p-1} \left(\frac{\mu_{r_j d}}{\beta_{r_j d}} \right)^{u+r-1} \left(\frac{\mu_{h_{I_i}}}{\beta_j} \right)^{-q-p} \left(\frac{\mu_K}{\beta_K} \right)^{-t-r} \gamma^{v+u+p+r-2} e^{-\left(\frac{\mu_{sr_j}}{\beta_{sr_j}} + \frac{\mu_{r_j d}}{\beta_{r_j d}} \right) \gamma} \right]
\end{aligned} \tag{3.18}$$

The PDF can then be derived by taking the derivation of (3.15) with respect to γ , both the definitions of Whittaker function W expressed in [41, Eq. 13.14.3] and Confluent Hypergeometric function represented in [41, Eq. 13.2.8] were used. In addition for applying the generalization rule for the derivation of collection product of function defined as $\{f_i\}_{i=1}^k$ and expressed in:

$$\frac{d}{dx} \left[\prod_{i=1}^k f_i(x) \right] = \sum_{i=1}^k \left(\frac{d}{dx} f_i(x) \prod_{j \neq i} f_j(x) \right) = \left(\prod_{i=1}^k f_i(x) \right) \left(\sum_{i=1}^k \frac{f'_i(x)}{f_i(x)} \right) \tag{3.19}$$

the PDF can then be derived and mathematically expressed as

$$\begin{aligned}
f_{\gamma_d}(\gamma) = & \frac{d}{d\gamma} \left[\prod_j^M \left[1 - \frac{1}{\Gamma(\mu_{cf})\Gamma(\mu_{r_j d})} \sum_{v=1}^{\mu_{sr_j}} \sum_{u=1}^{\mu_{r_j d}} \sum_{q=0}^{v-1} \sum_{t=0}^{u-1} \sum_{p=0}^{\infty} \sum_{r=0}^{\infty} \binom{v-1}{q} \binom{u-1}{t} \right. \right. \\
& \binom{-q - \mu_j N_j}{p} \binom{-t - \mu_K L}{r} (\mu_J N_j)_v (\mu_K L)_t \Gamma(\mu_{sr_j} - v + 1) \Gamma(\mu_{r_j d} - u + 1) \\
& \left. \left. \left(\frac{\mu_{sr_j}}{\beta_{sr_j}} \right)^{v+p-1} \left(\frac{\mu_{r_j d}}{\beta_{r_j d}} \right)^{u+r-1} \left(\frac{\mu_j}{\beta_j} \right)^{-q-p} \left(\frac{\mu_K}{\beta_K} \right)^{-t-r} \gamma^{v+u+p+r-2} e^{-\left(\frac{\mu_{sr_j}}{\beta_{sr_j}} + \frac{\mu_{r_j d}}{\beta_{r_j d}} \right) \gamma} \right] \right],
\end{aligned} \tag{3.20}$$

applying the generalization rule for the derivation of collection product of function in 3.19, the PDF can be mathematically expressed as

$$\begin{aligned}
f_{\gamma_d}(\gamma) = & \sum_{j=1}^M \left\{ \prod_{l \neq j} \left[1 - \frac{1}{\Gamma(\mu_{sr_j})\Gamma(\mu_{r_jd})} \sum_{v=1}^{\mu_{sr_j}} \sum_{u=1}^{\mu_{r_jd}} \sum_{q=0}^{v-1} \sum_{t=0}^{u-1} \sum_{p=0}^{\infty} \sum_{r=0}^{\infty} \binom{v-1}{q} \binom{u-1}{t} \right. \right. \\
& \binom{-q - \mu_j N_j}{p} \binom{-t - \mu_K L}{r} (\mu_j N_j)_q (\mu_K L)_t \Gamma(\mu_{sr_j} - v + 1) \\
& \Gamma(\mu_{r_jd} - u + 1) \left(\frac{\mu_{sr_j}}{\beta_{sr_j}} \right)^{v+p-1} \left(\frac{\mu_{r_jd}}{\beta_{r_jd}} \right)^{u+r-1} \left(\frac{\mu_j}{\beta_j} \right)^{-v-p} \left(\frac{\mu_K}{\beta_K} \right)^{-t-r} \\
& \left. \gamma^{v+u+p+r-2} e^{-\left(\frac{\mu_{sr_j}}{\beta_{sr_j}} + \frac{\mu_{r_jd}}{\beta_{r_jd}}\right)\gamma} \right] \left(-\frac{1}{\Gamma(\mu_{sr_j})\Gamma(\mu_{r_jd})} \sum_{v=1}^{\mu_{sr_j}} \sum_{u=1}^{\mu_{r_jd}} \sum_{r=0}^{v-1} \sum_{t=0}^{u-1} \sum_{p=0}^{\infty} \right. \\
& \sum_{r=0}^{\infty} \binom{v-1}{r} \binom{u-1}{t} \binom{-q - \mu_j N_j}{p} \binom{-t - \mu_K L}{r} (\mu_j N_j)_v (\mu_K L)_t \\
& \Gamma(\mu_{sr_j} - v + 1) \Gamma(\mu_{r_jd} - u + 1) \left(\frac{\mu_{sr_j}}{\beta_{sr_j}} \right)^{v+p-1} \left(\frac{\mu_{r_jd}}{\beta_{r_jd}} \right)^{u+r-1} \left(\frac{\mu_j}{\beta_j} \right)^{-q-p} \\
& \left(\frac{\mu_K}{\beta_K} \right)^{-t-r} \left((v+u+p+r-2) \gamma^{v+u+p+r-3} e^{-\left(\frac{\mu_{sr_j}}{\beta_{sr_j}} + \frac{\mu_{r_jd}}{\beta_{r_jd}}\right)\gamma} \right. \\
& \left. \left. - \left(\frac{\mu_{sr_j}}{\beta_{sr_j}} + \frac{\mu_{r_jd}}{\beta_{r_jd}} \right) \gamma^{v+u+p+r-2} e^{-\left(\frac{\mu_{sr_j}}{\beta_{sr_j}} + \frac{\mu_{r_jd}}{\beta_{r_jd}}\right)\gamma} \right) \right) \left. \right\}
\end{aligned} \tag{3.21}$$

3.4 Performance analysis

3.4.1 Outage Probability

Outage probability is a fundamental concept in wireless communication that quantifies the reliability of a communication link under varying conditions. It is defined as the probability that the signal-to-interference-and-noise ratio falls below a predetermined threshold necessary for successful data transmission, denoted as (γ_{Th}) . This threshold is critical for ensuring that the communication system meets specific performance criteria, such as acceptable bit error rates (BER) and overall quality of service (QoS). Essentially, outage probability serves as a measure of the likelihood that a communication channel will fail to support the required

information rate due to factors such as fading, interference, and noise.

The significance of outage probability extends beyond theoretical analysis; it has practical implications for the design and optimization of wireless communication systems. Various factors influence outage probability, including the distance between the transmitter and receiver, environmental conditions, and the presence of obstacles that can cause signal degradation. For instance, in scenarios involving unmanned aerial vehicles (UAVs), the height and distance from the communication base station are crucial for maintaining a reliable link. Analytical models can be employed to calculate outage probability based on these parameters, allowing engineers to optimize system performance and ensure robust communication even in challenging conditions.

Mathematically, outage probability can be expressed as the probability that the SINR at the output of a selection combiner does not meet the threshold (γ_{Th}). This relationship is vital for understanding how often the network fails to provide adequate service levels, which can be influenced by factors such as fading, interference, and the overall network architecture. By analyzing outage probability, network designers can identify potential weaknesses in the system and implement strategies to enhance performance, such as optimizing antenna configurations or adjusting power levels. The outage probability presented in [33, equation 6.46], and can be defined at output of the selection combiner as

$$P_{out} = \Pr(\gamma_d \leq \gamma_{th}) = P_{\gamma_d}(\gamma_{th}) = \int_0^{\gamma_{th}} f_{\gamma_d}(\gamma) d\gamma \quad (3.22)$$

substituting equation 3.15, the outage probability can be denoted by

$$\begin{aligned}
P_{out} = & \prod_j^M \left(1 - \frac{\left(\mu_{I_j} \bar{\beta}_{I_j}^{-\mu_{I_j}} \right)^{N_j} \left(\mu_K^{\mu_K} \bar{\beta}_K^{-\mu_K} \right)^L e^{\left(\frac{\mu_{I_j}}{\bar{\beta}_{I_j}} + \frac{\mu_K}{\bar{\beta}_K} \right)} e^{-\frac{1}{2} \left(\left(\frac{\mu_{sr_j}}{\bar{\beta}_{sr_j}} + \frac{\mu_{r_j d}}{\bar{\beta}_{r_j d}} \right) \gamma + \left(\frac{\mu_{I_j}}{\bar{\beta}_{I_j}} + \frac{\mu_K}{\bar{\beta}_K} \right) \right)}}{\Gamma(\mu_{sr_j}) \Gamma(\mu_{r_j d})} \right. \\
& \times \left(\frac{\mu_{sr_j}}{\bar{\beta}_{sr_j}} \gamma + \frac{\mu_{I_j}}{\bar{\beta}_{I_j}} \right)^{\frac{-\mu_{I_j} N_j - v - 1}{2}} \sum_{v=0}^{\mu_{sr_j} - 1} \sum_{u=0}^{\mu_{r_j d} - 1} \left(\frac{\mu_{sr_j}}{\bar{\beta}_{sr_j}} \gamma \right)^v \left(\frac{\mu_{r_j d}}{\bar{\beta}_{r_j d}} \gamma \right)^u \Gamma(\mu_{sr_j} - v) \\
& \times \Gamma(\mu_{r_j d} - u) \left(\frac{\mu_{r_j d}}{\bar{\beta}_{r_j d}} \gamma + \frac{\mu_K}{\bar{\beta}_K} \right)^{\frac{-\mu_K L - u - 1}{2}} W_{\frac{-\mu_{I_j} N_j + v + 1}{2}, \frac{-\mu_{I_j} N_j - k}{2}} \left(\frac{\mu_{sr_j}}{\bar{\beta}_{sr_j}} \gamma + \frac{\mu_{I_j}}{\bar{\beta}_{I_j}} \right) \\
& \left. \times W_{\frac{-\mu_K L + u + 1}{2}, \frac{-\mu_K L - u}{2}} \left(\frac{\mu_{r_j d}}{\bar{\beta}_{r_j d}} \gamma + \frac{\mu_K}{\bar{\beta}_K} \right) \right) \quad (3.23)
\end{aligned}$$

Equation (3.23) can be reduced for identical links with different values of fading coefficients (α and μ), such as Rayleigh and Nakagami-m fading channels. The outage probability can be evaluated for identical links with different values of fading coefficients such that:

- A. When $\mu = 1$ for all the non-identical links of the cooperative diversity network, the Outage probability can be evaluated as

$$P_{out} = \prod_j^M \left(1 - e^{-\gamma \left(\frac{1}{\bar{\gamma}_{sr_j}} + \frac{1}{\bar{\gamma}_{r_j d}} \right)} \left(\frac{\Lambda_j}{\gamma + \Lambda_j} \right)^{N_j} \left(\frac{\Upsilon_j}{\gamma + \Upsilon_j} \right)^L \right), \quad (3.24)$$

using the Binomial expansion, P_{out} is expressed as

$$P_{out} = \sum_{k_j=1}^M \binom{M}{k_j} (-1)^{k_j} e^{-\gamma \left(\frac{1}{\bar{\gamma}_{sr_j}} + \frac{1}{\bar{\gamma}_{r_j d}} \right) k_j} \left(\frac{\Lambda_j}{\gamma + \Lambda_j} \right)^{k_j N_j} \left(\frac{\Upsilon_j}{\gamma + \Upsilon_j} \right)^{k_j L}, \quad (3.25)$$

where $(\Lambda_j = \frac{\bar{\beta}_{sr_j}}{\bar{\beta}_j})$, is the average SIR at the j-th Relay node, and $(\Upsilon = \frac{\bar{\beta}_{r_j d}}{\bar{\beta}_k})$, is the average SIR at the Destination node.

B. When $\mu = 1$ for all the identical links of the cooperative diversity network, the Outage probability can be evaluated as

$$P_{out} = \prod_j^M \left(1 - e^{-\frac{2\gamma}{\bar{\gamma}_j}} \left(\frac{\Lambda_j}{\gamma + \Lambda_j} \right)^{2L} \right), \quad (3.26)$$

applying the Binomial expansion to (3.26), the outage probability is evaluated as

$$P_{out} = \sum_{k_j=1}^M \binom{M}{k_j} (-1)^{k_j} e^{-\frac{2k_j}{\bar{\gamma}_j} \gamma} \left(\frac{\Lambda_j}{\gamma + \Lambda_j} \right)^{2k_j L}, \quad (3.27)$$

where $(\Lambda_j = \frac{\bar{\beta}_{sr_j}}{\beta_j})$, is the average SIR at the j-th Relay node.

C. For different values of $\mu = m$, the outage probability for identical links can be evaluated as

$$\begin{aligned} P_{out} = & \prod_j^M \left(1 - \frac{1}{\Gamma(m_j)^2} \left(\frac{m_j}{\bar{\gamma}_{jj}} \right)^{2Lm_j} e^{\frac{m_j}{\bar{\gamma}_{jj}} - \frac{\gamma m_j}{\bar{\gamma}_j}} \left(\frac{m_j}{\bar{\gamma}_{jj}} + \frac{\gamma m_j}{\bar{\gamma}_j} \right)^{-Lm_j} \sum_{k=1}^{m_j} \Gamma(m_j - k + 1)^2 \right. \\ & \left(\frac{\gamma m_j}{\bar{\gamma}_j} \right)^{2k-2} \left(\frac{m_j}{\bar{\gamma}_{jj}} + \frac{\gamma m_j}{\bar{\gamma}_j} \right)^{-k} W_{\frac{k-Lm_j}{2}, \frac{-k-Lm_j+1}{2}}^2 \left(\frac{m_j}{\bar{\gamma}_{jj}} + \frac{\gamma m_j}{\bar{\gamma}_j} \right) - \frac{2}{\Gamma(m_j)^2} \\ & \left(\frac{m_j}{\bar{\gamma}_{jj}} \right)^{2Lm_j} \sum_{t=0}^{m_j-2} \sum_{j=t+1}^{m_j-1} \sum_{n=0}^t \sum_{s=0}^j \Gamma(m_j - t) \Gamma(m_j - j) \binom{t}{n} (Lm_j)_n \binom{j}{s} (Lm_j)_s \\ & \left. \left(\frac{\gamma m_j}{\bar{\gamma}_j} \right)^{i+j} e^{-\frac{2m_j}{\bar{\gamma}_j} \gamma} \left(\frac{m_j}{\bar{\gamma}_j} + \frac{\gamma m_j}{\bar{\gamma}_j} \right)^{-2Lm_j - n - s} \right), \quad (3.28) \end{aligned}$$

3.4.2 Average Error Probability

Average bit error probability (\bar{P}_e) is a critical metric in wireless communication that quantifies the likelihood of errors occurring during data transmission. It is particularly important for assessing the performance of communication systems under various conditions, including noise, interference, and fading.

Average bit error probability can be defined as the expected value of the probability of error for a given communication system. This metric is essential for evaluating the

reliability of the system and ensuring that it meets specific performance criteria, such as acceptable bit error rates and overall quality of service. In mathematical terms, the average bit error probability for Binary-Phase-Shift-Keying (BPSK) modulation, where the symbol error rate is the same as the bit error rate, can be expressed by [33, equation 6.50] as

$$\overline{P}_e = \int_0^\infty P_b(\gamma) f_{\gamma_d}(\gamma) d\gamma \quad (3.29)$$

where $P_b(\gamma)$ is the conditional bit error probability for a given SINR (γ), and is defined in [33, table 6.1]. For BPSK modulation, the average BER at the selection combining output is expressed as

$$\overline{P}_e = \int_0^\infty Q(\sqrt{2\gamma_d}) f_{\gamma_d}(\gamma) d\gamma \quad (3.30)$$

where $f_{\gamma_{SD}}$ is defined in equation (3.21), the average error rate can be expressed after the substitution as

$$\begin{aligned} \overline{P}_e = & \int_0^\infty Q(\sqrt{2\gamma_d}) \sum_{j=1}^M \left\{ \prod_{l \neq j} \left[1 - \frac{1}{\Gamma(\mu_{sr_j})\Gamma(\mu_{r_jd})} \sum_{v=1}^{\mu_{sr_j}} \sum_{u=1}^{\mu_{r_jd}} \sum_{q=0}^{v-1} \sum_{t=0}^{u-1} \sum_{p=0}^\infty \sum_{r=0}^\infty \binom{v-1}{q} \binom{u-1}{t} \right. \right. \\ & \binom{-q - \mu_j N_j}{p} \binom{-t - \mu_K L}{r} (\mu_j N_j)_q (\mu_K L)_t \Gamma(\mu_{sr_j} - v + 1) \\ & \Gamma(\mu_{r_jd} - u + 1) \left(\frac{\mu_{sr_j}}{\beta_{sr_j}} \right)^{v+p-1} \left(\frac{\mu_{r_jd}}{\beta_{r_jd}} \right)^{u+r-1} \left(\frac{\mu_j}{\beta_j} \right)^{-v-p} \left(\frac{\mu_K}{\beta_K} \right)^{-t-r} \\ & \left. \left. \gamma^{v+u+p+r-2} e^{-\left(\frac{\mu_{sr_j}}{\beta_{sr_j}} + \frac{\mu_{r_jd}}{\beta_{r_jd}}\right)\gamma} \right] \left(-\frac{1}{\Gamma(\mu_{sr_j})\Gamma(\mu_{r_jd})} \sum_{v=1}^{\mu_{sr_j}} \sum_{u=1}^{\mu_{r_jd}} \sum_{r=0}^{v-1} \sum_{t=0}^{u-1} \sum_{p=0}^\infty \right. \right. \\ & \sum_{r=0}^\infty \binom{v-1}{r} \binom{u-1}{t} \binom{-q - \mu_j N_j}{p} \binom{-t - \mu_K L}{r} (\mu_j N_j)_v (\mu_K L)_t \\ & \Gamma(\mu_{sr_j} - v + 1) \Gamma(\mu_{r_jd} - u + 1) \left(\frac{\mu_{sr_j}}{\beta_{sr_j}} \right)^{v+p-1} \left(\frac{\mu_{r_jd}}{\beta_{r_jd}} \right)^{u+r-1} \left(\frac{\mu_j}{\beta_j} \right)^{-q-p} \\ & \left(\frac{\mu_K}{\beta_K} \right)^{-t-r} \left((v+u+p+r-2)\gamma^{v+u+p+r-3} e^{-\left(\frac{\mu_{sr_j}}{\beta_{sr_j}} + \frac{\mu_{r_jd}}{\beta_{r_jd}}\right)\gamma} \right. \\ & \left. \left. - \left(\frac{\mu_{sr_j}}{\beta_{sr_j}} + \frac{\mu_{r_jd}}{\beta_{r_jd}} \right) \gamma^{v+u+p+r-2} e^{-\left(\frac{\mu_{sr_j}}{\beta_{sr_j}} + \frac{\mu_{r_jd}}{\beta_{r_jd}}\right)\gamma} \right) \right) \left. \right\} d\gamma \quad (3.31) \end{aligned}$$

The average bit error probability \overline{P}_e can be upper bounded as [49, Eq. 9.27].

$$\begin{aligned}
\overline{P}_e \leq & \frac{1}{2} \prod_{m=1}^M \int_0^\infty e^{-s\gamma} \left[\sum_{j=1}^M \left\{ \prod_{l \neq j} \left[1 - \frac{1}{\Gamma(\mu_{sr_j})\Gamma(\mu_{r_jd})} \sum_{v=1}^{\mu_{sr_j}} \sum_{u=1}^{\mu_{r_jd}} \sum_{q=0}^{v-1} \sum_{t=0}^{u-1} \sum_{p=0}^\infty \sum_{r=0}^\infty \binom{v-1}{q} \right. \right. \right. \\
& \binom{u-1}{t} \binom{-q - \mu_j N_j}{p} \binom{-t - \mu_K L}{r} (\mu_j N_j)_q (\mu_K L)_t \Gamma(\mu_{sr_j} - v + 1) \\
& \Gamma(\mu_{r_jd} - u + 1) \left(\frac{\mu_{sr_j}}{\beta_{sr_j}} \right)^{v+p-1} \left(\frac{\mu_{r_jd}}{\beta_{r_jd}} \right)^{u+r-1} \left(\frac{\mu_j}{\beta_j} \right)^{-v-p} \left(\frac{\mu_K}{\beta_K} \right)^{-t-r} \\
& \left. \left. \left. \gamma^{v+u+p+r-2} e^{-\left(\frac{\mu_{sr_j}}{\beta_{sr_j}} + \frac{\mu_{r_jd}}{\beta_{r_jd}}\right)\gamma} \right] \left(-\frac{1}{\Gamma(\mu_{sr_j})\Gamma(\mu_{r_jd})} \sum_{v=1}^{\mu_{sr_j}} \sum_{u=1}^{\mu_{r_jd}} \sum_{r=0}^{v-1} \sum_{t=0}^{u-1} \sum_{p=0}^\infty \right. \right. \right. \\
& \sum_{r=0}^\infty \binom{v-1}{r} \binom{u-1}{t} \binom{-q - \mu_j N_j}{p} \binom{-t - \mu_K L}{r} (\mu_j N_j)_v (\mu_K L)_t \\
& \Gamma(\mu_{sr_j} - v + 1) \Gamma(\mu_{r_jd} - u + 1) \left(\frac{\mu_{sr_j}}{\beta_{sr_j}} \right)^{v+p-1} \left(\frac{\mu_{r_jd}}{\beta_{r_jd}} \right)^{u+r-1} \left(\frac{\mu_j}{\beta_j} \right)^{-q-p} \\
& \left(\frac{\mu_K}{\beta_K} \right)^{-t-r} \left((v + u + p + r - 2) \gamma^{v+u+p+r-3} e^{-\left(\frac{\mu_{sr_j}}{\beta_{sr_j}} + \frac{\mu_{r_jd}}{\beta_{r_jd}}\right)\gamma} \right. \\
& \left. \left. \left. - \left(\frac{\mu_{sr_j}}{\beta_{sr_j}} + \frac{\mu_{r_jd}}{\beta_{r_jd}} \right) \gamma^{v+u+p+r-2} e^{-\left(\frac{\mu_{sr_j}}{\beta_{sr_j}} + \frac{\mu_{r_jd}}{\beta_{r_jd}}\right)\gamma} \right) \right] \right\} \Bigg|_{s=1} d\gamma \quad (3.32)
\end{aligned}$$

Finally, \overline{P}_e can be reduced for identical fading channel with coefficients of $\alpha = 2$ and $\mu = 1$, and using the binomial expansion and some mathematical manipulation, as

$$\overline{P}_e \leq 2^{M-1} \sum_{k=0}^M \binom{M}{k} \left(\frac{\overline{\beta}L}{\overline{\beta} + 2} \right)^k e^{\frac{2\Delta}{\overline{\beta}}k + \Lambda k} \times E_{2L+1}^k \left(\frac{\Lambda}{\overline{\beta}}(\overline{\beta} + 2) \right). \quad (3.33)$$

Where L is the interferes number at the j -th relay which is identical as the same number of interferes at the destination node, and $(\Lambda = \frac{\overline{\beta}_{sr_j}}{\beta_j})$ represents the average Signal to Interference Ratio (SIR) at the Relay node. In addition, $(\Upsilon = \frac{\overline{\beta}_{r_jd}}{\beta_K})$, is the average SIR at the relay and Destination node respectively.

3.5 Numerical results

3.5.1 Outage Probability Performance

Outage probability and error probability behavior are illustrated in this section over different conditions and fading channel parameters (α and μ). The results shown in figures (3.2) and (3.3) illustrate the behavior of the outage probability versus the normalized average SINR when there is no interference affecting any node of the network, for different values of ($\mu = 1$) and ($\mu = 2$) with the value of ($\alpha = 2$) fading parameter correspondingly. It's been illustrated that for different values of μ the outage probability decreases by increasing the number of diversity paths M that are received at the input of the selection combiner. On the other hand, it is noticed that increasing the value of μ decreases the outage probability over the same given conditions, thus; improving the performance of the network in the case of no interferers affecting any of the network nodes.

3.5.2 Effects of Interference on System Performance

As for the impact of interference at the cooperative diversity which is illustrated in figures (3.4) and (3.5), given that the number of interferers at the relay and destination nodes $N = L = 5$ with $INR = 3dB$ for different values of μ , improvement is clearly noticed in the network performance by increasing the number of combined branches when compared to the direct link transmission. Accordingly, increasing the number of diversity paths and increasing the value of μ for identical link, decreases the outage probability therefore improving the performance of the network compared to the direct link transmission.

3.5.3 Error Probability Analysis

The region of investigation in this chapter is the high SINR region, where a tight upper bound is considered to derive an approximated expression for the average error probability of the cooperative diversity where BPSK modulation technique is used, as illustrated and derived in section (3.4.2). Considering the relationship between the average bit error probability and the average SINR, it is found that the performance of the network is improved by increasing the number of diversity paths at the combiner input, though the interference affect the average error probability with adverse manner, as shown in figure (3.6) where different number of interferers are considered with $SINR = 30 \text{ dB}$ and links are identical with fading channel parameter $\mu = 1$. While maintaining a fixed number of interferers $N = L = 10$ with a value of $INR = 3 \text{ dB}$, the average error probability is enhanced by increasing the number of diversity paths even in the presence of interferers at the nodes. As can be observed in figure (3.7).

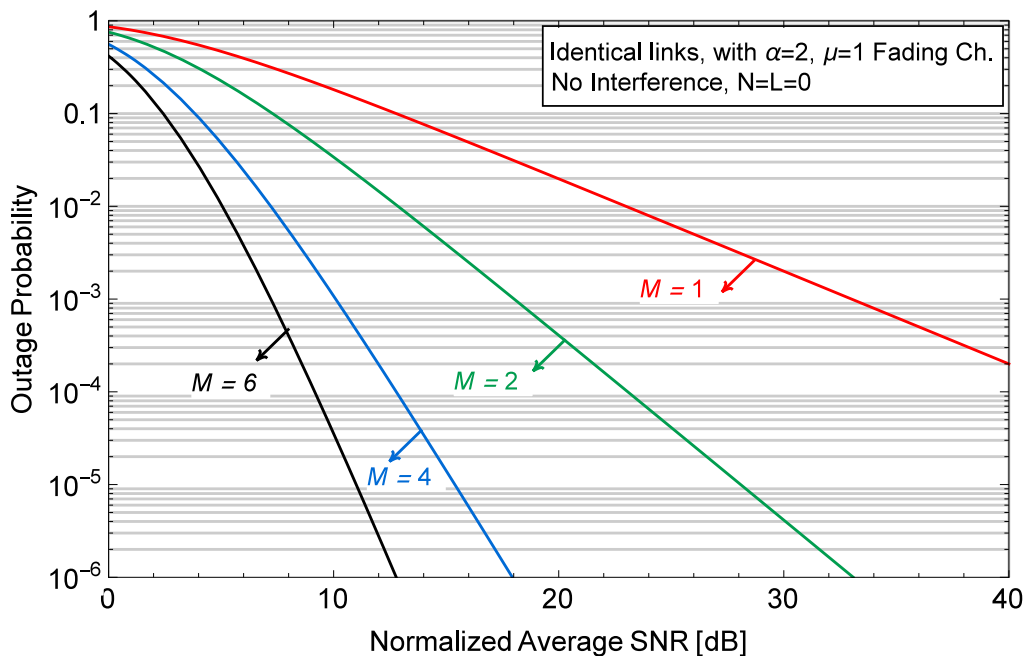


Figure 3.2: Outage probability of identical Fading channels with different coefficients, Selective Combining and without interference. Fading channels coefficients: $\alpha = 2$, $\mu = 1$.

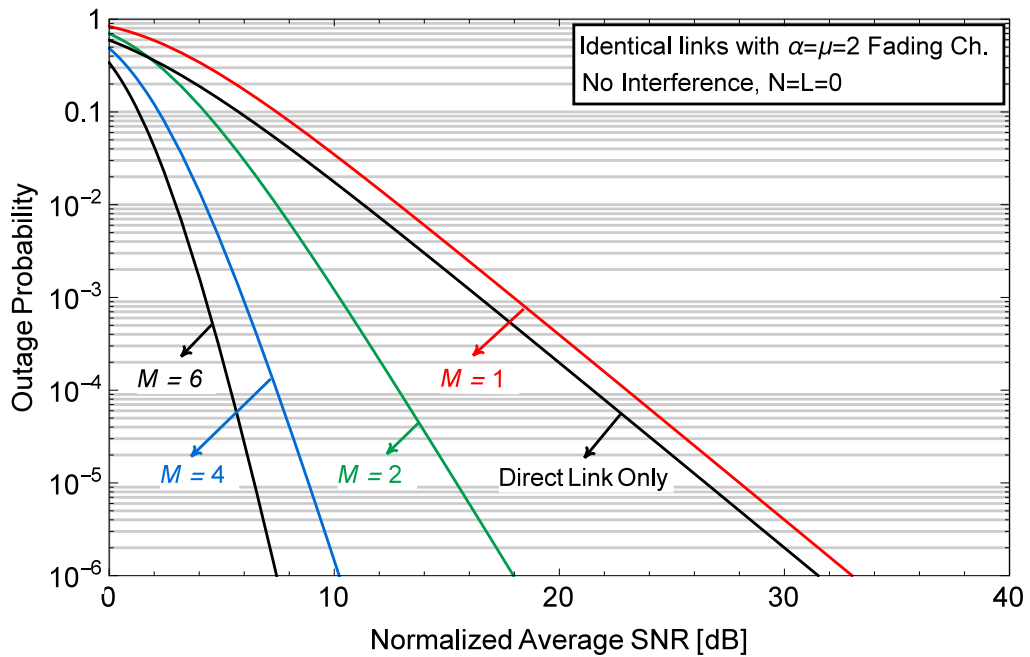


Figure 3.3: Outage probability of identical Fading channels with different coefficients, Selective Combining and without interference. Fading channels coefficients: $\alpha = 2$, $\mu = 2$.

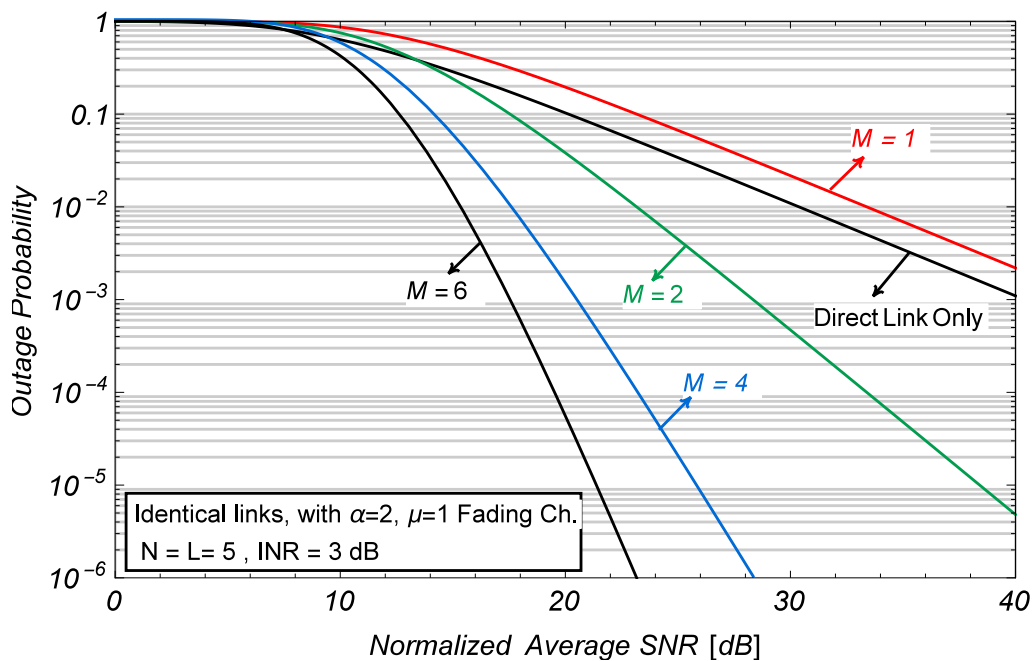


Figure 3.4: Outage probability of identical Fading channels with Selective Combining and 5-interferers and $INR = 3$ dB. Fading channels coefficients: $\alpha = 2$, $\mu = 1$.

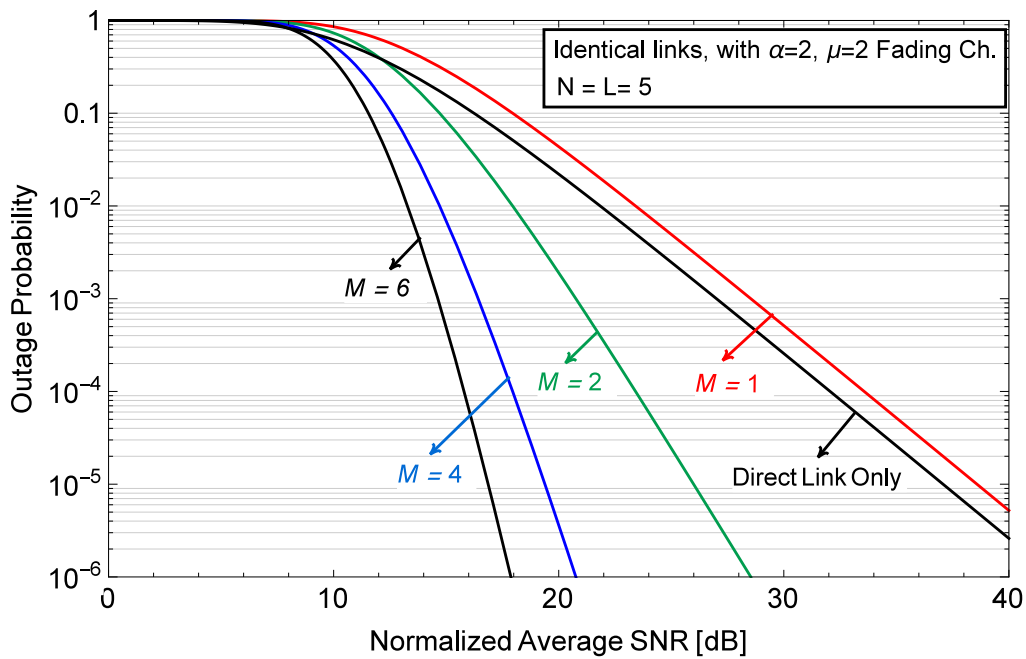


Figure 3.5: Outage probability of identical Fading channels with Selective Combining and 5-interferers and $INR = 3dB$. Fading channels coefficients: $\alpha = 2$, $\mu = 1$.

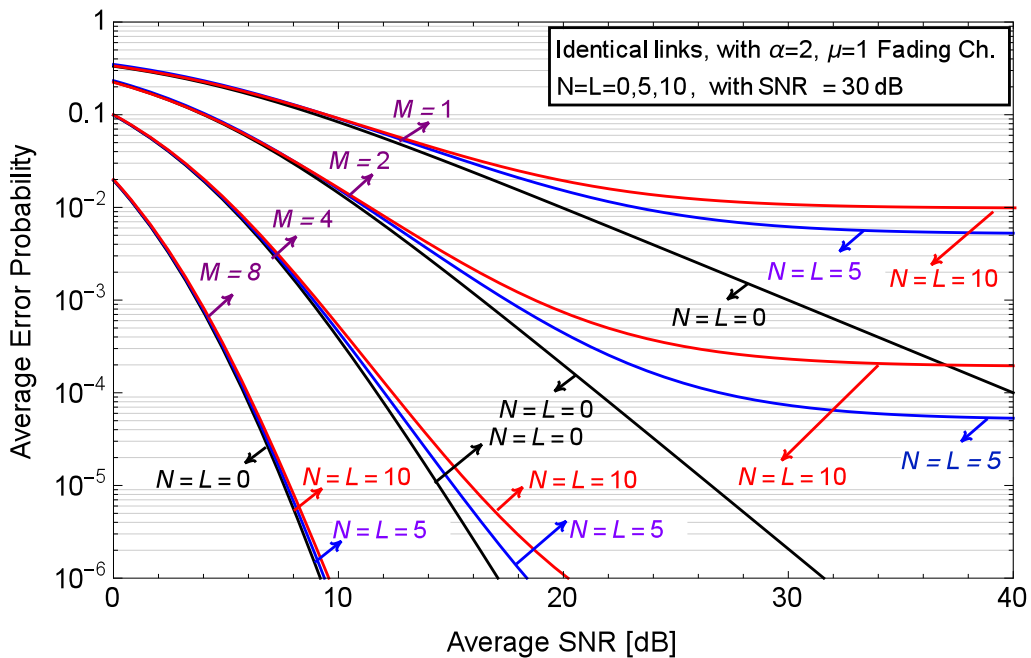


Figure 3.6: Average error probability of identical Fading channels with $SINR = 30 dB$ and SC scheme and various number of interferers (0,5,10). Fading channels coefficients: $\alpha = 2$, $\mu = 1$.

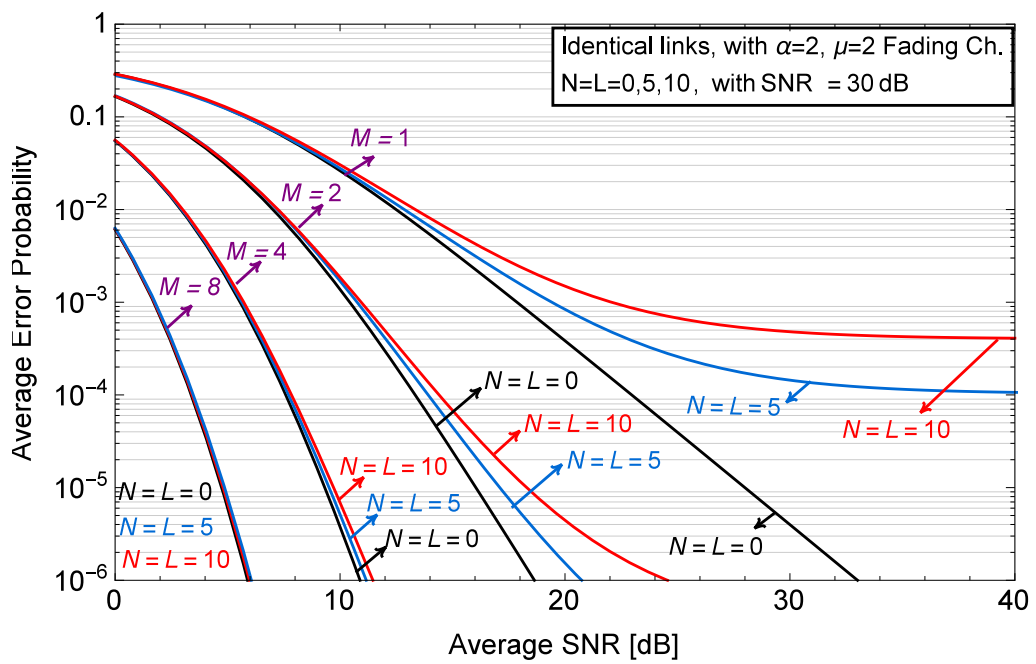


Figure 3.7: Average error probability of identical Fading channels with $SINR = 30$ dB and SC scheme and various number of interferers (0,5,10). Fading channels coefficients: $\alpha = 2, \mu = 2$.

3.6 Conclusion

In this chapter, I have investigated the error and outage performance of cooperative diversity networks over α - μ fading channels in the presence of co-channel interference. Both the probability density function and the cumulative distribution function of the upper bound of the SINR were developed in this chapter. In addition, the derived expressions of both the outage and error probability were used to investigate the performance of the proposed cooperative diversity network, where the relaying technique is assumed to be the amplify-and-forward, while the selective combining technique is introduced at the destination node. The derived expressions were used to extract other fading models such as Rayleigh ($\alpha = 2$ and $\mu = 1$), Nakagami-m ($\alpha = 2$ and $\mu = m$), and other fading models where the value $\alpha = 2$ with different values of μ .

Furthermore, as proved in the results, interference can majorly impact the system's performance. As the number of interferers increases, the outage probability increases, leading to a corresponding degradation in system performance. The same finding holds for the error probability, the system performance degrades by increasing the number of interferers introduced to the system nodes; also, interference caused the error probability curve to floor. Nevertheless, the average error probability can be enhanced by increasing the number of diverse paths even in the presence of number of interferers at the nodes.

Glossary — Chapter 3

Term	Description	Page
E_{ji}	The average received energy from the j -th interferer of the j -th relay node.	62
E_k	The average received energy from the k^{th} interferer node at the destination node.	62
E_{sr_j}	The average transmitted energy from the source to j -th relay node.	62
G_{AF_j}	The amplification gain of the j -th relay.	62
I_D	The interference at the destination node.	65
I_{r_j}	The interference at the j -th relay node.	64
L	The number of interferes at the destination node.	62
N_j	The number of interferes at the j -th relay node.	62
R_j	The j -th relay node.	62
h_{ji}	The channel gain of the i^{th} Co-Channel interference link at the j -th relay node.	62
h_{r_jd}	The channel fading coefficient from the j -th relay to the destination link.	62
h_{sr_j}	The channel fading coefficient of the source to the j -th relay node.	62
n_d	The AWGN at the destination node, and is considered to have zero-mean and variance $N_o \sim CN(0, N_o)$.	62
n_{r_j}	The AWGN at the j -th relay node, and is considered to have zero-mean and variance $N_o \sim CN(0, N_o)$.	62

Term	Description	Page
E_{r_j}	The average received energy from the j-th relay node.	62
d_{ji}	The received data from the j-th interferer of the j-th relay node.	62
d_{r_j}	The transmitted data from the j-th relay node.	62
d_{sr_j}	The transmitted data from source to the j-th relay node with unit energy	62
$\bar{\beta}_{I_j}$	The average SIR at the j-th relay node from the i^{th} interferes.	66
$\bar{\beta}_K$	The average SIR for the k^{th} interferes at the destination node.	66
$\bar{\beta}_{r_jd}$	The average SINR of the j-th relay to the destination $R_j \rightarrow D$ link.	66
$\bar{\beta}_{sr_j}$	The average SINR from the source node to the j-th relay node $S \rightarrow R_j$.	66
\bar{P}_e	The average bit error probability .	73
$F_{\gamma_{SC}}$	The $S \rightarrow R \rightarrow D$ link average SINR accumulative deinsity function (CDF).	66
γ_{gk}	The SINR of the k^{th} interfere at the destination node.	65
γ_{r_jd}	The SINR for the j-th relay node and the destination node link($R_j \rightarrow D$).	65
γ_{ji}	The SINR for the i^{th} interfere at the j-th relay node.	65
γ_{SC}	The SINR at the combiner output of the destination node which is the result of the best-relay SINR.	65
$f_{\gamma_{SC}}$	The $S \rightarrow R \rightarrow D$ link average SINR density function (pdf).	68
γ_{sr_j}	The SINR for the source and the j-th relay node link($S \rightarrow R_j$).	65
γ_{sr_jd}	The SINR for the j-th indirect path ($S \rightarrow R_j \rightarrow D$).	65
μ_{I_j}	The α - μ coefficient for the j-th reply node.	66
μ_k	The α - μ coefficient for the k^{th} interfere at the destination node.	66

Chapter 4

Deep Reinforcement Learning for Jointly Resource Allocation and Trajectory Planning in UAV-assisted Networks

4.1 Introduction

The beauty of Unmanned Aerial Vehicles (UAVs), which include drones, has recently attracted lots of researcher's attention in the industrial fields due to their ability to operate and monitor activities from remote locations; moreover, UAVs are well known for their portability, lightweight, low cost and flying without a pilot. UAV features make it suitable to be integrated into the fifth-generation (5G) and the networks beyond 6G wireless networks, where UAV can be deployed as aerial base stations into what is called the UAV-assisted [1], [50]. Such situations include quick service recovery after a natural disaster and offloading base stations or the Next Generation Node B (gNBs) at hotspots in case of failure or malfunction of the ground base station or the gNB. In addition, UAV can be used to enhance network coverage and performance, where the location of the UAV can be controlled and dynamically changed to optimize the network performance according to the users' needs and their mobility model. Such scenarios are represented in Figure 4.1.

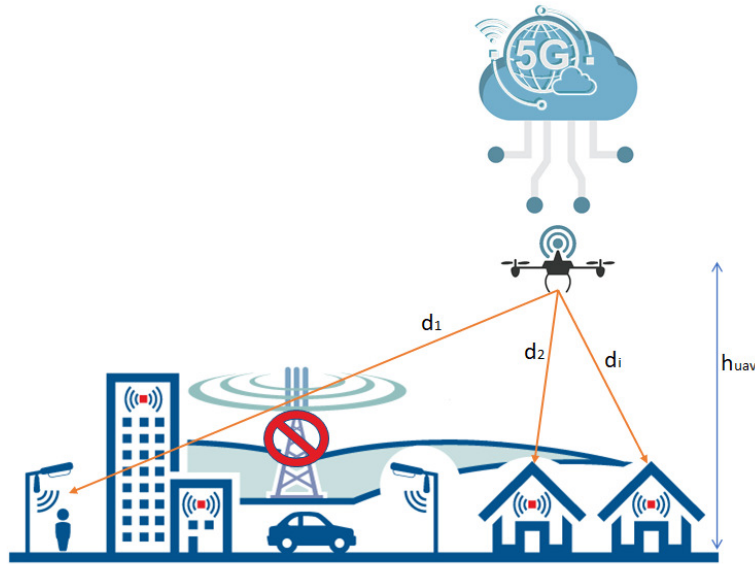


Figure 4.1: UAV emergency model.

A UAV-assisted application was investigated in terms of performance analysis, resource allocation, UAV placement and position optimization, channel modeling, and information security as in [51], [52] and [53]. UAV-assisted wireless

communications have three main types; the first type is called UAV-carried Evolved Node B (eNB) or gNB, where the UAV acts as an aerial base station and is used to extend the network coverage [2], [3] and [4]. The second type is called UAV relaying, where the UAVs are used as aerial relays to provide a wireless connection for users that cannot communicate with each other directly [5]-[6]. Finally, the third type is identified as a UAV-assisted Internet-of-Things (IoT) network, where UAVs assist the IoT network in collecting/disseminating data from/to its nodes or charging its nodes [7] and [8].

However, due to the UAV's limitations, only some applications use UAVs in the existing systems. The fundamental limitation is the battery life of the UAV, which is affected by the high power consumption dissipated in the hovering, horizontal, and vertical movements of the drone. Besides the battery life, the position of the UAV is also a significant concern in implementing real systems.

One of the significant applications of using the UAV in the communication system is during emergencies (such as floods or earthquakes, ... etc.) while the infrastructure is partially or totally unavailable, and the need to provide mobile service to the users is highly required. In these situations, the UAV can perform this task and provide mobile services to the user equipment (UEs) while granting the required quality-of-service (QoS). The main challenge for using the UAV-assisted network is to find the optimal position of the UAV in the cell area before getting a dead battery. Which is very complicated and challenging to determine, and the traditional optimization methods of artificial intelligence (AI) cannot solve those complicated optimization problems.

In order to address those two concerns, Reinforcement learning (RL) algorithms are applied, especially deep reinforcement learning, which has been proven to

outperform the existing traditional algorithm. In this chapter, we introduced deep RL algorithm to solve the UAV-assisted joint position and radio resource allocation optimization problem. The main target is to find the optimal position of the UAV that is dynamically changed concerning the UEs required QoS and consider the UAV battery energy level in each time step, in addition to the required energy to get back to the start point.

Our main contribution in this study is presented as follows. We developed a method that collaboratively optimizes communication resource allocation and position for the UAV based on reinforcement learning, where the position and radio resource allocation joint optimization problem is formulated to obtain the maximum cumulative discounted reward. For the non-convexity nature of the optimization problem, we designed and applied deep reinforcement learning algorithm which is Proximal Policy Optimization (PPO), for the UAV to solve the joint optimization issue.

Section 4.2 reviewed the related literature on optimizing the position and resource allocation in UAV-assisted networks. Also, we review the reinforcement learning application in such optimization problems for UAV-assisted wireless networks. System model and problem formulation are illustrated in Section 4.3, and simulation and results are presented in Section 4.4. The conclusion is discussed in Section 4.5.

4.2 Related work

The design of UAV position for improving various communication performance metrics has gained significant attention, as shown in various studies such as in [24], which focused on optimizing the spectrum efficiency and energy efficiency of a UAV-enabled mobile relaying system by adjusting the UAV's flying speed, position,

and time allocation. [25] aimed to optimize the global minimum average throughput through optimized UAV trajectories and OFDMA (orthogonal frequency-division multiple access) resource allocation. [26] explored the UAV-enabled wireless communication system with multiple UAVs and aimed to increase the minimum user throughput by optimizing communication scheduling, power allocation, and UAV trajectories. In [27], UAVs served as flying Base Stations (BSs) for vehicular networks, delivering data from vehicular sources to destination nodes. The authors determined the optimal UAV position and radio resource allocation by combining Linear Programming and successive convex approximation methods.

Despite the deployment optimization of UAVs, machine learning (ML) algorithms have been introduced to optimize different QoS network requirements. The reinforcement RL and deep learning (DL) received the foremost researchers' focus in this field. Such researches as in [28], where the authors proposed UAV autonomous indoor navigation and target detection approach based on a Q-learning algorithm. While in [29], the authors proposed multi-agent reinforcement learning to optimize the resource allocation of the multi-UAV networks, and the algorithm is designed to maximize the systems' long-term reward. The authors of [30] have considered RL algorithms to optimize UAV's position to maximize sensor network data collection under QoS constraints. Moreover, in [31], the researchers adopted deep learning RL based to dynamically allocate radio resources in heterogeneous networks. Moreover, in [P1], we addressed indoor localization based on the received signal strength (RSS) and we introduced a weighted-coefficient-approach (WCA) to estimate sensor positions by solving the compressive sensing (CS) problem.

Based on the related literature review, a limited number of researchers are solving the UAV position's joint optimization problem and the UEs resource allocation taking the UE mobility model into consideration. Motivated by that, we applied the deep

RL algorithms to solve this optimization problem using mainly the state-of-art PPO algorithm.

4.3 An RL-based approach

We considered a multi-rotor UAV with total battery energy E_{max} that is flying at a fixed altitude of h_{max} from a base point denoted by $s_0 = (x_0, y_0)$, where the UAV climbing movement to the fixed altitude is not considered in this study simulation. The UAV has an onboard gNB that will serve K subscribers within a specific area. At the beginning (τ_i) of time slot i , the gNB decides the assignment of Resource Blocks (RB) for each customer according to specific criteria; in our study, we adopt the customer's QoS requirements, and the channel quality, where the gNB can measure the channel quality of each user's device and allocate the RBs based on a minimum requirement to maintain the network performance. We assume that the gNB receives the channel quality indicator (CQI) values. ($CQI(k, i) = [CQI_{1,i}, CQI_{2,i}, \dots, CQI_{k,i}]$) of $k = \{1, \dots, K\}$ user equipment (UEs) at time instance τ_i where $i = 0, \dots$, which is in accordance with the time-slot operation of the gNB, so $\tau_{i+1} - \tau_i = \Delta$. At each time step $\tau_i = a \times i \times \Delta$, the UAV decides to continue flying or get back to the base point while monitoring the battery level. For this problem, we apply Reinforcement learning (RL) for flight control as follows:

- At each time step τ_i , the state $s_i = [(x_i, y_i, h_{max}, E_i), [CQI_{k,i}]] \quad \forall k \in [0, K]$ consists of UAV position, which can be denoted by the coordinates (x_i, y_i, h_{max}) and the UAV battery energy level, in addition to the received CQI values, from the UEs $CQI_{k,i} \forall k \in [1, K]$, and the UAV battery level E_i .
- We assume that the altitude of the UAV is fixed in this study, which can lead to the possible actions: backward (BW), forward (FW), left (L), right (R),

and hovering (HO) in the same location and (RE) returning to the base point. The action space is $\mathcal{A} = \{L, R, FW, BW, HO, RE\}$.

- The reward function is defined as the logarithmic function for the joint condition between the number of served UEs and the ratio of the allocated RB $N_{i,k}^{RB}$ to the total RB in each time step, where the reward function is used to maximize the number of served UEs with minimum allocated RBs, and denoted as

$$r_i = \left(\sum_{k=1}^K U_{i,k} \right) \times N_{tot}^{UE} + \frac{N_{tot}^{RB}}{\sum_{k=1}^K N_{i,k}^{RB}}, \quad (4.1)$$

where the binary variables $U_{i,k} \in \{0, 1\}, \forall k, i$, which is asserted if the UAV succeeded in serving the k -th UE at the i -th time slot, and allocated the required resources to guarantee the minimum throughput required to provide coverage for the cell in emergencies. Otherwise, $U_{i,k}$ is set to 0. In this study, we adopt the max CQI scheduling allocation of the UEs, where the UEs with the highest values of CQI are allocated while there are available resource blocks in the radio frame. While the other variable $N_{i,k}^{RB}, \forall k$ represent the sum of allocated RBs for the UEs that were allocated successfully and got mobile services in time slot i , the N_{tot}^{RB} represents the total number of RBs in the bandwidth. And finally, N_{tot}^{UE} denotes the total number of UEs that are requesting the mobile service in a certain cell area.

The energy consumption of the UAV consists of mainly two parts: one that is required to provide the onboard gNB with its energy to operate, and the other is the propulsion energy of the UAV so that it can fly around. The UAV will decide to get back to the base point by monitoring its battery energy level (E_i) at each time step τ_i , and compare it with the energy required to fly back to the start point $s_0 = (x_0, y_0)$ from its position point ($E_{i+1,r}$). The UAV battery energy constraints

is assumed to be:

$$E_i > E_{i,r} \text{ AND } E_{i+1} > E_{i+1,r}. \quad (4.2)$$

4.4 Simulation and analysis

4.4.1 Models used in simulation

4.4.1.1 User Mobility

User mobility modeled in this research is based on the Gauss–Markov Mobility Model [54]. Where the Mobile nodes (UEs) are located in random locations within the cell area, these nodes will set their speed as for the k -th UE the speed is denoted as $(V_{i,k})$ and its direction denoted as $(D_{i,k})$ for each specific step (i) . At every step i , the current position of the k -th UE coordinates $(x_{k,i}, y_{k,i})$ depends on the previous location $(x_{k,i-1}, y_{k,i-1})$, previous speed $V_{k,i-1}$ and previous direction $D_{k,i-1}$, assuming the directions values can be set to $\in [0, 90, 180, 270]$, to follow the proposed grid world model of the network cell. The k -th UE position at the i -th step, is expressed as

$$\begin{aligned} X_{k,i} &= X_{k,i-1} + V_{k,i-1} \cos D_{k,i-1}, \\ Y_{k,i} &= Y_{k,i-1} + V_{k,i-1} \sin D_{k,i-1}. \end{aligned} \quad (4.3)$$

Parameters $V_{k,i-1}$ and $D_{k,i-1}$ are chosen from a random Gaussian distribution with a mean equal to 0 and a standard deviation equal to 1.

4.4.1.2 RB scheduling algorithm

In our study, we adopt the best-CQI scheduling algorithm to allocate RB to the UE, where the gNB Scheduler allocates the RBs to the UEs that reported the highest CQI during Transmission Time Interval (TTI), where the higher CQI value means a better channel condition.

4.4.1.3 Energy Consumption Model for Multi-rotor UAV

In this chapter, we considered rotary-wing UAV, the UAV has four brushless motors which are powered by the carried battery, and they rotate at the same constant speed ω_{rotor} . The UAV will fly to a specific position and hover or continue flying to the next position. We follow the forces model in [55] to derive the energy consumption for both UAV motion phases. The propulsion power of the UAV is essential to support the UAV's hovering and moving activities either the vertical movement, where in our study, we assumed the UAV height is constant; thus, we will not consider this movement phase, the other movement type is the horizontal movement from one position to another in the cell grid.

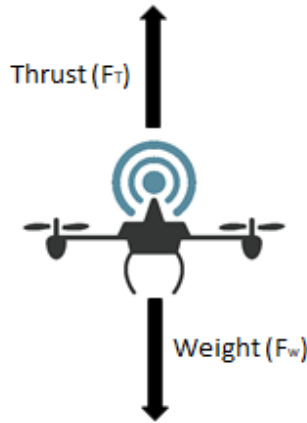


Figure 4.2: UAV hovering state forces.

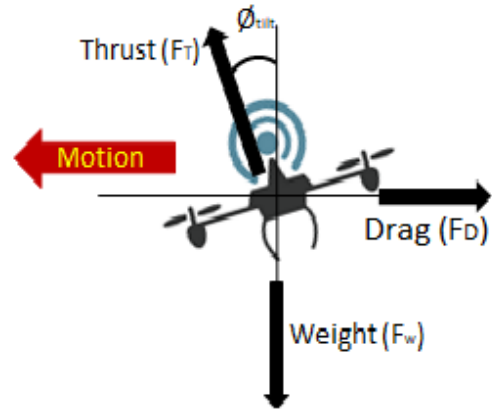


Figure 4.3: UAV forward state forces.

Hovering is a fundamental flight mode for drones, where the rotor-generated thrust exactly counteracts gravitational forces to maintain a stable position. The forces involved in this phase are illustrated in Figure 4.2. By applying the principles from [56, equations 2.14 and 2.15], [57, chapter 2], and [58], along with implementing [59, equations 2.24 and 2.25], we consider the drone's velocity to be zero during hover. In this state, the resultant velocity equals the motor speed, denoted as V_{hov} , which corresponds to the induced velocity of the rotor blades.

The total thrust force F_T produced during hover can be expressed by accounting for all N_{rotor} rotors of the quadcopter as follows

$$F_T = \frac{1}{2}\rho N_{rotor} A_{uav} V_{hov}^2, \quad (4.4)$$

where ρ is the air density and equals to (1.225 kg/m³), the rotor propeller area is A_{uav} and is equal to πr_{uav}^2 where r_{uav} is the propeller radius. Finally, the number of UAV rotors is represented by the variable N_{rotor} .

In the hovering phase, the thrust of the drone motors must be equal to the gravitational force ($F_T = m_{tot} \times g$), where the value of $V_{uav} = \sqrt{m_{tot} \times g / (2\rho A_{uav} N_{rotor})}$, and the earth gravitational acceleration g and equals to (9.81 \approx 10 kg/m²), and m_{tot} represents the total mass of the drone and it's cargo. Hovering energy in time step duration Δ [s] and the power is equal to $P_{hov} = F_T V_{hov}$, with the UAV velocity $V_{uav} = 0$, and the motor velocity represented by V_{hov} :

$$E_{hov} = F_T \times V_{hov} \times \Delta. \quad (4.5)$$

Then substituting the weight force that the drone has to defy, the energy consumed can be defined as

$$E_{hov} = m_{tot} \times g \times V_{hov} \times \Delta. \quad (4.6)$$

The drone rotor velocity in the hovering state is derived from the thrust equation and the force equilibrium as

$$V_{hov} = \sqrt{\frac{2m_{tot} \times g}{\rho A_{uav} N_{rotor}}}. \quad (4.7)$$

Accordingly, the energy that the battery must supply is only that to defy the weight force, is derived after substituting equation 4.7 into equation 4.6, then applying

mathematical manipulation, the final energy formula is represented by

$$E_{hov} = \sqrt{\frac{2(m_{tot} \times g)^3}{\rho A_{uav} N_{rotor}}} \times \Delta. \quad (4.8)$$

where m_{tot} is the total mass in kg and equals to the sum of UAV mass (m_{uav}), the payload (the carried gNB) (m_{pld}) and the battery (m_b), i.e $m_{tot} = m_{uav} + m_b + m_{pld}$.

To build a simulation that closely reflects real-world conditions, we account for the system efficiency of the UAV. The primary power-consuming components are the motors and propellers, whose efficiencies (η_{mot}) and (η_{pro}) dominate the energy balance. The motor efficiency in this case is metric to measure how well the motor converts electrical power into mechanical power, and the propellers efficiency is a metric to measure how well the propeller converts rotational power into thrust. Following [60, Chapter 7], the overall system efficiency is given by their product

$$\eta_{sys} = \eta_{mot} \times \eta_{pro} \quad (4.9)$$

Assuming the power draw of the flight controller and other electronics (e.g., gNB) is negligible compared to the propulsion system, the total energy required for hovering E_{hov} is derived as

$$E_{hov} = \sqrt{\frac{2(m_{tot} \times g)^3}{\rho A_{uav} N_{rotor}}} \times \frac{1}{\eta_{mot}\eta_{pro}} \times \Delta. \quad (4.10)$$

Maintaining steady horizontal flight requires the drone's thrust force (F_T) to precisely balance opposing forces, including aerodynamic drag (F_D) from forward motion and the weight force ($F_W = m_{tot} \times g$) from the combined mass of the drone, battery, and payload (the carried gNB in our study). This equilibrium, derived from Newton's First Law, becomes particularly challenging to estimate due to the nonlinear velocity dependence of F_D and complex interactions between propeller wake, airframe geometry, and environmental factors, making horizontal motion

the most demanding regime for accurate thrust prediction and energy estimation. Accordingly, under equilibrium conditions and assuming the UAV is moving at a constant velocity (steady flight), such that the vertical forces must balance. This equilibrium can be expressed mathematically as

$$\sum F_z = 0 \implies F_T \times \cos(\phi_{tilt}) = m_{tot} \times g \quad (4.11)$$

In steady forward flight, the horizontal equilibrium of a multi-rotor UAV is maintained when the forward component of thrust exactly balances the aerodynamic drag. This balance can be expressed as

$$\sum F_x = 0 \implies F_D = F_T \times \sin(\phi_{tilt}) \quad (4.12)$$

where F_T is the total thrust force, ϕ_{tilt} is the tilt angle of the drone, and F_D represents the drag force. The drag force is typically modeled using the standard aerodynamic equation [61]:

$$F_D = \frac{1}{2} C_D \rho A_{uav}^{eff} V_{UAV}^2, \quad (4.13)$$

where C_D represents the drag coefficient, and A_{uav}^{eff} represents the vertical projected area of the UAV and can be evaluated as

$$A_{uav}^{eff} = A_{uav}^{side} \sin(90^\circ - \phi_{tilt}) + A_{uav}^{top} \sin(\phi_{tilt}) \quad (4.14)$$

where A_{uav}^{side} and A_{uav}^{top} represents the side and top surface of the UAV, which can be approximated as $A_{uav}^{eff} \approx A_{uav}^{top} \sin(\phi_{tilt})$.

This equilibrium relationship demonstrates that the UAV attains a constant forward speed when the horizontal thrust exactly counterbalances aerodynamic drag. By substituting Equation 4.13 into 4.12 and performing the appropriate algebraic manipulations, we derive the steady-state velocity expression V_{uav} :

$$V_{uav} = \sqrt{\frac{2F_T \sin(\phi_{tilt})}{\rho C_D A_{uav}^{eff}}} \quad (4.15)$$

This formulation explicitly shows how the achievable forward speed depends on both the UAV's thrust capability and its aerodynamic properties. The square root relationship indicates that velocity increases proportionally with thrust but diminishes with larger drag coefficients or frontal areas, following fundamental aerodynamic principles.

Thrust can be expressed from solving equation 4.11 which can be manipulated mathematically as:

$$F_T = \frac{m_{tot} \times g}{\cos(\phi_{tilt})} \quad (4.16)$$

To analyze the energy expenditure during the horizontal motion of the UAV at constant velocity, we derive the required power expression by multiplying equations 4.16 by the UAV velocity. The horizontal propulsion power (P_{hor}) is formulated as

$$P_{hor} = \frac{m_{tot} \times g}{\cos(\phi_{tilt})} \times V_{uav} \quad (4.17)$$

After substituting the UAV velocity (from Equation 4.15) and the thrust force (given by Equation 4.16), further mathematical simplifications were applied to Equation 4.17, resulting in the following expression for (P_{hor}) as

$$P_{hor} = \frac{m_{tot} \times g}{\cos(\phi_{tilt})} \times \sqrt{\frac{m_{tot} \times g}{\cos(\phi_{tilt})} \times \frac{2 \sin(\phi_{tilt})}{\rho C_D A_{uav}^{eff}}} \quad (4.18)$$

after further mathematical manipulation, equation 4.18 can be expressed as

$$P_{hor} = \sqrt{\frac{2(m_{tot} \times g)^3}{C_D \rho A_{uav}^{eff} N_{rotor}}} \times \frac{\sin(\phi_{tilt})}{\cos^3(\phi_{tilt})} \quad (4.19)$$

The next step is to derive the energy for the horizontal movement E_{hor} is presented by

$$E_{hor} = P_{hor} \times \Delta \quad (4.20)$$

substituting 4.19, the electrical energy consumed by the battery while the drone is in horizontal movement, can be expressed after considering the system efficiency:

$$E_{hor} = \sqrt{\frac{2(m_{tot} \times g)^3}{C_D \rho A_{uav}^{eff} N_{rotor}}} \times \frac{\sin(\phi_{tilt})}{\cos^3(\phi_{tilt})} \times \frac{1}{\eta_{mot} \eta_{pro}} \times \Delta, \quad (4.21)$$

Here, (η_{mot}) and (η_{pro}) denote the motor and propeller efficiencies, respectively. The UAV simulation parameters, including its physical properties, are listed in table 4.1. Additionally, the battery specifications — modeled after the **DJI Matrice 600 Pro** drone's power system [62] — are provided in table 4.2. Further details on the gNB's energy, frequency, and dimensions can be found in Table 4.3, while the network configuration parameters are summarized in Table 4.4.

For a UAV following trajectory (x_i, y_i, h_{max}) with maximum battery capacity E_{max} , the remaining energy can be expressed as

$$E_i = E_{max} - \sum_{i=0}^i E_i. \quad (4.22)$$

4.4.1.4 Energy model of gNB

Path loss is modeled as the probability model that consists mainly of two components, i.e., Line-of-Sight (LoS) and Non-Line-of-Sight (NLoS). LoS connection probability between the receiver and transmitter is an essential factor and can be

Notations	Physical definition	Simulation value
m_{uav}	UAV Weight (6×TB48S batteries) [kg]	10
ρ	Air density in [kg/ m ³]	1.225
C_D	Drag coefficient	0.044
r_{uav}	Propeller radius in meter [m]	0.1905
A_{uav}^{top}	UAV top area [m ²]	0.3
V_{uav}	Max UAV speed [m/ s]	18
N_{rotor}	Number of rotors	6
ϕ_{tilt}	Tilt Angle values	25°
$N_{battery}$	Number of batteries	6
η_{mot}	Motor efficiency	0.8
η_{pro}	Propeller system efficiency	0.8

Table 4.1: UAV and Motor Simulation Parameters.

Parameter	Simulation value
Battery model	TB48S
Battery type	LiPo 6S
Weight	0.680 kg
Capacity (Q)	5700 mAh
Voltage	22.8 V
Energy	129.96 Wh

Table 4.2: UAV Battery Model Simulation Parameters.

Parameter	Simulation value
LTE Mode	TDD
Frequency Bands	400 MHz: (400-430) MHz 600 MHz: (566-626) MHz, (566-626) MHz, (606-678) MHz 1.4GHz: (1447-1467) MHz 1.8GHz: (1785-1805) MHz
Channel Bandwidth	5/10/15/20 MHz
Max Output Power	15 Watt
Power Supply	48V DC or 220V AC
Power Consumption	150 Watt
MIMO	2x2
Dimensions	330*260*110 mm
Weight	5.5 kg
Users	200
Working Temperature	-20° C to 60° C
Throughput	DL: ≤ 80 Mbps UL: ≤ 30 Mbps

Table 4.3: gNB Simulation Parameters.

formulated as [63]

$$p_{LoS,k}(i) = \frac{1}{1 + a_{LoS} \cdot \exp(-b_{LoS} (\phi_k(i) - a_{LoS}))}, \quad (4.23)$$

Parameter	Simulation value
Bandwidth	5 MHz, 10 MHz, 15 MHz, 25 MHz
Transmitted power	23 dBm
Frequency	2 GHz
Noise power density	-174 dBm
MIMO	2×2

Table 4.4: Mobile Network Simulation Parameters.

where (a_{LOS}) and (b_{LOS}) are environmental constants, and $(\phi_k(i))$ is the elevation angle in degree, and it depends on the UAV height as well as the distance between the UAV and user k , the elevation angle can be evaluated from $(\phi_k = -\frac{180^\circ}{\pi} \sin^{-1}(\frac{h(i)}{d_k(i)}))$. Furthermore, $(h(i))$ is the UAV height, and $(d_k(i))$ is the and defined by

$$d_k(i) = \sqrt{h^2(i) + (x(i) - x_k(i))^2 + (y(i) - y_k(i))^2}. \quad (4.24)$$

The probability of having NLoS communication between the UAV and k-th UE is denoted by

$$p_{NLoS,k}(i) = 1 - p_{LoS,k}(i). \quad (4.25)$$

Hence, the mean path loss model (in dB) I adopt the following equation from [63]

$$L_k(h, d_k, i) \text{ (dB)} = L_{LoS,k}(i) \times p_{LoS,k}(i) + L_{NLoS,k}(i) \times p_{NLoS,k}(i), \quad (4.26)$$

where, $L_{LoS,k}(i)$ [dB] and $L_{NLoS,k}(i)$ [dB] are the path loss for LoS and NLoS communication links and denoted by

$$L_{LoS,k}(i) = 10 \times \alpha_{pl,NLoS} \log \left(\frac{4\pi f_c d_k(i)}{c} \right) + \delta_{LoS}, \quad (4.27)$$

$$L_{NLoS,k}(i) = 10 \times \alpha_{pl,LoS} \log \left(\frac{4\pi f_c d_k(i)}{c} \right) + \delta_{NLoS}, \quad (4.28)$$

where $(\alpha_{pl,LoS})$ and $(\alpha_{pl,NLoS})$ are the path loss exponents for the LoS and NLoS paths respectively and its environment-dependent variable. Both the δ_{LoS} and δ_{NLoS}

are the mean losses due to LoS and NLoS communication links, ($c = 3 \times 10^8$ [m/s]) the speed of light and (f_c) is the network operating frequency.

With ($\gamma_k(i)$) represents the Signal-to-Noise Ratio (SNR) of the k -th UE at the i -th step, while assuming ($P_{r,k}(i)$) is the received signal power at the k -th UE, and (σ) represents the noise power which is assumed to be additive white Gaussian noise, AWGN), the SNR is defined as

$$\gamma_k(i) = \frac{P_{r,k}(i)}{\sigma^2}. \quad (4.29)$$

The SNR can be rewritten in terms of the path loss and transmitted UAV power as

$$\gamma_k(i) = \frac{P_k(i) \times L_k(i)}{\sigma^2}, \quad (4.30)$$

where ($P_k(i)$) is the transmitted power from the UAV to the k -th UE at the i -th step.

The 5G NR maximum data rate of the k -th UE can be evaluated in (Mbps) using the formula defined in [64], and expressed as

$$R_k(i) = 10^{-6} \cdot \sum_{j=1}^J \left(\Omega_{j,k} \cdot M_{j,k} \cdot \zeta_{j,k} \cdot C_{R,\max} \cdot \frac{N_{j,k}^{RB}(i) \cdot 12}{T_s^\mu} \cdot (1 - OH_{j,k}) \right), \quad (4.31)$$

where (J) represents the number of aggregated component carriers, ($\Omega_{j,k}$) is the maximum number of layers, and ($M_{j,k}$) is the modulation order. In contrast, ($\zeta_{j,k}$) is a scaling factor that has values of (1, 0.8, 0.75, and 0.4). The code rate is denoted by ($C_{R,\max}$), and is can have the values in Tables 5.1.3.1-1, 5.1.3.1-2 and 5.1.3.1-3 in 3gpp.38.214 with a maximum value of (948/1024). The numerology μ can have the values of [0, 1, 2, 3, 4] which responds to the subcarrier spacing (SCS) of 15 kHz, 30 kHz, 60 kHz, 120 kHz and 240 kHz. The variable T_s^μ represents the average OFDM symbol duration for certain μ and can be evaluated as ($T_s^\mu = \frac{10^3}{14 \times 2^\mu}$). The $N_{j,k}^{RB}(i)$ is

the number of allocated RBs to the k-th UE at the i-th step. Finally, $OH_{j,k}$ denotes the overhead and can have the values of (0.14, 0.18, 0.08, and 0.10).

Moreover, the data rate can have another formula to be evaluated according to [64], as

$$R_k(i) = 10^{-3} \cdot \sum_{j=1}^J TBS_{j,k}(i) \times 2^\mu, \quad (4.32)$$

where $TBS_{j,k}$ is the total maximum number of DL-SCH transport block bits received within a 1ms TTI for the k-th UE and j-th carrier.

4.4.1.5 NR frame Frame structure

The NR supports two frequency ranges of frame types (FR): FR1 (up to 6 GHz) and FR2 (millimeter wave range: 24.25 to 52.6 GHz). Also NR uses flexible subcarrier spacing (Δf [kHz]) derived from basic 15 kHz subcarrier spacing used in LTE. Where the numerology (μ) is introduced to determine the subcarrier spacing with the relation denoted as ($\Delta f = 2^\mu * 15$ [kHz]). The NR frame is presented in figure 4.4.

The NR radio frame consists of (10) subframes in the time domain, with subframe length (1ms), each subframe can have 2^μ slots and each slot consists of and (14) OFDM symbols. Slot length varies based on subcarrier spacing as presented in table 4.5.

μ	Δf [kHz]	Slot length [ms]	Max RBs	No. slot per subframe	No. slots per frame
0	15	1	275	1	10
1	30	0.5	275	2	20
2	60	0.25	275	4	40
3	120	0.125	275	8	80
4	240	0.0625	138	16	160

Table 4.5: NR frame slots and subframes based on numerology value.

4.4.1.6 5G frame Downlink Link Adaptation

Many link-to-system (L2SM) mapping approaches in 3GPP contributions and standards have been proposed [65], these algorithms use the concept of the effective

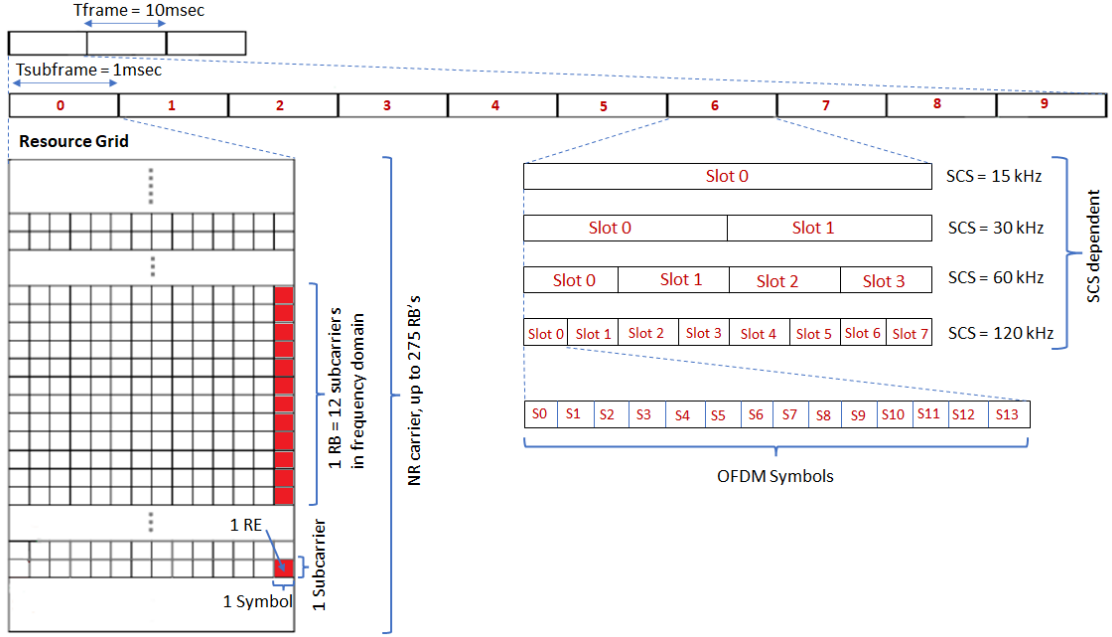


Figure 4.4: 5G NR Frame structure.

SNR (Signal-to-Noise Ratio) (γ_{eff}). Examples of mapping algorithms are the Exponential Effective SNR Metric (EESM) and Mutual Information Effective SNR mapping (MIESM), where the effective SNR is mapped another value that is denoted the CQI instead of dealing with the SNR directly. CQI is an information that is sent by the UE to the network to indicate its communication channel quality and to use this metric to determine the required throughput. The CQI report is a 4-bit word representing indices ranging from 0 to 15. NR defines four tables of 4-bit CQIs (Tables 5.2.2.1-2 to 5.2.2.1-5 in [66]).

The mapping procedure consists from two stages: 1) SNR compression, 2) Map to CQI value. The general form of all the forms of compression functions can be formulated for the single antenna case (SISO) as

$$\gamma_{\text{eff}}(\alpha_1, \alpha_2) = -\alpha_1 I^{-1} \left(\frac{1}{N^{RB}} \sum_{k=1}^{N^{RB}} I \left(-\frac{\gamma_k}{\alpha_2} \right) \right) \quad (4.33)$$

Herein, both (α_1) and (α_2) are the parameters to be optimized. The function (I) is the mapping function and its inverse function is denoted as (I^{-1}) . The SNR for the

k-th subcarriers is represented by (γ_k) and the variable (N^{RB}) is the total resource blocks. In the case of the EESM algorithm which is widely used for its simplicity over the other algorithms. EESM algorithm computes the information measure based on the exponential function, where the mapping function in the equation (4.33) is represented by exponential function as $(I = \exp\{\})$ and its inverse function denoted as $(I^{-1} = \ln\{\})$. The effective SNR then can be denoted as

$$\gamma_{eff}(\beta) = -\beta \ln \left(\frac{1}{N^{RB}} \sum_{k=1}^{N^{RB}} \exp \left(-\frac{\gamma_k}{\beta} \right) \right) \quad (4.34)$$

here the variable (N^{RB}) is the allocated RBs, and (γ_k) stands for the SNR measure at the k-th resource and can be defined by equation (4.29). Moreover, $(\beta = \alpha_1 = \alpha_2)$ is the fitting parameter which needs to be optimized. The parameter (β) is a calibration factor whose value is chosen to minimize the root mean square (RMS) error between the effective SNR, that is derived from the fading channel, and the average SNR which leads to the same BLER (block error rate) value in a AWGN channel (AWGN reference). (β) can be calculated following [67, equation 4], and denoted by

$$\beta = \min_{\beta} RMS(\gamma_{AWGN} - \gamma_{eff}(\beta)) \quad (4.35)$$

Then the effective SNR is to be mapped with the BLER, which is defined as the ratio of the number of erroneous blocks to the total number of blocks transmitted over the wireless channel. In addition, BLER depends on SNR, Modulation and coding scheme (MCS), and resource allocation.

Modulation and coding scheme (MCS) and the code rates are predefined in the NR with three tables: Table1 (up to 64-QAM), Table2 (up to 256-QAM), and Table3 (up to 64-QAM with low spectral efficiency), which are given by Tables 5.1.3.1-1 to 5.1.3.1-3 in [66]. Each MCS index is quantized by 5 bits. In this work, we focus on MCS tables 1 and 2 to determine the modulation order (Q_l) and the code rate

$(R_{l,i})$. In NR the transport block size (TBS) determination process is described as a sequence of algorithm summarized in the following steps.

To determine the TBS size the (N_{info}) is to be calculated for the k-th UE, the $(N_{info,i})$ is evaluated from equations in section 5.1.3.2 in [66], and denoted as

$$N_{info,i} = N_{RE,i} \times CR_{l,i} \times Q_{l,i} \times v_{l,i} \quad (4.36)$$

where $(N_{RE,i})$ is the number of resource elements (RE) in the slot and is evaluated from $(N_{RE,i} = \arg \min \{156, N'_{RE,i}\} \times n_{PRB})$, here (n_{PRB}) is the total number of allocated PRBs (Physical resource block) for the UE. Moreover, $(N'_{RE,i})$ represent the number of REs (Resource Element) allocated for PDSCH (Physical Downlink Shared Channel) within a PRB, and determined by the UE. The $(N'_{RE,i})$ is rounded down to 156 i.e. the UE can never consume more than 156RBs within the bandwidth of a single Resource Block, and it can be determined as

$$N'_{RE,i} = N_{SC}^{RE} \times N_{symp}^{sh} - N_{DMRS}^{PRB} - N_{OH}^{PRB} \quad (4.37)$$

Herein, (N_{SC}^{RE}) equals 12 which is the number of subcarriers in a PRB, (N_{symp}^{sh}) can have the values of 12 or 14 and represents the of symbols of the PDSCH allocation within the slot. (N_{DMRS}^{PRB}) is the number of the REs for DM-RS per PRB in the scheduled duration and includes the overhead of the DM-RS (Demodulation Reference Signal) groups without the data. The parameter (N_{OH}^{PRB}) can have the values of (0, 6, 12 or 18) and represent the overhead parameter. Finally, the modulation order $(Q_{l,i})$ and code rate $(R_{l,i})$ is determined from tables 5.1.3.1-1 and 5.1.3.1-2 in [66], by matching the MCS index value with the corresponding $(Q_{l,i})$ and $(R_{l,i})$.

The next step is the TBS determination from the value of $(N_{info,i})$. in this stage there are two approaches to calculate the TBS, the algorithm depends on the value of $(N_{info,i})$ and where it larger os smaller than the value of 3824. If $(N_{info,i} \leq 3824)$, the TBS can be found from the formula:

$$N'_{info,i} = \max \left(24, 2^{n_i} \cdot \left\lfloor \frac{N_{info,i}}{2^{n_i}} \right\rfloor \right)$$

where $[n_i = \max(3, \lfloor \log_2(N_{info,i}) \rfloor - 6)]$, then find the closest TBS value from table 5.1.3.2-1 in [66], but not greater than the value of N'_{info} .

On the other hand, where $(N_{info,i} > 3824)$, fist we need to check the code rate if it is larger than $(CR_i \leq 0.25)$ or not, then evaluate $(N_{info,i})$ and check if the value is lager than 8424 or not, the calculation algorithm for this stage is summarized in figure 4.5.

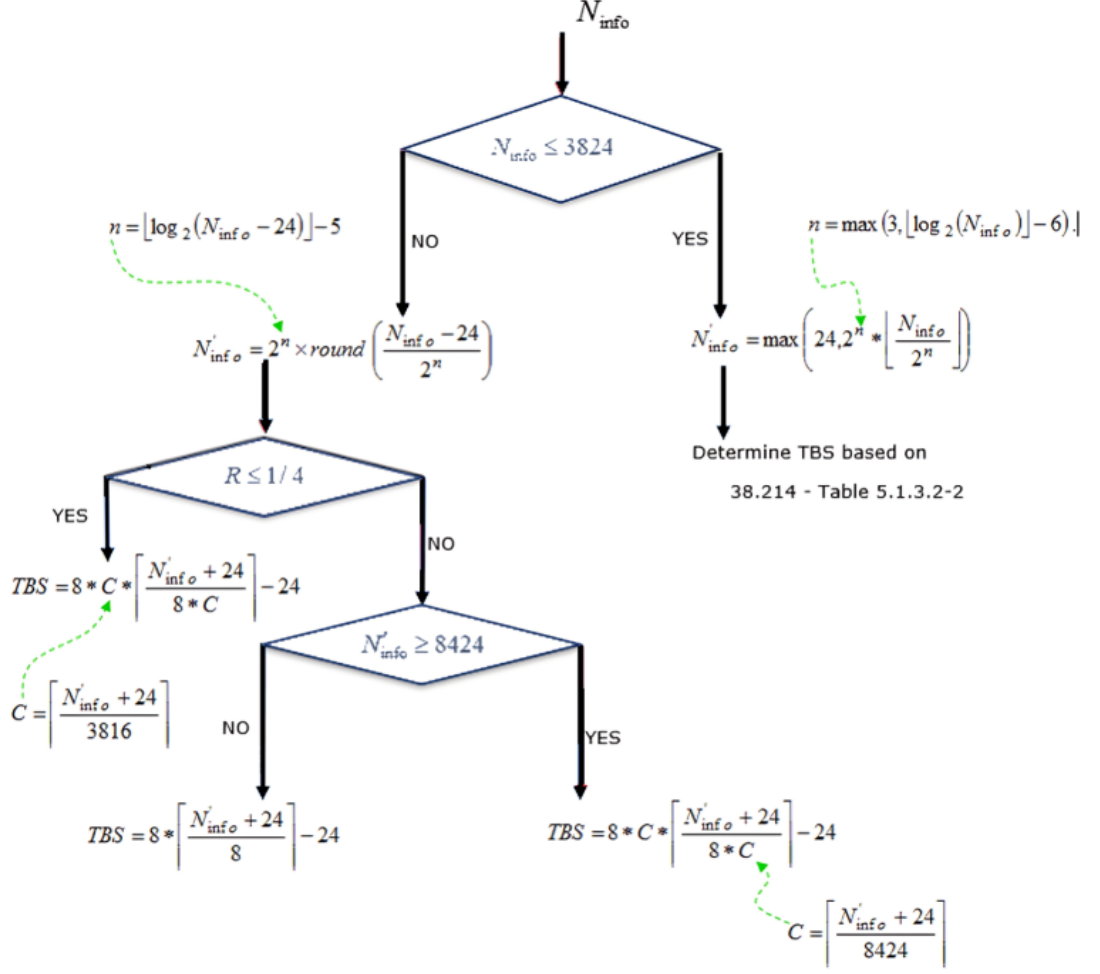


Figure 4.5: TBS size calculation algorithm flowchart.

4.4.2 Simulation results

In our case study, we considered one UAV that flies at a maximum altitude of $h_{max} = 200m$ over different grid area size (750×750) , (1000×1000) and (1500×1500) in $[m^2]$ units. The simulation parameters listed in tables 4.1, 4.2 and table 4.3 while the network settings are listed in Table 4.4.

The study involved deploying and training the Proximal Policy Optimization (PPO) deep reinforcement learning algorithm (DRL) in a UAV-assisted network environment. In this setup, the UAV carries the gNB and flies around the cell to provide mobile services to the maximum number of UEs. The battery capacity of the UAV was initialized with a value denoted by E_{max} . In the first simulation scenario,

there were four number of UEs which are positioned at the corners of a cell grid which has the dimensions of $(750 \times 750)m^2$. The maximum reward value, which is denoted by R^{max} , and is associated with the last position of the UAV before flying back to the starting base station was at the coordinates $(380, 380, 200)$ - the position is plotted in the red square on the map. The gNB allotted 16 RBs to all the four UE's located at the cell corners. The bandwidth used in this scenario was 5 MHz. Figure 4.6 depicted the UAV's path within the cell (top view) as it searched for the optimal position before returning to the base point, and Figure 4.7 it also illustrated the total reward function for each step in the trained episode.

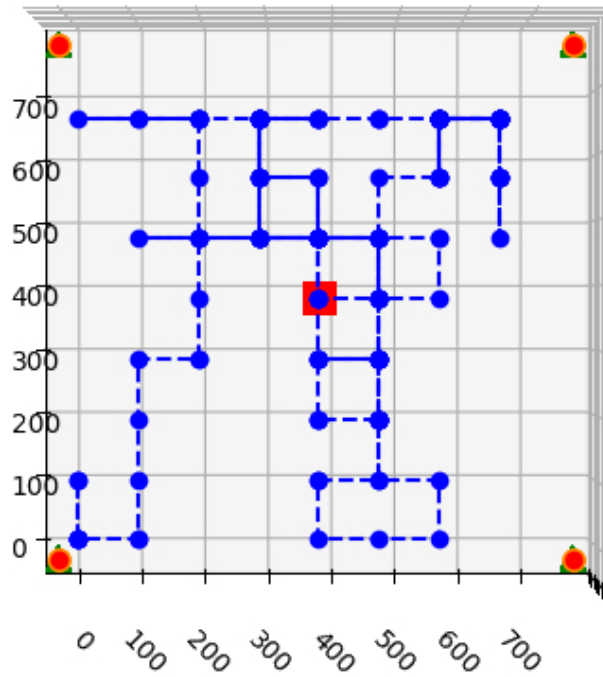


Figure 4.6: Cell grid with UAV trajectory path, for the scenario of 4 UEs positioned at the corners of $750m^2$ cell grid, BW=5 MHz.

In the second type of scenario, the UEs are randomly distributed within the cell grid, but they remain stationary and do not move within the cell. The number of UEs set to have 10 and 50 UEs. The results depicted in figure 4.9, and the UAV trajectory path in the cell is plotted in figure 4.8. The cell grid size is assumed to be $(1000 \times 1000)m^2$, and the BW value is 25 MHz. In this scenario, 10 number of UEs

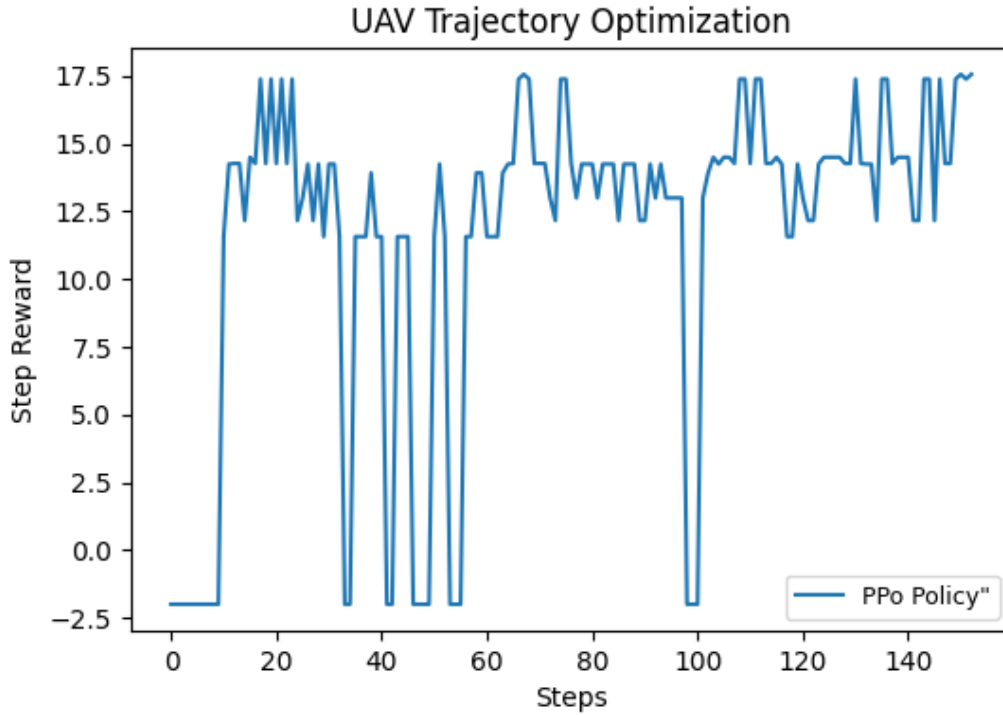


Figure 4.7: UAV trajectory and allocated RBs for the scenario of 4 UEs located at the corner of 750m^2 cell grid, $BW = 5\text{MHz}$.

are randomly distributed and stationary within the cell, with the maximum reward value associated with the UAV positioned at $(380, 190, 200)$ and the gNB allocates 23 RBs for all the UEs positioned in the cell grid. Furthermore, in figures 4.8 and 4.9, the cell grid size is assumed to be $(1000 \times 1000)\text{m}^2$, and the BW value is 25 MHz. In this scenario, 10 number of UEs are randomly distributed and stationary within the cell, with the maximum reward value associated with the UAV positioned at $(475, 665, 200)$ presented by the blue square at the cell grid map, and the gNB allocated 21 RBs for only 9 UEs out of the total number of UE which is 10. The last UAV position was at $(570, 380, 200)$ allocating 20 RBs to 8 UE's, the UAV position presented by the red square in figure 4.8.

Figures 4.10 and 4.11 depict the UAV's trajectory and reward-per-step function within a $1000\text{m} \times 10000\text{m}$ cell grid, showing maximum rewards at coordinates $(380, 475, 200)$ (blue square) and $(950, 285, 200)$ (red square) with 10 MHz bandwidth allocation, where 39 RBs were initially assigned to 20 randomly distributed

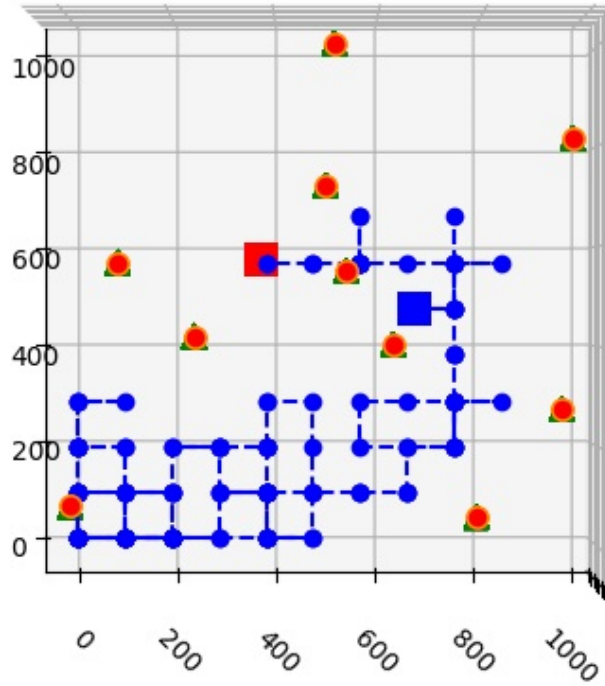


Figure 4.8: Cell grid with UAV trajectory path, for the scenario of 10 UEs randomly located and stationary in 1000 m^2 cell grid, $\text{BW}=25\text{ MHz}$.

stationary UEs; the UAV's final position at $(285, 570, 200)$ served 19 UEs with 38 RBs, demonstrating dynamic resource adaptation during the mission.

In the third type of scenario, the mobility of UE within a cell grid size of $(1500 \times 1500)\text{ m}^2$ is taken into account, with ground users moving at a different velocity values. Figure 4.12 illustrates the cell grid map for the case where 10 UEs are randomly distributed and moving at 10 m/s velocity. The UAV achieves maximum reward at the position of $(665, 665, 200)$, and 11 RBs are allocated for 9 UEs out of 10 in the cell grid. In this scenario, the bandwidth (BW) is set to 10 MHz . The reward per step function is plotted in figure 4.13. The red lines in the map plot illustrates the start and end point of the UE movement in the cell grid. Moving on to figure 4.14 and figure 4.15, the best position of the UAV is at $(380, 285, 200)$, with 38 RBs allocated to 15 UEs, while the last UAV position was at $(95, 475, 200)$ with 29 RBs allocated to 10 UEs. The bandwidth is set to 40 MHz .

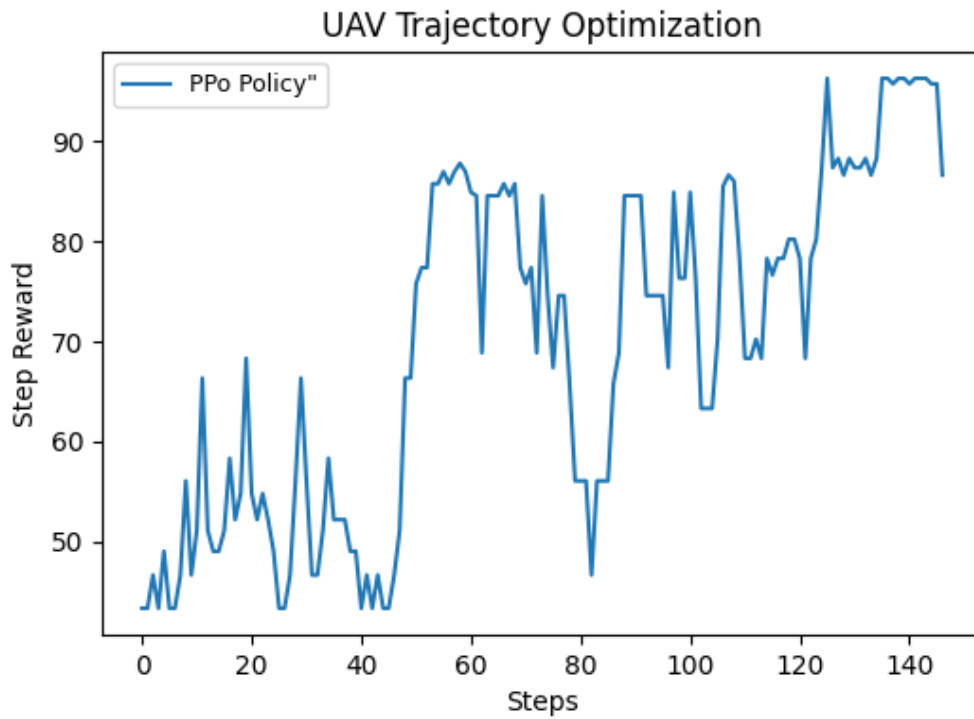


Figure 4.9: UAV trajectory and allocated RB, for the scenario of 10 UEs randomly located and stationary in 1000 m^2 cell grid, BW=25 MHz.

Finally, in figure 4.16 represents the scenario in which the simulation allocated 100 UEs in a $1700 \times 1700\text{ m}^2$ cell grid size. The RL agent succeeded to allocate 51 UE and served them with 151 total number of RBs. The step function is plotted in figure 4.17.

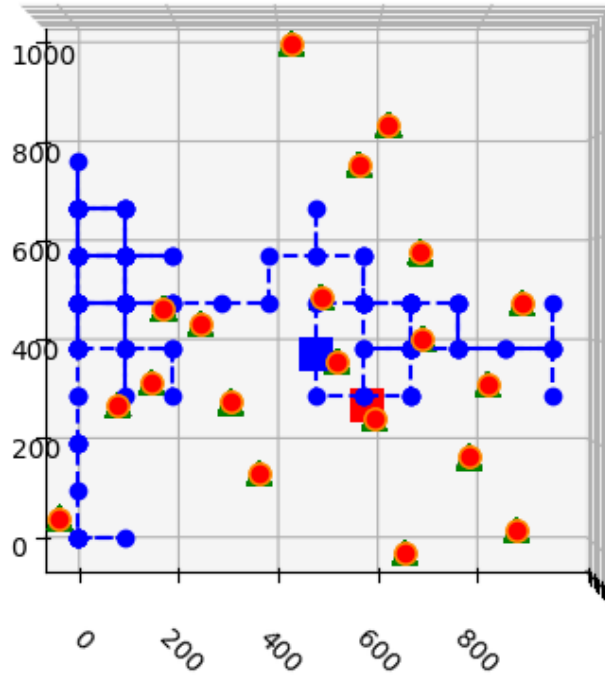


Figure 4.10: UAV trajectory and allocated RBs for the scenario of 20 UEs randomly located and stationary in 1000 m^2 cell grid, BW=25 MHz.

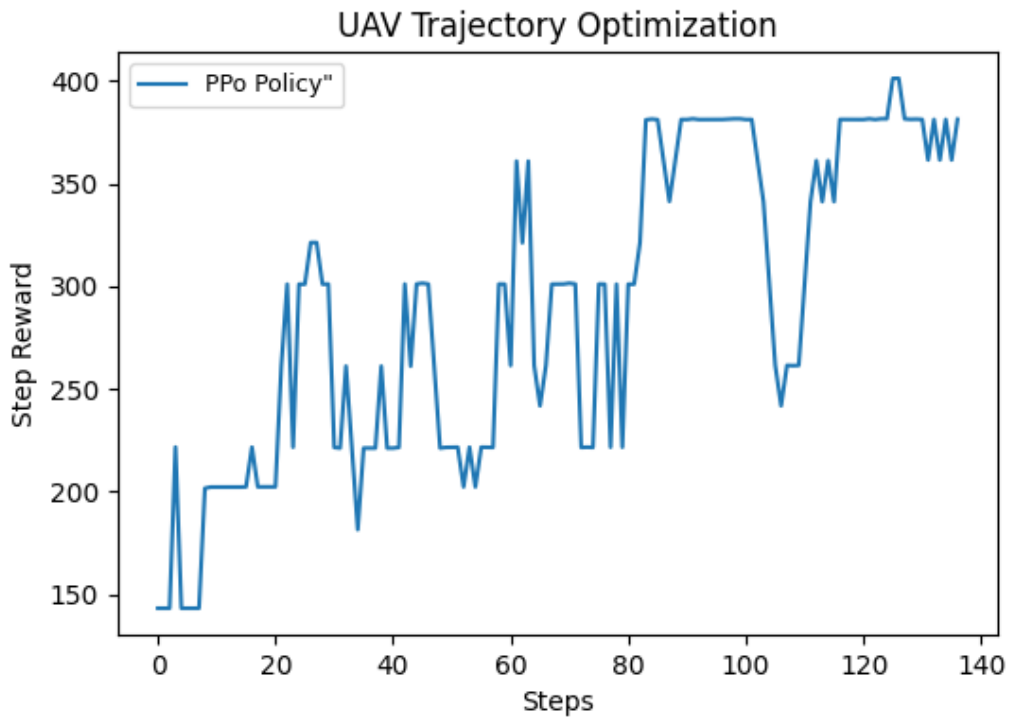


Figure 4.11: Cell grid with UAV trajectory path, for the scenario of 20 UEs randomly located and stationary in 1000 m^2 cell grid, BW=25 MHz.

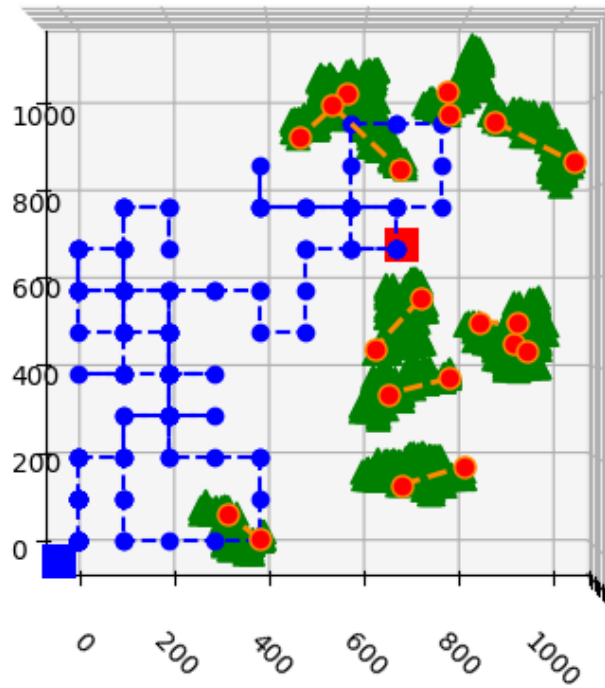


Figure 4.12: Cell grid with UAV trajectory path, 10 UEs with randomwalk model, BW=10 MHz, cell grid size= $1000 \times 1000m^2$

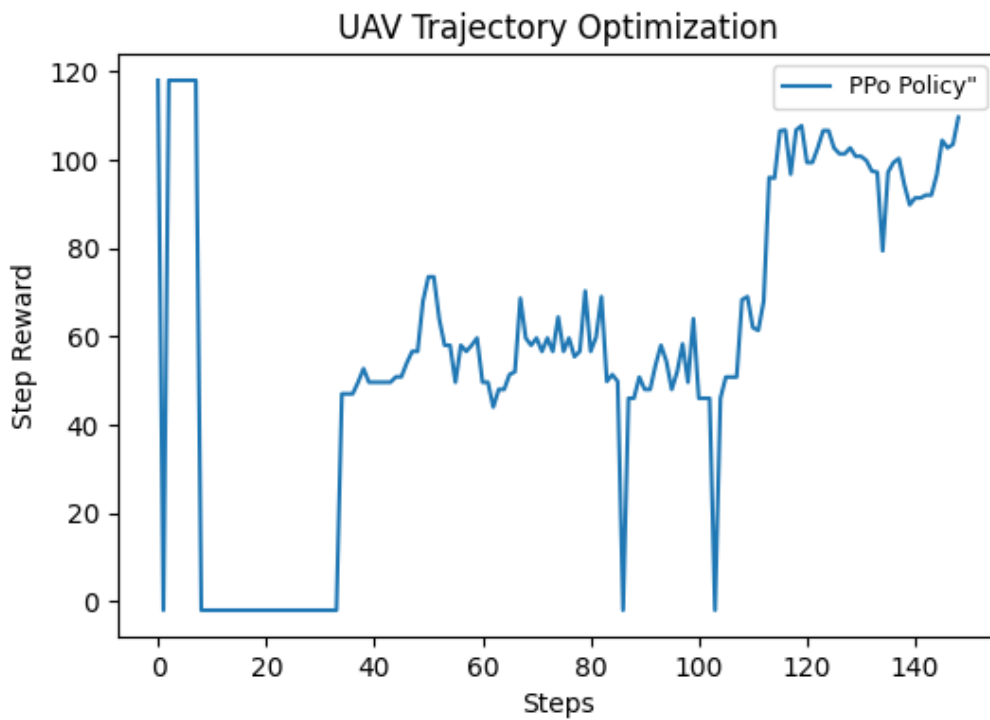


Figure 4.13: UE mobility scenario: 10 UEs with randomwalk model, BW=10 MHz, cell grid size= $1000m^2$

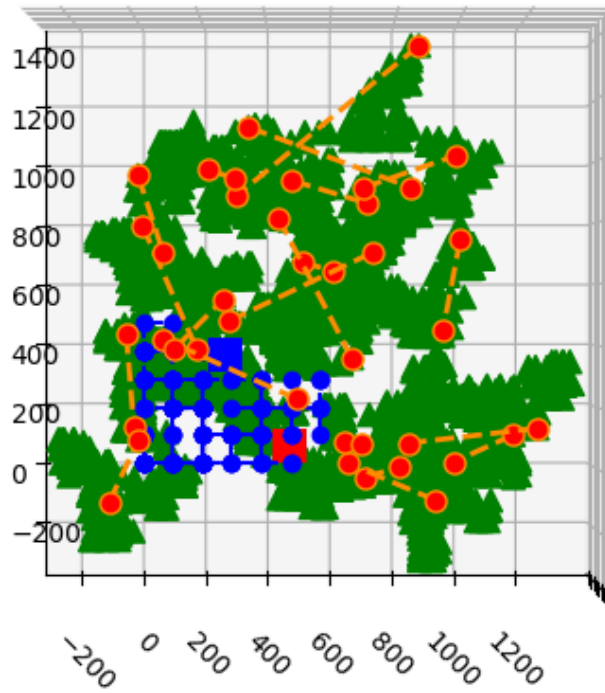


Figure 4.14: Cell grid with UAV trajectory path, 20 UEs with randomwalk model, BW=40 MHz, cell grid size= $1500 \times 1500m^2$.

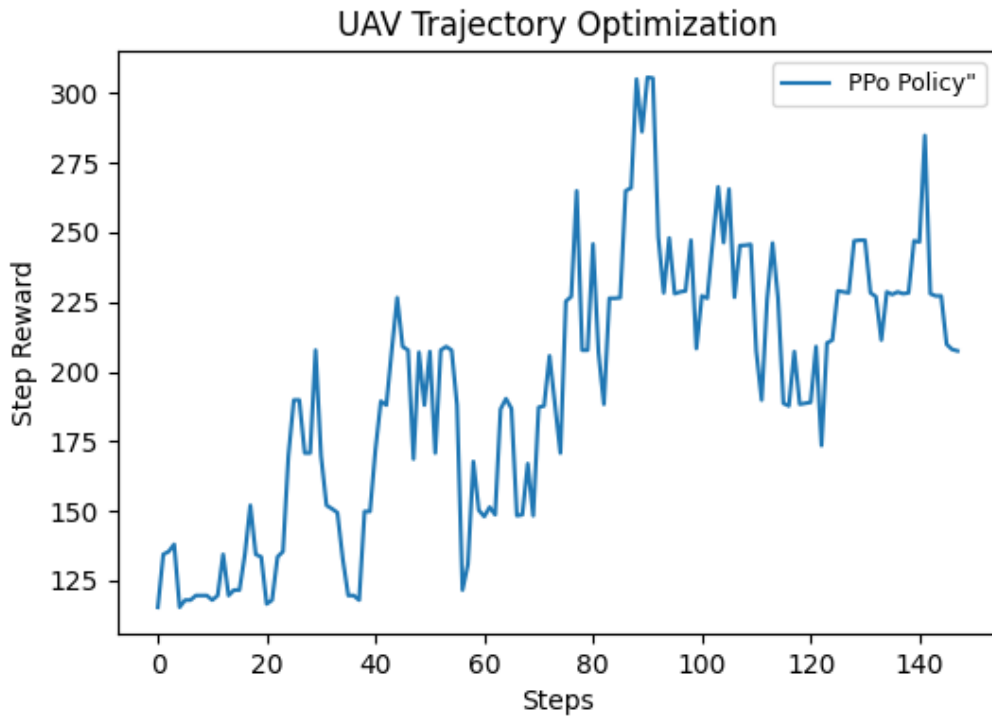


Figure 4.15: UE mobility scenario: 20 UEs with randomwalk model, BW=40 MHz, cell grid size= $1500 \times 1500m^2$.

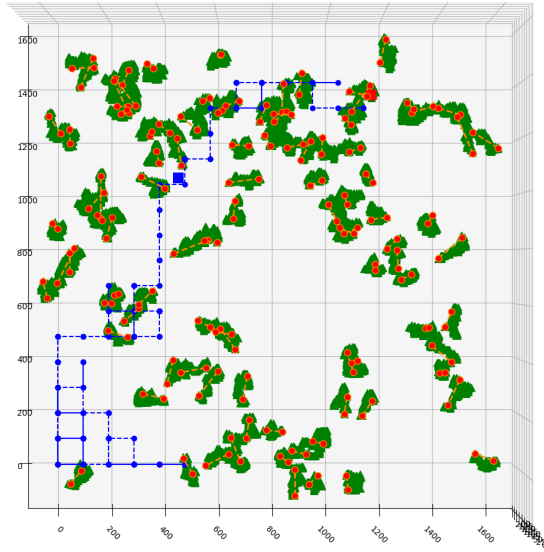


Figure 4.16: Cell grid with UAV trajectory path, 100 UEs with randomwalk model, BW=40 MHz, cell grid size= $1700 \times 1700m^2$.

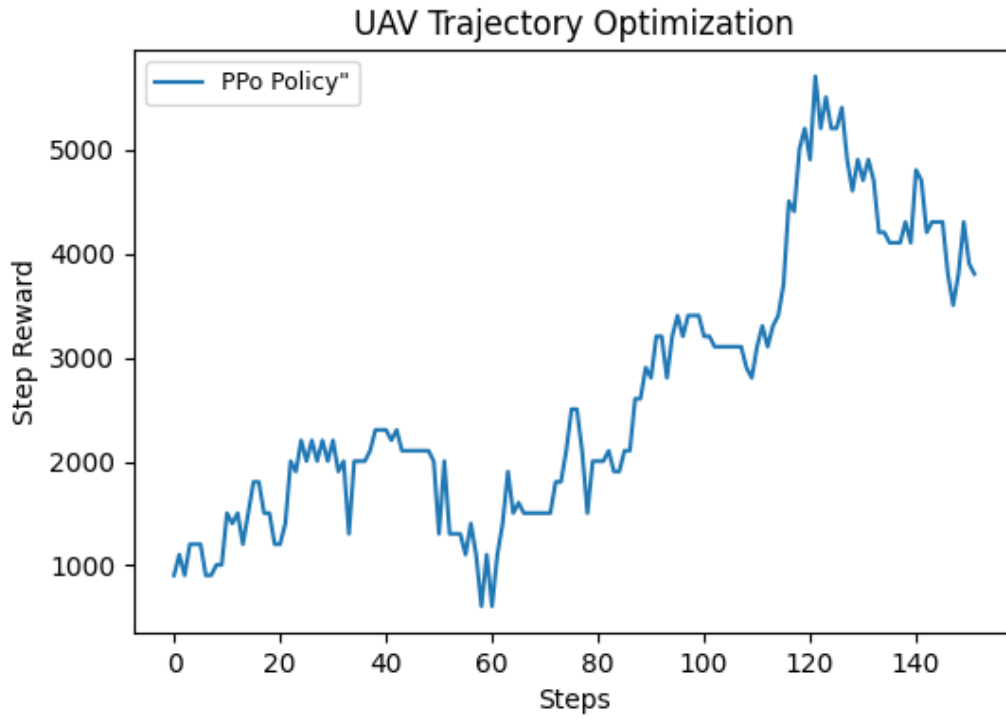


Figure 4.17: UE mobility scenario: 100 UEs with randomwalk model, BW=40 MHz, cell grid size= $1700 \times 1700m^2$.

4.5 Conclusion

This chapter presented a PPO-based reinforcement learning (RL) framework for autonomous UAV navigation in dynamic urban environments, addressing joint trajectory planning and resource allocation under critical constraints such as battery limits and user mobility. The algorithm's ability to learn efficient policies in stochastic settings was demonstrated through simulations, showcasing its potential for real-world UAV service delivery. While the current approach focuses on 2D navigation with discrete actions, future work could extend the model to 3D environments, incorporate real-time adaptive learning, and integrate multi-UAV coordination for large-scale deployments. The results highlight RL as a promising solution for intelligent UAV control, though further research is needed to bridge the gap between simulation and practical implementation under unpredictable real-world conditions.

Glossary — Chapter 4

Term	Description	Page
$(X_{k,i}, Y_{k,i})$	The k-th UE location coordinates at the i-th time slot.	90
A_{uav}	The UAV rotor propeller area.	91
A_{uav}^{eff}	The vertical projected area of the UAV.	94
$CQI(k, i)$	The i-th time slot CQI value of the k-th UE.	88
C_D	The drag coefficient.	94
$D_{i,k}$	The k-th UE direction at the i-th time slot.	90
E_{hor}	The horizontal propulsion energy.	96
E_{hov}	The required energy for the UAV hovering movement.	91
E_i	The UAV battery energy level value at each time slot.	89
E_{max}	The total energy of the multi-rotor UAV battery.	88
F_D	The UAV drag force.	94
F_x	The horizontal forces.	94
F_z	The vertical forces.	94
F_T	The UAV thrust force.	91
N_{tot}^{UE}	The total number of UEs that are requesting the mobile service in a certain cell area.	89
$N_{i,k}^{RB}$	The sum of allocated RBs for the UEs that were allocated successfully and got mobile services in time slot i .	89
N_{rotor}	The number of UAV rotors.	91
P_{hor}	The horizontal propulsion power.	95

Term	Description	Page
$U_{i,k}$	The i-th time slot CQI value of the k-th UE.	88
V_{hov}	The UAV hovering velocity.	91
$V_{i,k}$	The k-th UE speed at the i-th time slot.	90
ρ	The air density and equals to (1.225 kg/ m ³).	91
ω_{rotor}	The UAV motors rotation speed.	91
$\alpha_{pl,LoS}$	The path loss exponents for the LoS path.	98
$\alpha_{pl,NLoS}$	The path loss exponents for the NLoS path.	98
δ_{LoS}	The mean losses due to LoS communication link.	98
δ_{NsLoS}	The mean losses due to NLoS communication link.	98
$d_k(i)$	The network operating frequency.	98
f_c	The network operating frequency.	98
g	The earth gravitational acceleration and is equal to (9.81 \approx 10 kg/ m ²).	91
h_{max}	The UAV altitude (m).	88
k	The total number of subscribers that were located the served cell.	88
m_{tot}	The total mass of the drone and it's cargo.	92
$p_{LoS,k}(i)$	The probability of having LoS communication between the UAV and k-th UE.	98
$p_{NLoS,k}(i)$	The probability of having NLoS communication between the UAV and k-th UE.	98
r_i	The i-th reward value.	89
s_0	The UAV start point in the grid.	88
N_{tot}^{RB}	The total number of RBs in the bandwidth.	89
τ_i	The i-th time slot.	88

Own Publications

- [P1] R. Ramadan, A. Jwaifel, H. Al-Tous, and I. Barhumi, “Compressive sensing with weighted coefficient approach for indoor source localization,” in *2017 40th International Conference on Telecommunications and Signal Processing (TSP)*, pp. 243–246, 2017.
- [P2] A. M. J. Jwaifel, I. Ghareeb, and S. Shaltaf, “Impact of co-channel interference on performance of dual-hop wireless ad hoc networks over α - μ fading channels,” *International Journal of Communication Systems*, vol. 33, no. 14, p. e4500, 2020.
- [P3] A. M. Jwaifel, I. Ghareeb, and T. Van Do, “Impact of Co-channel Interference on the Performance of Cooperative Diversity Systems over α - μ Fading Channels,” *International Journal of Wireless Information Networks*, vol. 29, p. 232–239, 2022.
- [P4] A. M. Jwaifel and T. Van Do, “Deep reinforcement learning for jointly resource allocation and trajectory planning in uav-assisted networks,” in *Computational Collective Intelligence* (N. T. Nguyen, J. Botzheim, L. Gulyás, M. Núñez, J. Treur, G. Vossen, and A. Koziarkiewicz, eds.), (Cham), pp. 71–83, Springer Nature Switzerland, 2023.

Bibliography

- [1] M. Mozaffari, W. Saad, M. Bennis, Y. Nam, and M. Debbah, “A tutorial on UAVs for wireless networks: Applications, challenges, and open problems,” *IEEE Communications Surveys Tutorials*, vol. 21, no. 3, pp. 2334–2360, 2019.
- [2] H. Zhao, H. Wang, W. Wu, and J. Wei, “Deployment algorithms for UAV airborne networks toward on-demand coverage,” *IEEE Journal on Selected Areas in Communications*, vol. 36, no. 9, pp. 2015–2031, 2018.
- [3] N. Sharma, M. Magarini, D. N. K. Jayakody, V. Sharma, and J. Li, “On-demand ultra-dense cloud drone networks: Opportunities, challenges and benefits,” *IEEE Communications Magazine*, vol. 56, no. 8, pp. 85–91, 2018.
- [4] Q. Zhang, M. Mozaffari, W. Saad, M. Bennis, and M. Debbah, “Machine learning for predictive on-demand deployment of UAVs for wireless communications,” in *2018 IEEE Global Communications Conference (GLOBECOM)*, 2018, pp. 1–6.
- [5] X. Chen, X. Hu, Q. Zhu, W. Zhong, and B. Chen, “Channel modeling and performance analysis for UAV relay systems,” *China Communications*, vol. 15, no. 12, pp. 89–97, 2018.
- [6] G. Zhang, H. Yan, Y. Zeng, M. Cui, and Y. Liu, “Trajectory optimization and power allocation for multi-hop UAV relaying communications,” *IEEE Access*, vol. 6, pp. 48 566–48 576, 2018.

- [7] C. Zhan, Y. Zeng, and R. Zhang, "Energy-efficient data collection in UAV enabled wireless sensor network," *IEEE Wireless Communications Letters*, vol. 7, no. 3, pp. 328–331, 2018.
- [8] J. Xu, Y. Zeng, and R. Zhang, "UAV-enabled wireless power transfer: Trajectory design and energy optimization," *IEEE Transactions on Wireless Communications*, vol. 17, no. 8, pp. 5092–5106, 2018.
- [9] S. Ikki and S. Aissa, "Performance analysis of dual-hop relaying systems in the presence of co-channel interference," in *Proc. IEEE Global Telecommunications Conference, GLOBECOM*, 2010, pp. 1–5.
- [10] C. Zhong, S. Jin, and K.-K. Wong, "Outage probability of dual-hop relay channels in the presence of interference," in *Proc. IEEE 69th Vehicular Technology Conference, VTC Spring*, 2009, pp. 1–5.
- [11] F. S. Al-Qahtani, C. Zhong, K. A. Qaraqe, H. Alnuweiri, and T. Ratnarajah, "Performance analysis of fixed-gain AF dual-hop relaying systems over Nakagami-m fading channels in the presence of interference," *EURASIP journal on Wireless Communications and Networking*, vol. 2011, no. 1, pp. 1–10, 2011.
- [12] S. S. Ikki and S. Aissa, "Performance Evaluation and Optimization of Dual-Hop Communication over Nakagami-m Fading Channels in the Presence of Co-Channel Interferences," *IEEE Communications Letters*, vol. 16, no. 8, pp. 1149–1152, 2012.
- [13] A. Salhab, F. Al-Qahtani, S. Zummo, and H. Alnuweiri, "Performance analysis of amplify-and-forward relay system with interference-limited destination in different fading environments," in *Proc. International Symposium on Wireless Communication Systems, ISWCS*, 2012, pp. 196–200.
- [14] G. Nauryzbayev, K. M. Rabie, M. Abdallah, and B. Adebisi, "On the Performance Analysis of WPT-Based Dual-Hop AF Relaying Networks in $\alpha - \mu$ Fading," *IEEE Access*, vol. 6, pp. 37 138–37 149, 2018.

- [15] G. Nauryzbayev, M. Abdallah, and K. Rabie, "Outage Probability of the EH-Based Full-Duplex AF and DF Relaying Systems in $\alpha - \mu$ Environment," in *2018 IEEE 88th Vehicular Technology Conference (VTC-Fall)*, 08 2018, pp. 1–6.
- [16] A. Magableh, T. Aldalgamouni, and N. Jafreh, "Capacity analysis of dual-hop wireless communication systems over α - μ fading channels," *Computers & Electrical Engineering*, vol. 40, 01 2013.
- [17] M. A. Amer and S. Al-Dharrab, "Performance of two-way relaying over α - μ fading channels in hybrid RF/FSO wireless networks," 2019.
- [18] S. Ikki and M. Ahmed, "Performance analysis of cooperative diversity using equal gain combining (EGC) technique over Rayleigh fading channels," in *Proc. IEEE International Conference on Communications, ICC*, 2007, pp. 5336–5341.
- [19] S. S. Ikki and M. H. Ahmed, "Performance of multiple-relay cooperative diversity systems with best relay selection over Rayleigh fading channels," *EURASIP Journal on Advances in Signal Processing*, vol. 2008, p. 145, 2008.
- [20] S. Ikki and M. Ahmed, "Performance of cooperative diversity using Equal Gain Combining (EGC) over Nakagami-m fading channels," *IEEE J WCOM*, vol. 8, no. 2, pp. 557–562, 2009.
- [21] A. Afana, S. Ikki, T. M. N. Ngatched, and O. A. Dobre, "Performance analysis of cooperative networks with optimum combining and co-channel interference," in *2015 IEEE International Conference on Communication Workshop (ICCW)*, 2015, pp. 949–954.
- [22] H. Yu, I. Lee, and G. L. Stuber, "Outage probability of decode-and-forward cooperative relaying systems with co-channel interference," *IEEE Transactions on Wireless Communications*, vol. 11, no. 1, pp. 266–274, 2012.
- [23] A. M. Salhab, F. Al-Qahtani, S. A. Zummo, and H. Alnuweiri, "Exact outage probability of opportunistic DF relay systems with interference at both the relay

- and the destination over Nakagami-m fading channels,” in *2012 IEEE Global Communications Conference (GLOBECOM)*, 2012, pp. 4560–4565.
- [24] J. Zhang, Y. Zeng, and R. Zhang, “Spectrum and energy efficiency maximization in UAV-enabled mobile relaying,” in *2017 IEEE International Conference on Communications (ICC)*, 2017, pp. 1–6.
- [25] Q. Wu and R. Zhang, “Common Throughput Maximization in UAV-Enabled OFDMA Systems With Delay Consideration,” *IEEE Transactions on Communications*, vol. 66, no. 12, pp. 6614–6627, 2018.
- [26] Y. Xu, L. Xiao, D. Yang, Q. Wu, and L. Cuthbert, “Throughput maximization in multi-UAV enabled communication systems with difference consideration,” *IEEE Access*, vol. 6, pp. 55 291–55 301, 2018.
- [27] M. Samir, M. Chraïti, C. Assi, and A. Ghrayeb, “Joint optimization of UAV trajectory and radio resource allocation for drive-thru vehicular networks,” in *2019 IEEE Wireless Communications and Networking Conference (WCNC)*, 2019, pp. 1–6.
- [28] A. Guerra, F. Guidi, D. Dardari, and P. M. Djurić, “Reinforcement learning for UAV autonomous navigation, mapping and target detection,” in *2020 IEEE/ION Position, Location and Navigation Symposium (PLANS)*, 2020, pp. 1004–1013.
- [29] J. Cui, Y. Liu, and A. Nallanathan, “Multi-agent reinforcement learning-based resource allocation for UAV networks,” *IEEE Transactions on Wireless Communications*, vol. 19, no. 2, pp. 729–743, 2020.
- [30] J. Cui, Z. Ding, Y. Deng, A. Nallanathan, and L. Hanzo, “Adaptive UAV-trajectory optimization under quality of service constraints: A model-free solution,” *IEEE Access*, vol. 8, pp. 112 253–112 265, 2020.

- [31] F. Tang, Y. Zhou, and N. Kato, “Deep Reinforcement Learning for Dynamic Uplink/Downlink Resource Allocation in High Mobility 5G HetNet,” *IEEE Journal on Selected Areas in Communications*, vol. 38, no. 12, pp. 2773–2782, 2020.
- [32] D. Tse and P. Viswanath, *Fundamentals of wireless communication*. USA: Cambridge University Press, 2005.
- [33] A. Goldsmith, *Wireless Communications*. Cambridge University Press, 2005.
- [34] M. Yacoub, “The α - μ distribution: A physical fading model for the stacy distribution,” *IEEE Transactions on Vehicular Technology*, vol. 56, no. 1, pp. 27–34, 2007.
- [35] Proakis, *Digital Communications 5th Edition*. McGraw Hill, 2007.
- [36] R. S. Sutton and A. G. Barto, *Reinforcement Learning: An Introduction*. Cambridge, MA, USA: A Bradford Book, 2018.
- [37] J. Schulman, F. Wolski, P. Dhariwal, A. Radford, and O. Klimov, “Proximal policy optimization algorithms,” *CoRR*, vol. abs/1707.06347, 2017.
- [38] K. J. R. Liu, A. K. Sadek, W. Su, and A. Kwasinski, *Cooperative Communications and Networking*. USA: Cambridge University Press, 2009.
- [39] H. Ilhan, “Performance Analysis of Cooperative Vehicular Systems with Co-channel Interference Over Cascaded Nakagami-m Fading Channels,” *Wireless Personal Communications*, vol. 83, 07 2015.
- [40] A. Papoulis and S. U. Pillai, *Probability, random variables, and stochastic processes*. Tata McGraw-Hill Education, 2002.
- [41] F. W. Olver, D. W. Lozier, R. F. Boisvert, and C. W. Clark, *NIST Handbook of Mathematical Functions*, 1st ed. USA: Cambridge University Press, New York, NY, 2010.

- [42] P. Z. Peebles, *Probability, random variables, and random signal principles*. New York : McGraw-Hill, 1987.
- [43] M. O. I. Prudnikov A. P., Brychkov I. A., *Integrals and Series: Volume 3: More Special Functions*. Gordon and Breach Science publishers, 1990.
- [44] Wolfram, *Wolfram Research, Mathematica Edition: Version 10.0*. Wolfram Research, Inc., 2015. Wolfram, 2007.
- [45] S. Ikki and S. Aissa, “Investigations on the effects of co-channel interference on dual-hop transmission in Nakagami-m fading,” in *Personal Indoor and Mobile Radio Communications (PIMRC), 2011 IEEE 22nd International Symposium on*, 2011, pp. 894–898.
- [46] I. R. I.S. Gradshteyn, *Table of integrals, series, and products*. Elsevier, 2014.
- [47] M. O. I. Prudnikov A. P., Brychkov I. A., *Integrals and Series: Volume 1: Elementary Functions*. Gordon and Breach Science publishers, 1986.
- [48] M. Abramowitz and I. A. Stegun, *Handbook of Mathematical Functions, With Formulas, Graphs, and Mathematical Tables*,. USA: Dover Publications, Inc., 1974.
- [49] M. K. Simon and M. S. Alouini, *Digital Communication over Fading Channels; 2nd ed.* Newark, NJ: Wiley, 2005.
- [50] Y. Zeng, R. Zhang, and T. J. Lim, “Wireless communications with unmanned aerial vehicles: opportunities and challenges,” *IEEE Communications Magazine*, vol. 54, no. 5, pp. 36–42, 2016.
- [51] Q. Wu, L. Liu, and R. Zhang, “Fundamental trade-offs in communication and trajectory design for UAV-enabled wireless network,” *IEEE Wireless Communications*, vol. 26, no. 1, pp. 36–44, 2019.

- [52] Q. Wu, W. Mei, and R. Zhang, “Safeguarding wireless network with UAVs: A physical layer security perspective,” *IEEE Wireless Communications*, vol. 26, pp. 12–18, 10 2019.
- [53] X. Lin, V. Yajnanarayana, S. D. Muruganathan, S. Gao, H. Asplund, H. Maattanen, M. Bergstrom, S. Euler, and Y. . E. Wang, “The sky is not the limit: LTE for unmanned aerial vehicles,” *IEEE Communications Magazine*, vol. 56, no. 4, pp. 204–210, 2018.
- [54] T. Camp, J. Boleng, and V. Davies, “A survey of mobility models for ad hoc network research,” *Wireless Communications and Mobile Computing*, vol. 2, no. 5, pp. 483–502, 2002. [Online]. Available: <https://onlinelibrary.wiley.com/doi/abs/10.1002/wcm.72>
- [55] K. P. Valavanis and G. J. Vachtsevanos, *Handbook of Unmanned Aerial Vehicles*. Springer Publishing Company, Incorporated, 2014.
- [56] J. G. Leishman, *Principles of helicopter aerodynamics*, ser. Cambridge aerospace series 12. Cambridge ;: Cambridge University Press, 2000.
- [57] J. Seddon, S. Newman, P. Belobaba, J. Cooper, and A. Seabridge, *Basic Helicopter Aerodynamics*, ser. Aerospace Series. Wiley, 2011. [Online]. Available: <https://books.google.jo/books?id=xUN75AXYhFgC>
- [58] H. V. Abeywickrama, B. A. Jayawickrama, Y. He, and E. Dutkiewicz, “Comprehensive energy consumption model for unmanned aerial vehicles, based on empirical studies of battery performance,” *IEEE Access*, vol. 6, pp. 58 383–58 394, 2018.
- [59] W. Z. Stepniewski and C. Keys, *Rotary-wing aerodynamics*. Courier Corporation, 1984.
- [60] W. Johnson, *Rotorcraft Aeromechanics*, ser. Cambridge Aerospace Series. Cambridge University Press, 2013.

- [61] M. Orsag and S. Bogdan, “Influence of forward and descent flight on quadrotor dynamics,” in *Recent Advances in Aircraft Technology*, R. K. Agarwal, Ed. Rijeka: IntechOpen, 2012, ch. 7. [Online]. Available: <https://doi.org/10.5772/37438>
- [62] DJI, “DJI matrice 600 prospecs,” <https://www.dji.com/hr/matrice600-pro/info#specs>, accessed: 2023-03-20.
- [63] A. Al-Hourani, S. Kandeepan, and S. Lardner, “Optimal lap altitude for maximum coverage,” *IEEE Wireless Communications Letters*, vol. 3, no. 6, pp. 569–572, 2014.
- [64] 3GPP, *5G, NR, User Equipment (UE) radio access capabilities*, 15th ed. 3GPP TS, 2018.
- [65] R. Patidar, S. Roy, T. R. Henderson, and A. Chandramohan, “Link-to-System Mapping for Ns-3 Wi-Fi OFDM Error Models,” in *Proceedings of the Workshop on Ns-3*, ser. WNS3 '17. New York, NY, USA: Association for Computing Machinery, 2017, p. 31–38. [Online]. Available: <https://doi.org/10.1145/3067665.3067671>
- [66] 3GPP, “NR; Physical layer procedures for data,” 3rd Generation Partnership Project (3GPP), Technical Specification (TS) 38.214, 03 2025, version 17.13.0.
- [67] W. Anwar, K. Kulkarni, N. Franchi, and G. Fettweis, “Physical layer abstraction for ultra-reliable communications in 5g multi-connectivity networks,” in *2018 IEEE 29th Annual International Symposium on Personal, Indoor and Mobile Radio Communications (PIMRC)*, 2018, pp. 1–6.
- [68] Y. Chen, W. Feng, and G. Zheng, “Optimum placement of UAV as relays,” *IEEE Communications Letters*, vol. 22, no. 2, pp. 248–251, 2018.

- [69] Y. Chen, N. Zhao, Z. Ding, and M. Alouini, "Multiple UAVs as relays: Multi-hop single link versus multiple dual-hop links," *IEEE Transactions on Wireless Communications*, vol. 17, no. 9, pp. 6348–6359, 2018.
- [70] S. Zhang, H. Zhang, Q. He, K. Bian, and L. Song, "Joint trajectory and power optimization for UAV relay networks," *IEEE Communications Letters*, vol. 22, no. 1, pp. 161–164, 2018.
- [71] Y. Zeng, J. Xu, and R. Zhang, "Energy minimization for wireless communication with rotary-wing UAV," *IEEE Transactions on Wireless Communications*, vol. 18, no. 4, pp. 2329–2345, 2019.
- [72] "IWAVE airborne 4G LTE base station," <https://www.iwavecomms.com/>, accessed: 2023-03-20.
- [73] I. Ghareeb and A. Atiani, "Gaussian class multivariate alpha - mu distribution: Theory and applications over correlated fading channels," in *Vehicular Technology Conference (VTC Fall), 2014 IEEE 80th*, 2014, pp. 1–5.
- [74] A. M. Magableh and M. M. Matalgah, "Moment generating function of the generalized α - μ distribution with applications," *IEEE Communications Letters*, vol. 13, no. 6, pp. 411–413, 2009.
- [75] P. Fahlstrom, T. Gleason, P. Belobaba, J. Cooper, R. Langton, and A. Seabridge, *Introduction to UAV Systems: Fifth Edition*. Wiley, 04 2022.

Index

Chapter 2

P_{out} , 39

$M_{\gamma_{n_i}}(s)$, 21

$P_b(\gamma)$, 42

$\Gamma(z)$, 15

γ_{h_i} , 21

μ , 15

$\bar{\beta}_I$, 23

$\bar{\beta}_K$, 26

$\theta(t)$, 16

$f_{\gamma_{n_i}}(\gamma)$, 21

f_c , 16

$h(t)$, 16

$n(t)$, 16

$r(t)$, 16

$s(t)$, 16

$s_l(t)$, 16

v , 17

$\hat{\psi}$, 15

d_i , 12

d_k , 13

d_S , 12

E_i , 12

E_k , 13

E_R , 13

E_S , 12

g_k , 13

h_i , 12

h_{rd} , 13

h_{sr} , 12

n_{rd} , 13

n_{sr} , 12

x_i , 12

Chapter 3

E_{ji} , 62

E_k , 62

E_{sr_j} , 62

G_{AF_j} , 62

I_D , 65

I_{r_j} , 64

L , 62

R_j , 62

$F_{\gamma_{SC}}$, 66

\bar{P}_e , 73

$f_{\gamma_{SC}}$, 68	E_{hor} , 96
μ_{I_j} , 66	E_{hov} , 91
μ_k , 66	E_i , 89
$\bar{\beta}_{I_j}$, 66	E_{max} , 88
$\bar{\beta}_K$, 66	F_D , 94
$\bar{\beta}_{r_j d}$, 66	F_x , 94
$\bar{\beta}_{sr_j}$, 66	F_z , 94
γ_{SC} , 65	F_T , 91
γ_{gk} , 65	N_{tot}^{UE} , 89
$\gamma_{r_j d}$, 65	$N_{i,k}^{RB}$, 89
$\gamma_{sr_j d}$, 65	N_{rotor} , 91
γ_{sr_j} , 65	P_{hor} , 95
γ_{ji} , 65	$U_{i,k}$, 88
h_{ji} , 62	V_{hov} , 91
$h_{r_j d}$, 62	$V_{i,k}$, 90
h_{sr_j} , 62	$\alpha_{pl,LoS}$, 98
n_d , 62	$\alpha_{pl,NLoS}$, 98
n_{r_j} , 62	δ_{LoS} , 98
E_{r_j} , 62	δ_{NsLoS} , 98
d_i , 62	ω_{rotor} , 91
d_{ji} , 62	ϕ_{tilt} , 94
d_{r_j} , 62	ρ , 91
Chapter 4	τ_i , 88
$(X_{k,i}, Y_{k,i})$, 90	$d_k(i)$, 98
A_{uav} , 91	f_c , 98
A_{uav}^{eff} , 94	g , 91
$CQI(k, i)$, 88	h_{max} , 88
C_D , 94	k , 88
$D_{i,k}$, 90	m_{tot} , 92

$p_{LoS,k}(i)$, 98

$p_{NLoS,k}(i)$, 98

r_i , 89

s_0 , 88

N_{tot}^{RB} , 89

Chapter 2

D Destination node, 12

R Relay node, 12

S Source node, 12

Acronyms

3GPP	3rd generation partnership project
5G	Fifth-generation mobile system
6G	Sixth-generation mobile system
AF	Amplify and forward
AMC	Adaptive modulation and coding
AWGN	Additive white gaussian noise
BEP	Bit error probability
BER	Bit error rate
BPSK	Binary phase shift keying
CCI	Co-channel interference
CDF	Commutative distribution function
CSI	Channel state information
dB	Decibels
DF	Decode and forward
DPSK	Differential phase shift keying
ECC	Error-Correcting Codes
EGC	Equal gain combining
eNB	Evolved node-b
GCD	Greatest Common Divisor
gNB	Next-generation node-b
I.I.D.	Independent and identically distributed

I.N.I.D.	Independent and non identically distributed
IEEE	Institute of electrical and electronics engineer
INID	Independent but not identically distributed
ISI	Inter-symbol Interference
LoS	Line-of-sight
LTE	Long term evolution
MCS	Modulation and coding scheme
MDP	Markov decision problem
MGF	Moment generating function
MIMO	Multiple-input multiple-output
ML	Machine learning
MRC	Maximal ratio combining
MSK	Minimum shift keying
NR	New radio
PDF	Probability density function
PPO	Proximal policy optimization
PRB	Physical resource block
QAM	Quadrature amplitude modulation
QoS	Quality of service
R-D	Relay to destination link
RB	Resource block
RL	Reinforcement learning
RSRP	Received signal
S-R	Source to relay link
SC	Selective combining
SINR	Signal to interference plus noise ratio
SISO	Single-input and single-output
SNR	Signal to noise ratio

TBS	Transport block size
TDD	Time division duplex
TTI	Transmission time interval
UAV	Unmanned aerial vehicles
UE	User equipment
WLAN	Wireless local area network
WPT	Wireless power transfer